



The development of rhenium(III) oxide nanoradiopharmaceuticals

by

Sinelizwi Veronica Joseph

**Submitted in partial fulfilment of the requirements for the degree of MSc
Chemistry (Nanoscience) at the Nelson Mandela University**

May 2018

Supervisor: Prof. Z.R. Tshentu

Co-supervisor: Prof. C. Frost

DEDICATION

This is for my late dad and my late sister

DECLARATION

I, Sinelizwi Veronica Joseph (s216666945), hereby declare that the mini-treatise for student qualification to be awarded is my own work and that it has not previously been submitted for assessment or completion of any postgraduate qualification to another University or for another qualification.

A handwritten signature in black ink, appearing to read 'S. V. Joseph', written in a cursive style.

Sinelizwi Veronica Joseph

ABSTRACT

The study details the experimental work on the development of rhenium(III) oxide nanoradiopharmaceuticals for imaging and therapy of disease states. The nanoparticles (NPs) were capped with covalently linked tetraaminophthalocyanine-folate and ethylenediamine-folate to enhance their targeting ability. The capping agents were successfully synthesised and structurally characterised using Ultraviolet-Visible Spectroscopy (UV-Vis), Fourier Transform-Infrared Spectroscopy (FT-IR), Proton Nuclear Magnetic Resonance ($^1\text{H-NMR}$), and Liquid Chromatography-Mass Spectroscopy (LC-MS). The nanoparticles were characterised using UV-Vis, spectrofluorimetry, Transmission Electron Microscopy (TEM), dynamic light scattering (DLS) and Zeta potential. Nanoparticles of sizes between 10 and 100 nm size were envisaged to be suitable for applications in biological systems. The preferred surface charge for the uptake of NPs must be between -30 and +30 mV, Re_2O_3 NPs capped with ethylenediamine were found to have a surface charge of -49 mV as compared with NPs capped with ethylenediamine-folate which gave -18.6 mV. The cytotoxicity studies of the nanoparticles were tested against four different cell lines: MDA-MB-468, MDA-MB-231, MCF-7, and MCF-10A. The cell survival rate after treatment was done with different capped rhenium(III) oxide nanoparticles obtained at a 10 μM concentration showed more than 80% cell viability. A comparison was conducted based on different nanoparticle sizes of capping agents across the four cell lines of varying folate receptor. All the cell lines were compared, and it was observed that MCF-7 had high percentage of cell viability especially with the cells treated with folate conjugated nanoparticles. Further investigation was done on the effects of folate conjugates and the effects of size. It was observed that the tetraaminophthalocyanine-folate favoured the MCF-7, for large-sized nanoparticles. However, further work is required to test the cancer cell internalisation of the nanoparticles using TEM as well as the correct size for endocytosis. Thereafter, the mice model study will be carried out for investigation of biodistribution of particles in tumour tissue using hot isotopes ($^{186/188}\text{Re}$) and this will be done in a radiopharmaceutical laboratory.

Key words: Radiopharmaceuticals, rhenium nanoparticles, capping agent, biomolecules, cell lines

ACKNOWLEDGEMENTS

“For I know the plans I have for you, declares the Lord, the plans to prosper you and not to harm you, plans to give you hope and future” (Jeremiah 29:11, New International Version). I am grateful to the God almighty for opening this wonderful opportunity and allowing me to complete my work, it was not by me, but it was his will.

I would like to thank my supervisor, Professor Zenixole Richman Tshentu, for giving me this opportunity to work as his research student and for trusting me with this project. His great support and guidance is greatly appreciated, without it I would not be where I am today. He really taught me a lot and I will represent him wherever I go.

I would also like to thank my co-supervisor, Professor Carminita Frost, for her valuable support and advice towards the study, especially with the biochemistry studies.

I would like to extend my sincere gratitude to Dr. Natasha Beukes for her assistance with the biological studies, without her the biological studies would not be possible.

I would like to extend my appreciation to the person I was working with, Mr Sendibityosi Gandidzanwa, my peer, for helping me with the understanding of biological studies.

I would also like to extend my sincere gratitude to the following people Ms Candice Blom, Mr Arno Janse Van Vuuren, Ms Shirley Pinchuck and Mr Marvin Randall for assisting with HR-TEM and TEM samples.

The following people are also much appreciated, Dr J. Ngororabanga, Mr T. Dembaremba, Mr S. Mgawu and Mr S. Ntsimango for their support.

To our Lab Technician, Mr Henk Schalekamp, I want to say thank you for ordering chemicals throughout this study and for always reminding us about the safety cautions to be taken when working in the laboratory.

I would like to thank my entire group, Inorganic research group (lab 114) for their advice, reliable help and support. I also wish to express my appreciation to the Biochemistry research group for the cell work experience and being patient with me.

Special thanks to my mother and little sister for their moral support and prayers for the successful completion of this work. I would like to thank my mother for all her efforts and motherly care and for the support she has given me throughout my educational journey both moral and financial.

I would like to acknowledge DST Nanotechnology platform for providing financial support through a bursary.

Finally, I would like to thank Nelson Mandela University for their scholarship and for allowing me to use their facilities.

TABLE OF CONTENTS

DEDICATION.....	I
DECLARATION	II
ABSTRACT	III
ACKNOWLEDGEMENTS.....	IV
TABLE OF CONTENTS	VI
LIST OF FIGURES	X
LIST OF TABLES.....	XV
CHAPTER 1 : INTRODUCTION	1
1.1 Motivation	1
1.2 Statistics of cancer	2
1.3 Treatment of Cancer	3
1.3.1 Nuclear medicine	4
1.3.1.1 Radiopharmaceuticals.....	5
1.4 Nanotechnology.....	7
1.4.1 Nanoparticles.....	8
1.4.1.1 A brief history of nanoparticles.....	9
1.4.2 Different methods of synthesizing nanoparticles.....	10
1.4.2.1 Bottom-up (chemical approach)	11
1.4.2.2 Top-down (physical approach).....	11
1.4.3 Nanoparticles in medicine	12
1.4.3.1 Nanomedicine	13
1.4.3.2 Nanoradiopharmaceuticals.....	15
1.4.3.3 Rhenium nanomaterials.....	16

1.5	Capping agents: phthalocyanines versus diamines	17
1.5.1	Phthalocyanines (Pcs)	17
1.5.2	Ethylenediamine (EDA)	19
1.6	Targeting biomolecules	20
1.6.1	Folate (FA)	20
1.7	Scope of the study.....	21
 CHAPTER 2 : MATERIALS, TECHNIQUES AND EXPERIMENTAL METHODS		23
2.1	General reagents for synthesis	23
2.2	Instrumentation	24
2.2.1	Spectroscopic techniques	24
2.2.1.1	Nuclear magnetic resonance (NMR spectroscopy).....	24
2.2.1.2	Infrared spectroscopy (FT-IR).....	24
2.2.1.3	UV-Vis electronic spectroscopy (UV-Vis)	24
2.2.1.4	Spectrofluorimetry.....	25
2.2.1.5	Powerwave spectrophotometer (Biotek)	25
2.2.1.6	Liquid chromatography-mass spectroscopy (LC-MS)	25
2.2.2	Transmission electron microscopy (TEM).....	25
2.2.3	Zeta potential (ZS).....	25
2.2.4	Other instruments.....	26
2.2.4.1	Melting point.....	26
2.2.4.2	Centrifuge.....	26
2.2.4.3	Class 2 Microbiological safety cabinet	26
2.2.4.4	Incubator	26
2.2.4.5	Microscope.....	26
2.3	Methodology	27

2.3.1	Synthesis <i>N</i> -BOC-ethylenediamine-folate	27
2.3.1.1	<i>N</i> -boc-ethylenediamine-folate (<i>N</i> -BOC-EDA-FA)	27
2.3.1.2	Synthesis of ethylenediamine-folate (EDA-FA) (deprotection step)	28
2.3.2	Synthesis of Tetraaminophthalocyanine (TAPc).....	29
2.3.2.1	Tetranitro-zinc-phthalocyanine (TNZnPc).....	29
2.3.2.2	Tetraamino-zinc-phthalocyanine (TAZnPc).....	30
2.3.2.3	Tetraaminophthalocyanine (TAPc)	31
2.3.2.4	Synthesis of TAPc-folate conjugate.....	32
2.3.3	Synthesis of rhenium(III) oxide nanoparticles	32
2.3.4	Cell culture and maintenance	34
2.3.5	Cell viability assay	35
2.3.6	Statistics	36
2.3.7	Cell accumulation studies: Transmission electron microscope.....	36

CHAPTER 3 : SYNTHESIS AND CHARACTERISATION OF CAPPING AGENTS AND NANOPARTICLES	39
3.1 General introduction	39
3.2 Results and discussion.....	40
3.2.1 Ethylenediamine-folate conjugate	40
3.2.2 Tetraaminophthalocyanine-folate (TAPc-FA) conjugate	45
3.2.3 Rhenium(III) oxide nanoparticles.....	49
3.2.3.1 General introduction.....	49
3.2.3.2 Synthetic aspects.....	49
3.2.3.3 Spectroscopic characterization	51
3.2.3.4 TEM characterization	54
3.2.3.5 Zeta potential analysis	58
3.2.4 General conclusion	61

CHAPTER 4 : BIOCHEMICAL STUDIES	62
4.1 General introduction	62
4.1.1 Cell cytotoxicity studies	63
4.1.2 General conclusion	75
CHAPTER 5 : CONCLUSION, RECOMMENDATIONS, AND FUTURE WORK	77
5.1 Conclusion	77
5.2 Recommendations and future work	79
REFERENCES	80

LIST OF FIGURES

Figure 1.1: [A] Different kinds of cancer for both man and woman, [B] Cancer growth and progression, [C] Cancer cells dividing rapidly, [D] Cancer cells metastasised to other parts of the body.....	1
Figure 1.2: Some few examples of nanomaterials used in different fields.	8
Figure 1.3: Photographs of the famous Lycurgus cup which displays a different colour depending on whether it is illuminated, externally A or internally B, colour changes depend on the size and shape of gold and silver nanoparticles.	9
Figure 1.4: Engineered approach for prepared of tumour targeted stable nanoparticles for the siRNA delivery.....	15
Figure 1.5: APTES-PEG coated iron oxide nanoparticles conjugated to rhenium ¹⁸⁸ Re labelled rituximab.	17
Figure 1.6: Chemical structure of phthalocyanine	18
Figure 1.7: The structure of folate showing the pteridine ring (red), 4-aminobenzoate (blue) and the glutamate.....	20
Figure 2.1: Proposed synthetic route of protecting one side of ethylenediamine with <i>tert</i> -Butyloxycarbonyl protecting group.	27
Figure 2.2: Synthetic route of ethylenediamine-folate conjugate.....	28
Figure 2.3: Synthetic route of deprotecting the <i>tert</i> -Butyloxycarbonyl (BOC) protecting group.	29
Figure 2.4: The synthesis of tetranitro-zinc-phthalocyanine (TNZnPc) from 4-phthalonitrile.....	30
Figure 2.5: The synthesis of tetraamino-phthalocyanine (TAPc) and tetranitro-phthalocyanine.....	31
Figure 2.6: Conjugation of tetraamino-phthalocyanine (TAPc) to folate.....	32
Figure 2.7: Synthetic route of capped rhenium (III) oxide nanoparticles with ethylenediamine-folate	33
Figure 2.8: Photographs of the sample vials containing ammonium perrhenate in water (100 mM), (A) before and after adding ethylenediamine, and ethylenediamine-folate	

as capping agents and sodium borohydride as reducing agent. (B) before and after adding tetraaminophthalocyanine, and tetraaminophthalocyanine-folate as capping agents and sodium borohydride as reducing agent.	34
Figure 3.1: FT-IR spectra of <i>N</i> -boc-ethylenediamine-folate (<i>N</i> -BOC-EDA-FA) and ethylenediamine-folate (EDA-FA)	41
Figure 3.2: UV-Vis spectra of <i>N</i> -Boc-ethylenediamine-folate (<i>N</i> -BOC-EDA-FA) and ethylenediamine-Folate (EDA-FA).....	42
Figure 3.3: ¹ H-NMR of Conjugated folate with <i>N</i> -boc-ethylenediamine	42
Figure 3.4: ¹ H-NMR ethylenediamine- folate (EDA-FA) after deprotection	43
Figure 3.5: LC-MS of ethylenediamine- folate (EDA-FA).....	44
Figure 3.6: UV-Vis spectra of tetranitrophthalocyanine (TNZnPc), tetraamino-zinc-phthalocyanine (TAZnPc) and tetraaminophthalocyanine (TAPc).....	46
Figure 3.7: FT-IR spectra of tetranitro-zinc-phthalocyanine (TNZnPc), tetraamino-zinc-phthalocyanine (TAZnPc) and tetraaminophthalocyanine (TAPc).....	47
Figure 3.8: LC-MS of tetraaminophthalocyanine-folate (TAPc-FA)	48
Figure 3.9: Optical spectra of rhenium oxide nanoparticles capped with ethylenediamine	51
Figure 3.10: Optical spectra of rhenium oxide nanoparticles with an increase concentration of EDA-FA compared with the spectra of rhenium(III) oxide nanoparticles capped with ethylenediamine.	52
Figure 3.11: Optical spectra of rhenium(III) oxide nanoparticles with an increase in concentration of tetraaminophthalocyanine-folate (TAPc-FA)	53
Figure 3.12: Emission spectra of rhenium(III) oxide nanoparticles with different capping agents in various concentrations.....	54
Figure 3.13: TEM micrographs of rhenium(III) oxide-ethylenediamine (Re-EDA NPs) and their subsequent particles size distributions approximately 2 and 6 nm. These small size nanoparticles capped with ethylenediamine resulted from the following optimised conditions: 60 µL of ammonium perrhenate (100 mM) , 700 µL of freshly prepared NaBH ₄ (100 mM) and 800 µL of EDA-FA solution in DMSO (10 mg/ml). However, 6 nm sizes resulted from an increase in the concentration of	

perrhenate (80 μL) and with decreasing the amount of the reducing agent (500 μL). 55

Figure 3.14: TEM micrographs of rhenium(III) oxide-ethylenediamine-folate (Re-EDA-FA NP) and their subsequent particles size distributions with 2 and 154 nm displayed larger spherical with trace amounts of capping agent surrounding the particle. The small-sized nanoparticles resulted from the following optimised conditions : 60 μL of ammonium perrhenate (100 mM), 700 μL of freshly prepared NaBH_4 (100 mM) and 700 μL of EDA-FA solution in DMSO (10 mg/ml). However, 154 nm resulted from an increase of concentration of perrhenate (80 μL) and with decreased amount of the reducing agent (500 μL). 56

Figure 3.15: TEM micrographs of rhenium(III) oxide capped with ethylenediamine-folate (Re-EDA-FA NP) and tetraaminophthalocyanine-folate (Re-TAPc-FA NP) with their subsequent particles size distributions. The image of rhenium(III) oxide capped with conjugated EDA-FA with average size 52 nm resulted from the following optimised conditions: 80 μL of ammonium perrhenate (100 mM), 700 μL of NaBH_4 (100 mM) and 600 μL of EDA-FA. However, medium (12 nm) size nanoparticles capped with TAPc-FA resulted from the following optimised conditions: 60 μL of ammonium perrhenate (100 mM), 500 μL of NaBH_4 (100 mM) and 600 μL of TAPc-FA. An increase in the concentration of perrhenate (80 μL) and 500 μL of NaBH_4 resulted in the medium size (32 nm) nanoparticles. 56

Figure 3.16: Dynamic light scattering (DLS) measurements of rhenium(III) oxide nanoparticles capped with ethylenediamine (Re-EDA NP s) from Zeta-sizer..... 59

Figure 3.17: Dynamic light scattering (DLS) measurements of rhenium(III) oxide nanoparticles capped with ethylenediamine-folate (Re-EDA-FA NP s) from Zeta-sizer..... 59

Figure 3.18: Dynamic light scattering (DLS) measurements of rhenium(III) oxide nanoparticles capped with ethylenediamine (Re-EDA NP m) from Zeta-sizer. 60

Figure 3.19: Dynamic light scattering (DLS) measurements of rhenium(III) oxide nanoparticles capped with ethylenediamine-folate (Re-EDA-FA NP s) from Zeta-sizer..... 60

Figure 4.1: The viability profiles of rhenium(III) oxide nanoparticles studied using MDA-MB-468 at 100 μ M. Different colors represent the following: controls (green), small-sized nanoparticles (blue) and large (big)- sized nanoparticles (grey). The following compounds were investigated; folate (FA), methotrexate (MTX), ethylenediamine (EDA), tetraaminophthalocyanine (TAPc), ethylenediamine-folate (EDA-FA), tetraaminophthalocyanine-folate (TAPc-FA), small and big-sized sodium borohydride capped nanoparticles (Re NP), small and big-sized ethylenediamine capped nanoparticles (Re-EDA NP), small and big-sized tetraaminophthalocyanine capped nanoparticles (TAPc-NP), small and big-sized ethylenediamine-folate capped nanoparticles (Re-EDA-FA NP), and small and big-sized tetraaminophthalocyanine-folate capped nanoparticles (Re-EDA-FA NP). The untreated cells were used as a neutral control, with methotrexate as a positive control. The small-sized nanoparticles are between 1–10 nm and big-sized nanoparticles are between 10–100 nm. Statistics analysis was done using ANOVA, $P^* < 0,05$, and 3 experiments were done ($N = 3$) for each cell line. 64

Figure 4.2: The viability profiles of rhenium(III) oxide nanoparticles studied using MDA-MB-468 at 10 μ M. Different colors represent the following: controls (green), small-sized nanoparticles (blue) and large (big)- sized nanoparticles (grey). The following compounds were investigated; folate (FA), methotrexate (MTX), ethylenediamine (EDA), tetraaminophthalocyanine (TAPc), ethylenediamine-folate (EDA-FA), tetraaminophthalocyanine-folate (TAPc-FA), small and big-sized sodium borohydride capped nanoparticles (Re NP), small and big-sized ethylenediamine capped nanoparticles (Re-EDA NP), small and big-sized tetraaminophthalocyanine capped nanoparticles (Re-TAPc NP), small and big-sized ethylenediamine-folate capped nanoparticles (Re-EDA-FA NP), and small and big-sized tetraaminophthalocyanine-folate capped nanoparticles (Re-TAPc-

FA NP). The untreated cells were used as a neutral control, with methotrexate as a positive control. The small-sized nanoparticles are between 1–10 nm and big-sized nanoparticles are between 10–100 nm. Statistics analysis was done using ANOVA, $P^* < 0,05$, and 3 experiments were done ($N = 3$) for each cell line. . 66

Figure 4.3: The viability profiles of rhenium(III) oxide nanoparticles studied using MDA-MB-321 at 10 μ M. Different colors represent the following: controls (green), small-sized nanoparticles (blue) and large (big)- sized nanoparticles (grey). The following compounds were investigated; folate (FA), methotrexate (MTX), ethylenediamine (EDA), tetraaminophthalocyanine (TAPc), ethylenediamine-folate (EDA-FA), tetraaminophthalocyanine-folate (TAPc-FA), small and big-sized sodium borohydride capped nanoparticles (Re NP), small and big-sized ethylenediamine capped nanoparticles (Re-EDA NP), small and big-sized tetraaminophthalocyanine capped nanoparticles (Re-TAPc NP), small and big-sized ethylenediamine-folate capped nanoparticles (Re-EDA-FA NP), and small and big-sized tetraaminophthalocyanine-folate capped nanoparticles (Re-EDA-FA NP). The untreated cells were used as a neutral control, with methotrexate as a positive control. The small-sized nanoparticles are between 1–10 nm and big-sized nanoparticles between 10–100 nm. Statistics analysis was done using ANOVA, $P^* < 0,05$, and 3 experiments were done ($N = 3$) for each cell line. 68

Figure 4.4: The viability profiles of rhenium(III) oxide nanoparticles studied using MCF-10A at 10 μ M. Different colors represent the following: controls (green), small-sized nanoparticles (blue) and large (big)- sized nanoparticles (grey). The following compounds were investigated; folate (FA), methotrexate (MTX), ethylenediamine (EDA), tetraaminophthalocyanine (TAPc), ethylenediamine-folate (EDA-FA), tetraaminophthalocyanine-folate (TAPc-FA), small and big-sized sodium borohydride capped nanoparticles (Re NP), small and big-sized ethylenediamine capped nanoparticles (Re-EDA NP), small and big-sized tetraaminophthalocyanine capped nanoparticles (Re-TAPc NP), small and big-sized ethylenediamine-folate capped nanoparticles (Re-EDA-FA NP), and small

and big-sized tetraaminophthalocyanine-folate capped nanoparticles (Re-EDA-FA NP). The untreated cells were used as a neutral control, with methotrexate as a positive control. The small-sized nanoparticles are between 1–10 nm and big-sized nanoparticles are between 10–100 nm. Statistics analysis was done using ANOVA, $P^* < 0,05$, and 3 experiments were done ($N = 3$) for each cell line. 70

Figure 4.5: The viability profiles of rhenium(III) oxide nanoparticles studied using MCF-7 at 10 μ M. Different colors represent the following: controls (green), small-sized nanoparticles (blue) and large (big)- sized nanoparticles (grey). The following compounds were investigated; folate (FA), methotrexate (MTX), ethylenediamine (EDA), tetraaminophthalocyanine (TAPc), ethylenediamine-folate (EDA-FA), tetraaminophthalocyanine-folate (TAPc-FA), small and big-sized sodium borohydride capped nanoparticles (Re NP), small and big-sized ethylenediamine capped nanoparticles (Re-EDA NP), small and big-sized tetraaminophthalocyanine capped nanoparticles (Re-TAPc NP), small and big-sized ethylenediamine-folate capped nanoparticles (Re-EDA-FA NP), and small and big-sized tetraaminophthalocyanine-folate capped nanoparticles (Re-EDA-FA NP). The untreated cells were used as a neutral control, with methotrexate as a positive control. The small-sized nanoparticles are between 1–10 nm and big-sized nanoparticles between 10–100 nm. Statistics analysis was done using ANOVA, $P^* < 0,05$, and 3 experiments were done ($N = 3$) for each cell line. 74

LIST OF TABLES

Table 1.1:	Profiles of potential radionuclides for nanotargeted therapy and imaging.....	6
Table 2.1:	General reagents used in this study.	23
Table 2.2:	Reagents used for biological studies.....	24
Table 2.3:	Preparation of the media for cell culture:	35
Table 3.1:	Chemical structure and molecular ions from of ethylenediamine- folate (EDA-FA) obtained from the Electrospray Ionization (ESI) using LC-MS.	44
Table 3.2:	Analyzed chemical and molecular ions of tetraaminophthalocyanine-folate (TAPc-FA) obtained from the Electrospray Ionization (ESI) usng LC-MS.	48
Table 3.3:	Optimisation synthesis of rhenium(III) oxide nanoparticles capped with different capping agents.	50
Table 3.4:	Summarised results of rhenium(III) oxide nanoparticles sizes (Zeta-sizer) and charge (Zeta potential).....	61
Table 4.1:	Different cell lines with the various receptors they express.	65
Table 4.2:	Overall comparison on how the different cell lines responded to the control treatments.....	75
Table 4.3:	Overall comparison on how the different cell lines responded to the nanoparticle treatments.....	76

LIST OF ABBREVIATIONS

^{186}Re – Rhenium-186

^{188}Re – Rhenium-188

$^{99\text{m}}\text{Tc}$ – Metastable 99-Technetium

BOC – *tert*-Butyloxycarbonyl

EPR – Enhanced Permeation and Retention effect

FA – Folate

FA-EDA – Folate conjugated ethylenediamine

FA-TAPc – Folic acid conjugated tetraaminophthalocyanine

FR – Folate receptors

FT-IR – Fourier Transform Infrared Spectroscopy

NMR – Nuclear Magnetic Resonance

NPs – Nanoparticles

NRPs – Nanoradiopharmaceuticals

Pcs – Phthalocyanines

PDT – Photodynamic therapy

Re Pcs – Rhenium phthalocyanine

RP – Radiopharmaceuticals

SPECT – Single Photon Emission Computed Tomography

TEM – Transmission Electron Microscopy

UV- Vis – Ultra Violet-Visible Spectroscopy

Chapter 1 : Introduction

1.1 Motivation

Cancer is defined as a class of diseases that is characterized by out of control cell growth (**Figure 1.1: [B]**). There are over 100 different types of cancer, each being classified by the type of cell that is initially affected (**Figure 1.1: [A]**). Cancer damages the body, as the cells that are rapidly dividing (**Figure 1.1: [C]**) form lumps called tumours and it eventually prohibits normal function. Leukaemia is an exception as it does not create a tumour but prohibits normal blood function. Tumours grow and interfere with the nervous, digestive and circulatory systems with release of hormones that affect the body function [1, 2].

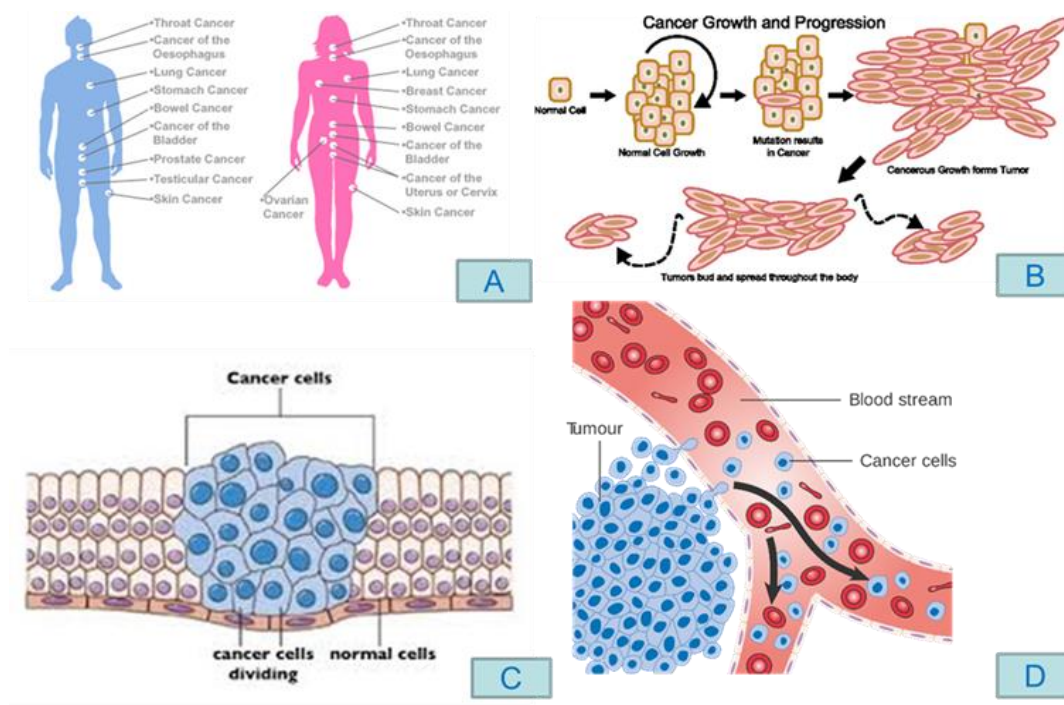


Figure 1.1: [A] Different kinds of cancer for both man and woman [3], [B] Cancer growth and progression [4], [C] Cancer cells dividing rapidly, [D] Cancer cells metastasised to other parts of the body [5].

Tumours that stay in one area and demonstrate limited growth are generally considered to be benign. A malignant tumour is considered as a developed cancer where the cancer cells have entered the blood vessels and invaded neighbouring tissues. Metastatic cancerous cells manage to move throughout the body using the blood or lymph systems, destroying healthy tissue in a process called invasion. When a cell manages to divide and grow, it makes new blood vessels and thus feed itself through a process called angiogenesis, where a tumour develops and spreads to other parts of the body. It invades and destroys other healthy tissues and it is then said to have metastasised [6] (**Figure 1.1: [D]**).

1.2 Statistics of cancer

In 2018, roughly 1,735,350 new cancer cases and 609,640 cancer deaths are projected to occur in the United States. Over the past decade of data, the cancer incidence rate was stable in women and declined by approximately 2% annually in men, while the cancer death rate declined with about 1.5% annually in both men and women in 2006 to 2015. It was estimated that 135 430 cases of colorectal cancer were diagnosed in 2017 with 50 260 deaths in the United State [7].

Without action, the worldwide cancer burden is expected to reach 21 million new diagnoses and 13 million deaths by 2030, with the most rapid increases occurring in low- and middle-income countries [8]. Cancer deaths worldwide for 2017 were estimated at over 25 000 per day, of which this also includes the economically developing countries. South Africa is one of these countries [9].

Cancer affects every South African either financially or emotionally in some way. Cancer in South Africa is an emerging health problem, with breast cancer being one of the leading cancers in women, following similar worldwide statistics. Lifetime risks of developing breast cancer vary from a low of one in 81 African women (similar to Japan) to a high of one in 13 among white women, which is similar to the rates in Western countries. Age and stage at diagnosis vary considerably between the different races and populations (urban or rural) living in South Africa [9, 10].

Millions of people diagnosed with cancer extend their life due to early identification and treatment. The most common causes of cancer death are cancers of the lung and bronchus, prostate, and colorectal in men, and breast and colorectal cancers in women. The lifetime probability of being diagnosed with an invasive cancer is higher for men than women [11]. The disease is not contagious. It cannot be spread from person to person through the air, by contact or *via* transfusion of blood. Rather the risk of cancer can be inherited. This means that it can be passed genetically from parents to children. This risk factor increases the chance of getting cancer. Other factors are tobacco use, high fat diet, being overweight, excessive exposure to sunlight, drinking too much alcohol, X-ray sources of radioactivity, certain geographic areas, chemicals and other substances in the environment (carcinogens) [11, 12].

1.3 Treatment of Cancer

The treatment for cancer patients has come a long way in the past decades. It started with surgery, and now it is more precise and less harmful due to the new techniques that are being developed. Detecting cancer at its early stages increases the chances of it being treated or even cured using chemicals instead of surgery, especially patients that are diagnosed with breast and colon cancer. Radiation therapy can be tailored to patients, depending on the tumour type, the size and location of the tumour. This technique can cure several early-stage cancers. Patients are now receiving a specific combination of surgery along with chemotherapy and other treatments like immunotherapy, hormone and nuclear medicine [13].

These techniques are being used although they are still presenting a lot of drawbacks. For example, radiotherapy is a special technique that uses X-rays/gamma rays/beta rays to destroy the DNA of cancer cells, thus stopping them from dividing and growing. Unfortunately, the side effect of radiation occurs for both cancer cells and the normal cells, however normal cells repair faster than the cancer cells, although not all the good cells (normal cells) are repaired. During radiation therapy the patient can experience severe side effects like losing weight, vomiting, losing hair, etc. [14].

All controlled drug delivery systems aim to improve the therapeutic drug efficacy and reduce the side effects by the augmentation of the local drug concentration (control of distribution), the desired control, and sustained release (control of time). Conventional anti-cancer drugs exhibit a lack of specificity, poor solubility and distribution, unfavourable pharmacokinetics and high tissue damage or toxicity [15].

Modern medicine demands progressively more sophisticated methods for the accurate diagnosis and treatment of disease states, and there is a massive worldwide research effort into developing and improving imaging techniques. Images can be produced either by measuring the absorption of externally applied radiation (e.g. X-ray, ultrasound, MRI imaging), or by administering a small amount of a radioactive compound and detecting the radiation escaping from the body. In addition, development of anticancer agent that localise specifically on cancer tumours is important [14].

1.3.1 Nuclear medicine

Nuclear medicine is a medical speciality of radiology that involves administering a small amount of radioactive material (called radiopharmaceutical or radiotracers) to a patient by injection, inhalation or pill. The radiopharmaceutical accumulates in an organ or area of the body where it gives off energy in the form of gamma or beta rays. Targeted therapy with a radiopharmaceutical (radioactive compounds) used in nuclear medicine has a great potential for the treatment of cancer, especially for cancer cells that have migrated from primary tumours to lymph nodes and secondary organs such as bone marrow [16, 17]. These disseminated tumour cells can be difficult to treat with a single targeting agent, hence there are dramatic differences in the number of targetable receptors on each cell [18, 19].

1.3.1.1 Radiopharmaceuticals

Cancer continues to claim more lives every year despite the efforts that have been attempted to find a cure for many years. Most of the conventional ways of treating cancer still present many side effects. However, current research in the field of nuclear medicine continues to

yield promising results. In modern medicine, early diagnosis of disease plays an important part in improving the lives and reducing health care costs to society [20].

Properties of potential radionuclides are presented in **Table 1.1**. Technetium-99m (^{99m}Tc) is one of the most commonly used radioisotopes for diagnostic and imaging purposes in nuclear medicine worldwide. The coordination chemistry of Tc has been successfully extended to rhenium (Re) since they are congeners [21]. Of particular interest are two Re radioisotopes (^{186}Re and ^{188}Re), due to their nuclear properties that can be applied in the diagnosis and therapy of cancer. With the growing interest of employing nanoparticles in medicine coupled with nuclear properties of $^{186}\text{Re}/^{188}\text{Re}$, the focus is on the development of novel rhenium nanoradiopharmaceuticals (NRPs). There are several reviews available on Tc but Re is still under investigation [22]. More research is being carried out on the radionuclides such as ^{186}Re , ^{188}Re , ^{64}Cu , ^{67}Cu , ^{198}Au , ^{199}Au , ^{77}As , ^{105}Rh , ^{111}Ag , ^{194}Ir and ^{99m}Tc . ^{99m}Tc is being used as a source of gamma radiation in SPECT image analysis for bone, kidney and brain imaging, and only one analogue of Re for bone metastasis is in the clinic today [21].

Table 1.1: Profiles of potential radionuclides for nanotargeted therapy and imaging [23].

Radionuclide	Emission type	E max (keV)	Half-life	production
^{99m} Tc	γ	140	6.0 h	⁹⁹ Mo/ ^{99m} Tc-generator
¹¹¹ In	Auger, γ	171,245	67.2 h	¹¹¹ Cd(p,n) ¹¹¹ In
⁶⁷ Ga	γ	93, 184, 300, 393	78.3 h	⁶⁸ Zn(n,p) ⁶⁷ Ga
¹³¹ I	γ (81.2%), β	284, 364, 637	8.0 days	¹³⁰ I(n,γ) ¹³¹ Te(β) ¹³¹ I
¹²³ I	Auger, γ	159	13.2 h	¹²¹ Sn(α, 2n) ¹²³ I
^{5m} Te	γ	-	57.4 days	¹²⁵ Sn(β-) ¹²⁵ Sb (β-)
¹¹ C	Positron	960	20.4 min	¹⁴ N(p, α) ¹¹ C
¹⁵ O	-	1720	2.07 min	¹⁴ N(d,n) ¹⁵ O
¹³ N	-	1190	9.96 min	¹⁶ O(p, α) ¹³ N
¹²⁴ I	-	Eβ+2134, 1533	100.2 h	¹²⁴ Te (p,n) ¹²⁴ I
¹⁸ F	-	Eβ+635	1.83 h	¹⁸ O(p,n) ¹⁸ F
⁷⁶ Br	-	Eβ+ 3961	16.0 h	⁷⁶ Se(p,n) ⁷⁶ Br
⁶⁴ Cu	-	Eβ+656	12.7 h	⁶⁴ Ni(p,n) ⁶⁴ Cu
⁶⁷ Cu	β	0.42	67 h	¹¹¹ Cd (n, p) ¹¹¹ In
¹¹¹ In	Auger, γ	0.19	2.6 d	⁶⁴ Ni (α, p) ⁶⁷ Cu
⁹⁰ Y	β	2.28	64.1 h	⁹⁰ Sr/ ⁹⁰ Y- generator
¹⁸⁸ Re	β, γ (15.1%)	2.12	17 h	¹⁸⁸ W/ ¹⁸⁸ Re-generator
¹⁸⁶ Re	β, γ (15.1%)	1.07	89.2 h	¹⁸⁵ Re (n, γ)
²²⁵ Ac	α	5.83	10 h	²²⁵ Ra-genegetor
¹⁷⁷ Lu	β	0.49	16 h	¹⁷⁶ Lu (n, γ) ¹⁷⁷ Lu
¹⁶⁶ Ho	β, γ (6.7%)	1.85	26.9 h	¹⁶⁵ Ho(n, γ) ¹⁶⁶ Ho
⁸⁹ Sr	β	1.46	52.7 d	⁸⁸ Sr (n, γ) ⁸⁹ Sr

Table 1.1: Continued.

³² P	β	1.71	14.3 d	¹² S (n, p) P
²¹¹ Pt	α	5.87	7.2 h	Accelerator
²¹³ Br	α	5.869	45.7 min	²²⁵ Ra-generator

1.4 Nanotechnology

Having witnessed the advances and successes in the field of nanotechnology, scientists across various disciplines have applied nanotechnology as another approach to address the issue of diseases. Nanotechnology is the “work horse” of nanoscience, that is, nanoscience focuses on discovering novel behaviours and properties of materials with dimensions in the nanoscale, which varies roughly between 1 and 100 nm [24]. Nanotechnology is the application of the discoveries made in nanoscience. In other words, nanotechnology is the art of building and using materials, devices, and machines at the nanometer scale. “Nano”- is a Greek word for “dwarf”, which means (10^{-9}), or one-billionth. In the case of nanotechnology, it means one-billionth of a meter or 1 nanometer (nm). To put the nano-size into context, 1 nanometer is equivalent to 3 atoms long [25].

Nanotechnology offers potential prospects to produce better materials and products. Scientists have discovered different nanomaterials using different materials such as metal-based nanocomposites, thin films, carbon and dendrimers to name a few (**Figure 1.2**). In recent years, nanomaterials have attracted a significant attention in the vast array of scientific disciplines, by the virtue of their unusual magnetic, electrical, optical and mechanical properties [26].

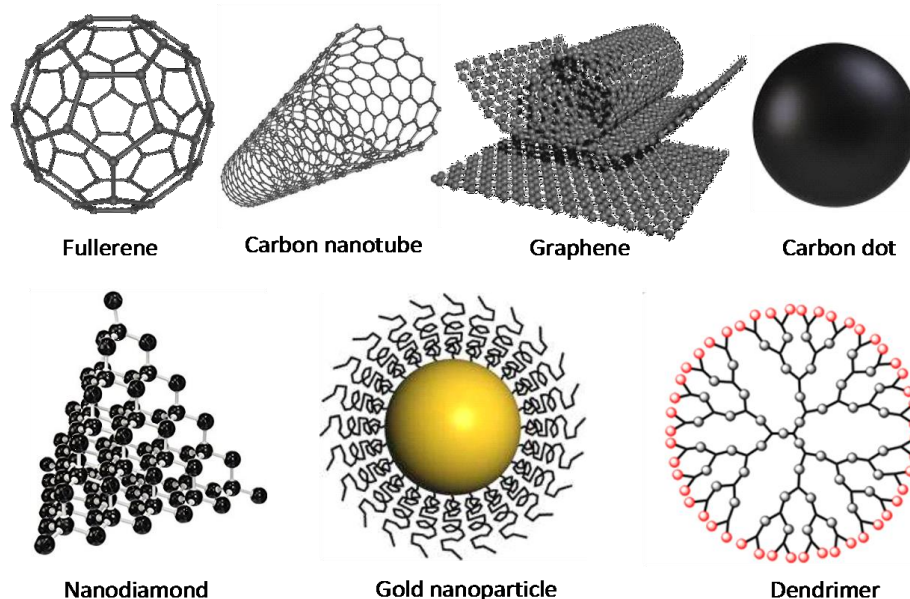


Figure 1.2: Some few examples of nanomaterials used in different fields [27, 28].

There are many different types of nanomaterials that have been produced by researchers across the world such as carbon-based nanomaterials with varied applications, gold nanoparticles (GNPs) capped with different capping agents for targeted therapy, and dendrimers used as drug delivery systems [27] (**Figure 1.2**).

Nanomaterials are being exploited in many other areas due to their fascinating physical and chemical properties and for their application in devices. Among these materials, transition metals are of interest because they represent an important family of elements that are proven to be useful as thermo-electric, magnetic semiconductor, superconductors, sensors and photovoltaics [28].

1.4.1 Nanoparticles

Nanoparticles (NPs) are defined as particles with a diameter smaller than 100 nm. They are increasingly used in different applications, including drug carrier systems and to pass organ barriers such as the blood-brain barrier. Nanoparticles are typically very small pieces of material that can be measured by a few atoms across. They are small enough that they can

easily interact on the same level with macroscopic pathogens such as bacteria and viruses [29].

Nanoparticles have surfaces that are easily modified, a small size, large surface area to volume ratio, are highly reactive to the living cells, stable over high temperatures and can undergo translocation into the cells [30]. Nanoparticles also display unique optical properties, making them capable of producing the quantum effects suitable for imaging applications [31, 32]. The properties of bulk materials change when they are reduced to nanoparticles. This is due to nanoparticles having a greater surface area per weight than the larger particle thus this causes the nanoparticles to be more reactive when they react with other molecules [33].

1.4.1.1 A brief history of nanoparticles

Nanoparticles have been around for centuries, this is evident from the presence of gold nanoparticles from the sculptures and paintings even before the 4th century AD (*anno domini*). The most famous example is the Lycurgus cup (fourth century AD) in **Figure 1.3**. Gold and silver nanoparticles are found in the windows of old cathedrals that were built in the middle ages [34].

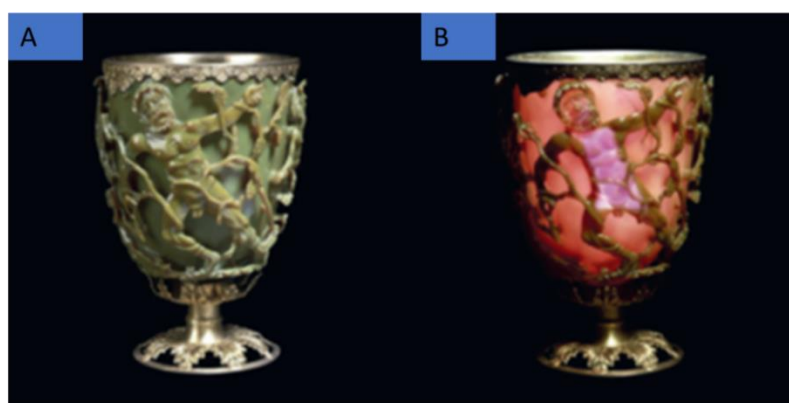


Figure 1.3: Photographs of the famous Lycurgus cup which displays a different colour depending on whether it is illuminated, externally A or internally B, colour changes depend on the size and shape of gold and silver nanoparticles [34].

Since the 1990's the nanomaterial field has grown as a research field. The oldest gold nanoparticle synthesis was reported as early as the 19th century [35, 36], and the recent interest now is focusing on the miniaturization of electronic devices to nanometer scale. It has been established that the properties of nanoparticles such as melting point and the band gap of a semiconductor are dependent on the size of a crystal, thus the nanometer material does not share the same properties as bulk material based on two factors that are responsible for this phenomenon, namely surface area and quantum size effects of the crystal [37].

Although the nanocrystals can be very small, a large fraction of the atoms are present on their surface. Thermodynamic properties of the material are affected by the surface atoms that have a contribution of free energy and the density of the electronic energy is transformed. This is known as a quantum size effect. This can affect the excited state in the material, although it increases the size of the energy spacing between the states. Thus, the optical excitations and the electrical transport properties are affected by the metal size and the semiconducting material [38].

Carbon nanotubes were first discovered in the 1990's with their unique properties (mechanical, thermal and electrical) which make them easily used to fabricate composites [39]. Carbon nanotubes form closed tubular structures consisting of a nested cylindrical graphitic layer sometimes capped with fullerene-like ends with a hollow internal cavity. Nanotubes consist of either one cylindrical graphene sheet i.e. single wall (SWNT), or several nested cylinders with an interlayer spacing of 0.34–0.40 nm, termed multi wall nanotube (MWNT). The discovery of nanotubes has revolutionised research in several directions. Light or high strength nanotubes are considered to be an ideal structure for designing nanostructured instruments [40].

1.4.2 Different methods of synthesizing nanoparticles

Nanoparticles synthesis can be achieved using materials of various chemical nature, such as biomolecules, carbon, metals, metal oxide, non-oxide ceramics, organics, polymers and silicates. Nanoparticles exist with greatly different morphology such as spheres, cylinders, platelets and tubes. Nanoparticles are generally designed in such a way that their surfaces can be modified to meet the needs of specific applications.

The enormous diversity of the nanoparticles are arising from their wide chemical nature, shape and morphologies, the medium in which the particles are present, the state of dispersion of the particles and most importantly the numerous possible surface modifications the nanoparticles can be subjected to make this an important active field of science now-a-days [41]. The same chemical can generate a wide variety of nanoparticles [42]. The composition of nanoscale structures and other devices can be achieved *via* bottom up and top down methods.

1.4.2.1 Bottom-up (chemical approach)

Small building blocks are assembled to prepare a large structure in the bottom up approach. A few examples of this method are chemical synthesis, laser induced assemblies (laser trapping), self-assembly and colloidal-aggregation. Eventually, physical limits may be included such as perturbations, e.g. molecular vibrations that can influence the smallest of the nanoscopic structures. Since in the bottom up approach molecular components arrange themselves to become more complex assemblies, the concept of molecular self-assembly is being used. An example of a bottom up approach that is mostly used to synthesize nanoparticles is a colloidal dispersion. Although a bottom up and a top down approach may seem to be approaches that are opposite, there is an approach where both techniques are utilized it is known as a hybrid approach. Lithography is an example (of a hybrid approach) in which the thin films that are growing refers to a bottom up approach and etching refers to a top down approach [43].

1.4.2.2 Top-down (physical approach)

In top down synthesis, large scale production is limited. In this approach the nanoparticles become reactive after they are being processed and they have a high surface energy which is decreased by adsorption or agglomeration of a certain species, hence some additional reaction occurs. During the synthesis of nanoparticles specific materials are being used up to coat the nanomaterials and this controls a further interaction with other particles. High-energy mechanical milling is used to synthesize metal-ceramic composite powders that allow the metal and the ceramic phases to unite in the same particle. A suitable precursor is chosen to produce a nanoparticle of a particular material [44].

Large objects are modified to compose smaller features in the top down method such as lithography techniques, e.g. ultraviolet (UV), electron or ion beam, scanning probe, optical near field, film deposition and growth, laser beam processing and mechanical techniques, e.g. machining, polishing and grinding [45].

1.4.3 Nanoparticles in medicine

Recently, there has been an exponential growth in the use of nanoparticles in biomedical research [31]. The use of nanoparticles in nanomedicine will radically change the way we approach diagnosis and therapy of diseases states such as cancer and others, since they possess the ability to overcome the shortcomings that are presented by traditional drugs such as drug resistance at the cellular level, distribution, clearance of anticancer drugs in the body, drug resistance at the tumour level due to physiological barriers and biotransformation [46].

Important properties of nanoparticles in the development of radiopharmaceuticals include particle size, dispersity, shape, surface, crystallinity and composition. The nanoparticle's ability to penetrate biological membranes, accessibility to remote tissues and increased residence time in the body offer a more diverse portfolio of treatment options and improve efficacy through both local and systemic targeting [46]. The size of nanoparticle controls its interactions with biological systems, this includes absorption distribution, cellular internalisation, metabolism and excretion of nanoparticles from the body [47].

Nanoparticles with a diameter of 50 nm are more efficiently internalized by cells than smaller (15–30 nm) or larger particles (70–240 nm) [48]. Nanoparticles with a diameter of 30–50 nm efficiently interact with membrane receptors and are subsequently taken up by receptor-mediated endocytosis [49]. Nanoparticles with sizes around 400 nm is the upper boundary for harnessing the effect of EPR [50]. Particles with diameters less than 200 nm will be cleared much less rapidly than particles with diameters over 200 nm. Varying particle sizes of 50 nm and above showed higher levels of agglomeration of the larger nanoparticles in the liver [51]. Therefore, to be an effective drug carrier, the nanoparticle should have a diameter of 10–150 nm. This size range will ensure longer circulation time and increased accumulation in the tumour interstitial [52].

1.4.3.1 Nanomedicine

Cancer nanotherapeutics is progressing at a steady rate; research and development in this field has experienced an exponential growth since the early 2000's [53]. Although the path to a successful cancer drug is still long to be discovered, there is considerable excitement that nanotechnologies may contribute to the success of the oncology drug development. The pace at which pharmaceutical companies have formed partnerships to use proprietary nanoparticle technologies has accelerated considerably. It is now recognized that by enhancing the efficacy of new drug candidates, nanotechnology can meaningfully contribute to create differentiated products and improved clinical outcome [54].

More than 40 years ago, the foundation was established for nanotechnologies to deliver therapeutic and diagnostic agents in a safer and more efficient manner [55]. Achieving this nanotechnology vision of delivering therapeutic and diagnostic agents became more realistic in recent years, with increasing numbers of nanotherapeutics and nanodiagnostics having reached the clinical stage. In 2010, the first clinical evidence of gene silencing was obtained by systemically-administered targeted nanoparticles (NPs) delivering siRNA therapeutics [56].

Nanoparticles offer the possibility to encapsulate poorly soluble drugs [57], protect therapeutic molecules [58], and modify their blood circulation and tissue distribution profiles

[48, 55]. These properties are attractive in oncology to encapsulate drugs exhibiting wide-ranging toxicities and physicochemical properties. The parameters governing effective passive transport and retention of NPs in tumours hold through actively-targeted NPs which are decorated with ligands [59]. The active-targeted NPs recently made its way to human clinical trials, a prominent clinical example of an active targeting ligand, is a transferrin (Tf), glycoprotein responsible for delivering iron to cells. The transferrin receptor (TfR) is highly expressed on the surface of many cancer cells [60], therefore incorporation of Tf in nanoparticle formulations allows for preferential uptake. Nanoparticles are also tailorable such that they can be synthesized to bind and stabilize difficult-to-formulate hydrophobic drugs.

Several nanoparticle-based drugs have moved into clinical trials [61]. Two well-known passively targeted nanoparticle therapies are Doxil and Abraxane. Doxil is a liposomal drug containing doxorubicin and Abraxane is a formulation of paclitaxel and albumin. The nanoparticles help to improve the solubility of the chemotherapeutics, allowing them to remain in circulation longer, while ameliorating some of the adverse side-effects of the free drugs [62]. While Doxil has been approved for treatment of ovarian cancer, recent clinical trials have been focused on combinational therapies, with efficacy seen when Doxil is combined with panitumumab to treat platinum-resistant epithelial ovarian cancer [63]. Abraxane is currently used to treat metastatic breast cancer [64] and ovarian cancer [65], and is finding clinical success against pancreatic cancer [66], non-small cell lung carcinoma [67] and drug resistant metastatic cervical cancer [68]. Camptothecin is most efficacious when applied continuously to the tumour cells; however, prolonged exposure is associated with severe bone marrow suppression and hemorrhagic cystitis. Incorporation of camptothecin into polymeric nanoparticles improved delivery to solid tumour cells and was well tolerated in patients, with stable disease reported in 64% of patients [69].

Understanding the biological processes involved in the distribution and retention of nanomaterials inside the tumours is therefore essential to the development of personalized

nanomedicine approaches. The concepts apply to therapeutic nanomaterials in general, whether its drug carriers or nanoparticulate therapy mediators responding to external stimuli to exert therapeutic effects such as light [70], magnetic field [71] or ultrasounds [72].

1.4.3.2 Nanoradiopharmaceuticals

The application of nanotechnology in medicine has been extended to radiopharmaceuticals. In this direction, a novel and promising science called nanoradiopharmaceuticals (NRPs) has been developed. Nanoradiopharmaceuticals are radiolabelled nanomaterials designed to deliver therapeutic doses of ionizing radiation to specific cancerous sites with high specificity in the body. These are already in clinical tests [73]. There are two possible approaches that are used to synthesize nanoradiopharmaceuticals. They can be prepared through direct nano-encapsulation of radioactive radiopharmaceuticals. The second approach involves direct radiolabelling of nanoparticles coated with a non-radioactive ligand by a radioisotope.

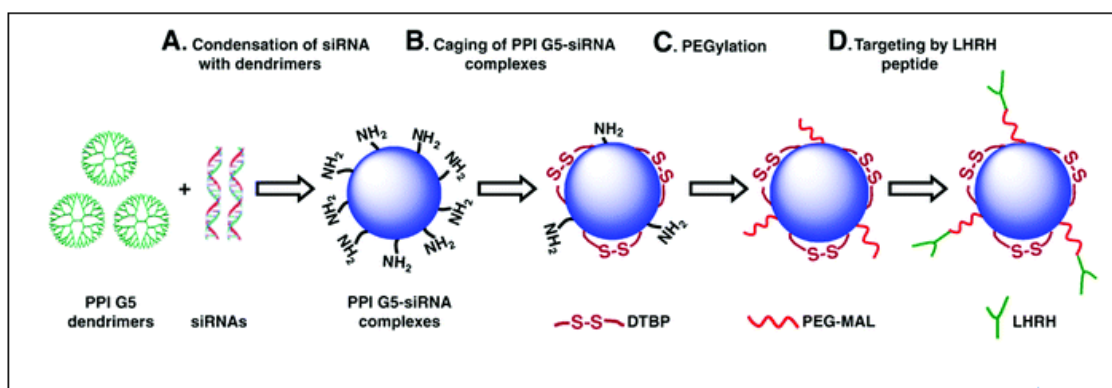


Figure 1.4: Engineered approach for prepared of tumour targeted stable nanoparticles for the siRNA delivery [74].

Trau *et al.* [74] reported the synthesis of nano-encapsulated microcrystalline nanoparticles for super-amplified biochemical assays (**Figure 1.4**). The radiolabelled molecules were encapsulated within ultra-thin polyelectrolyte layers of poly(allylamine hydrochloride) and poly(sodium 4-styrenesulfonate) that are functionalized with targeting molecules and are released in the tumour site [74].

Nanoparticles have been successfully radiolabelled with both α -emitters, e.g. ^{211}At and ^{225}Ac and β -emitters (e.g. ^{90}Y , ^{67}Cu , ^{131}I , ^{186}Re , and ^{188}Re) [75]. Hong and other co-workers reported the synthesis of radiolabelled iron oxide nanoparticles which have been designed for use in SPECT/MRI and PET/MRI dual techniques. Both these approaches yield the nanoradiopharmaceuticals [76].

1.4.3.3 Rhenium nanomaterials

Even though molecular imaging techniques have advanced, there is no single technique that is ideal to acquire all the required information for experimental questions [76]. For example, there are drawbacks associated with quantifying fluorescence signals in biological systems, specifically in deep tissues; magnetic resonance imaging (MRI) has a very high resolution but it has low sensitivity; and radionuclide-based imaging methods possess high sensitivity yet they suffer from poor resolution [77]. The combination of various molecular imaging techniques can be advantageous compared to a single technique.

Rhenium stands as a good candidate for nanoradiopharmaceuticals because of its good nuclear properties, physical half-life, and decay characteristics. Despite the plethora of literature available on the synthesis of metal oxide nanoparticles, little is known about rhenium oxide nanoparticles. Re_2O_7 based nanostructures that are immobilized within Al_2O_3 and SiO_2 have been synthesized for catalytic purposes [78]. Pawlak *et al.* reported on the synthesis of Re_2S_7 nanostructures, which have the potential to be applied in nuclear medicine [79].

Most of the literature reports on the synthesis of rhenium nanoparticles from various precursors, using different approaches that do not employ sodium borohydride reduction processes. However, the synthesis of rhenium oxide nanoparticles from perrhenate (ReO_4^-) ion using sodium borohydride as the reducing agent has been reported for catalytic applications [80]. The synthesis of transition metal nanostructures and their oxides has been widely explored due to their fascinating physical and chemical properties. Diverse methodologies for

the synthesis of transition metal nanoparticles such as gold [81], platinum [82], rhodium [83], silver [84] and palladium [85] as well as metal oxide nanoparticles [86] have been reported.

The applications of these nanomaterials in different areas such as optics, electronics, catalysis, and medicine have been broadly studied and they show promising results. Rhenium, being part of the transition metals group, has gained significant attention as it poses a unique combination of properties that position it as a high-performance engineering material. A few examples of rhenium-incorporating nanoradiopharmaceuticals have emerged in the literature. Azadbakht and co-workers have studied rhenium-188 labelled with silane-polyethylene glycol that was coated with iron oxide nanoparticles, and the therapeutic effect and targeting efficacy were evaluated [87, 88].

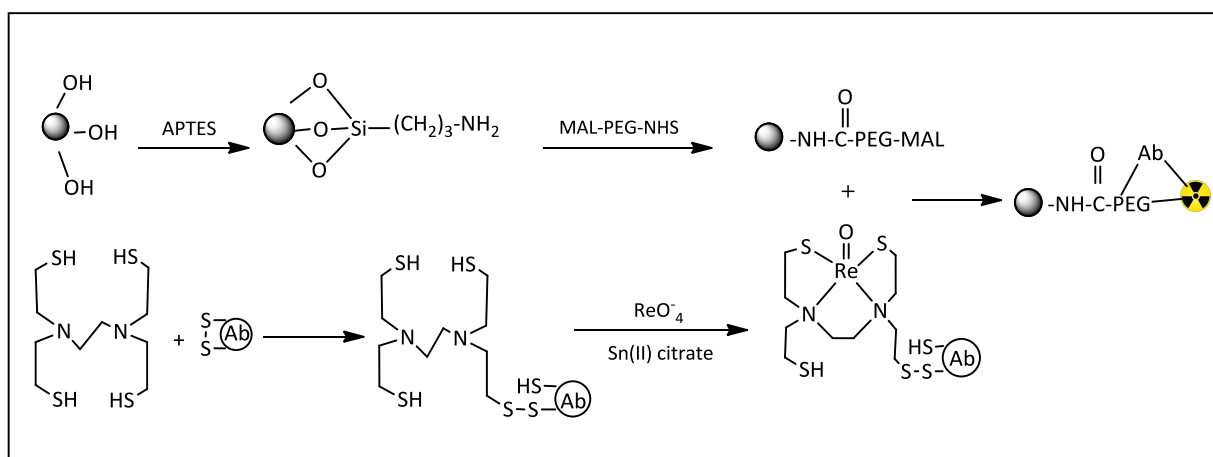


Figure 1.5: APTES-PEG coated iron oxide nanoparticles conjugated to rhenium ^{188}Re labelled rituximab [88].

Rhenium and technetium with poly(pyrazolyl)borates have been extensively studied by several research groups, allowing the introduction of a great variety of oxo, carbonyl and polyhydride complexes but these compounds were difficult to obtain under the conditions required for the preparation of materials [21]. Anantharaj and co-workers synthesized ultra-small rhenium nanoparticles that were immobilised on DNA scaffolds and this material was used for surface enhanced Raman scattering and catalysis studies [89]. Rojas and Castano have achieved their

milestone of synthesising rhenium nanoparticles in the form of Re_xO_y by gamma irradiation [90].

1.5 Capping agents: Phthalocyanines versus diamines

1.5.1 Phthalocyanines (Pcs)

Phthalocyanines (**Figure 1.6**) are classified as aromatic macrocyclic compounds with 18 p -electron cloud delocalised over an arrangement of staggered carbon and nitrogen atoms with tetrapyrrole rings [91]. Phthalocyanine forms upon heating various phthalic acid derivatives containing nitrogenous functional groups, e.g. phthalonitriles and diiminoisoindole [92, 93]. Interestingly, phthalocyanines are analogues of naturally occurring porphyrins and other compounds like chlorins. Pcs have a very wide range of usage in many different fields such as in producing inks, dyes, pigments and in laser technology [94].

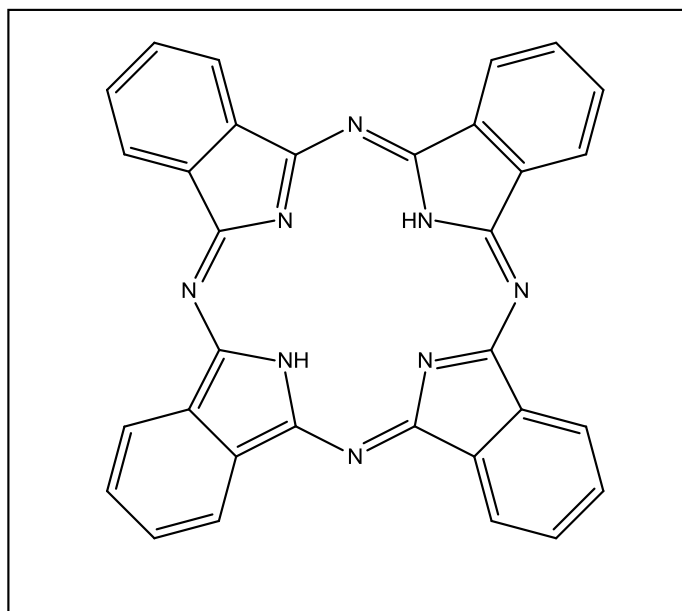


Figure 1.6: Chemical structure of phthalocyanine.

Phthalocyanine derivatives are currently under investigation for use in photodynamic therapy, which is a promising cancer treatment. These compounds display favourable uptake in cancerous cells and present high fluorescence yields that can be used for tumour detection [95]. The Pcs have also attracted many applications because of their redox flexibility, stability towards thermal-chemical conditions and intense colour. However, their poor solubility in

industrial organic solvents causes problems for different type of applications; and because of this reason improvement on the synthesis of soluble phthalocyanine derivatives is still an important task [95,96]. The solubility of Pcs can be increased by using substituents such as alkyl, alkoxy, aryloxy, and alkylthio chains and bulky groups [96]. These Pcs have intense absorptions at long wavelengths (above 670 nm) and an extraordinary ability for generating singlet oxygen with good yields.

The major disadvantage of the Pcs in technological applications is intermolecular interactions, known as aggregation, between Pc macrocycles. Therefore, many structural modifications, such as modifying of the position and type of substituents have been made to prevent the aggregation of Pcs. Bulky substituents prevent the planar Pc rings from approaching each other [97–99]. In this application, an aminated Pc will be attached to the particle as a capping agent and conjugated to folate as a targeting biomolecule.

1.5.2 Ethylenediamine (EDA)

Ethylenediamine is an organic compound, known to act as a bidentate ligand in complexing with metals. This colourless sticky liquid is widely used in chemical synthesis. Ethylenediamine is manufactured industrially from 1,2-dichloroethane or ethanolamine and ammonia under high pressure at 180°C in an aqueous medium [100].

Mono-functionalisation of symmetrical or unsymmetrical diamines is an essential step for the synthesis of biologically important pharmacores and materials [101]. Recently there is more interest on chemical and biological chip production of monofunctionalised diamines to hold functional molecules at the one end while the other end is free to be attached on the solid surface of the nanoparticle [102]. Therefore, a facile and large-scale synthetic method is urgent for the preparation of a monoprotected diamine [103, 104].

Ethylenediamine is used in different fields such as: as a precursor to chelation agents, drugs, agrochemicals. A most prominent derivative of ethylene diamine is the chelating agent,

ethylenediaminetetraacetic acid [100]. It is a pharmaceutical ingredient in the most common bronchodilator drugs [105]. It also plays an important role in the production of polymers [106]. In this study, a folate-conjugated diamine will be used to cap the rhenium oxide nanoparticles.

1.6 Targeting biomolecules

1.6.1 Folate (FA)

Folic acid is known as pteroylglutamic acid with the chemical formula of $C_{19}H_{19}N_7O_6$ (**Figure 1.7**). Folate (pteroylglutamate) is a stable, water-soluble, inexpensive, and non-immunogenic chemical, and has a high affinity for cell surface folate receptor [107, 108].

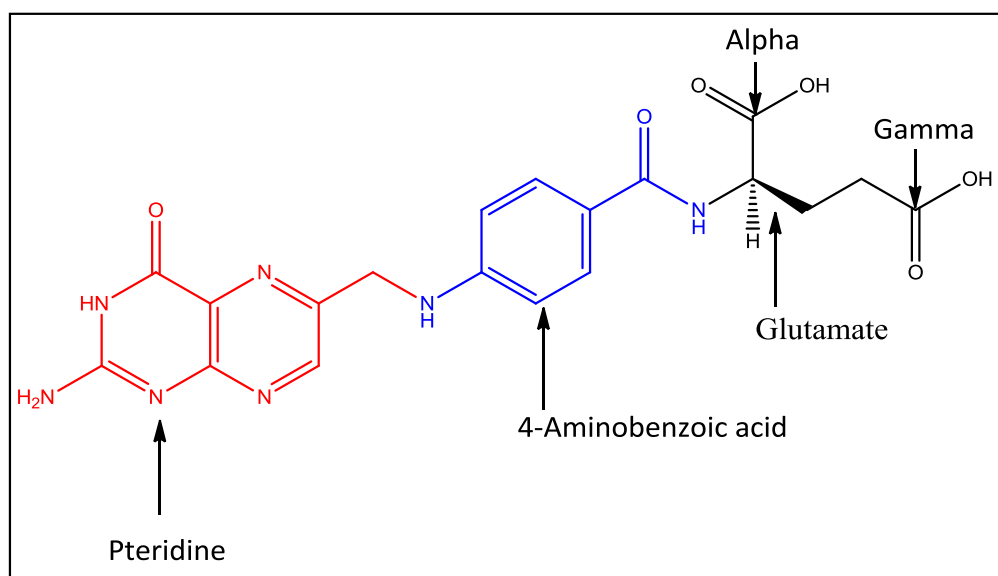


Figure 1.7: The structure of folate showing the pteridine ring (red), 4-aminobenzoate (blue) and the glutamate (black).

Folic acid is an important vitamin required for the healthy functioning of all cells. Folate is necessary for the DNA nucleotide synthesis and cell division. Folic acid is known to bind with a folate receptor existing on the surface of tumoural cells. Rapidly dividing cells require much more folate than a healthy cell. The deficiency of folate include fetal neural tube defects, cardiovascular disease and cancers [109, 110], hence it can be exploited for targeting cancer cells.

Folate antagonists are folate analogs that inhibit vitamin B9 (folic acid) cellular uptake, *via* widely expressed membrane transporters. Folate receptors (FRs) transport folate *via* endocytosis with high affinity and are proposed targets for the specific delivery of new classes of folate conjugates to tumours. There are specific antifolates that have been developed namely, pemetrexed, aminopterin, and methotrexate. They are commonly used since they have similar structures to that of folate [111].

Although all cells express the folate receptor for normal DNA replication and cell division, however cancerous cells express a much greater amount of folate receptors. Cancer cells overexpress the folate receptor as a result, the high affinity of folic acid for folate receptors provides a unique opportunity to use it as a targeting ligand to deliver nanoparticles to cancer cells [112]. Because of the low expression level of folate receptors in healthy cells and its overexpression in cancerous tissues, folate behaves as a suitable targeting biomolecule.

The folate receptor is upregulated in many human cancers, to name a few malignancies of the ovary, brain, kidney, breast, myeloid cells and lung. The ability of folate to access these folate receptor locations can be limited due to the apical membrane of polarised epithelia and the density of folate receptor that appears to increase as the stage of cancer worsens [113].

1.7 Scope of the study

The key to the development of nanoradiopharmaceuticals is selective localisation of the compounds to the cancerous sites. Therefore, the primary aim of this study was to design new radiopharmaceuticals based on the rhenium-nuclide. In this case, the size of the nanoparticles will be exploited due to enhanced permeation and retention effect (EPR effect) as well as the incorporation of folate for targeting. The hot isotopes of rhenium would be used at a later stage to fully assess the behaviour of nanoparticles in some biological systems for diagnosis and therapy of cancer tumours.

The aim of the study was addressed by completing the following objectives:

- Synthesis of diamines and phthalocyanine linked with folate for stabilisation and making nanoparticles recognisable by cells through folate receptors.

- The synthesis and characterization of the rhenium(III) oxide nanoparticles.
- The viability studies using non-tumourigenic and cancerous cells to investigate the effects of the nanoparticles at non-cytotoxic concentrations.
- The investigation of tumour internalisation ability of the Re_2O_3 -diamine-folate NPs using the *in vitro* model (cancer cell lines).

Due to the nature of the treatise, the investigation of the localisation of nanoparticles on cancer cells by TEM is currently being done as part of the bigger scope of the project. This mini thesis will present work achieved up to cell viability studies.

Chapter 2 : Materials, techniques and experimental methods

2.1 General reagents for synthesis

Table 2.1 provides the list of reagents used in the study as well as their purity and suppliers.

Table 2.1: General reagents used in this study.

Chemical name	% Purity	Supplier
Acetic acid	Glacial	Sigma-Aldrich
Acetone	98.0	Merck-Chemicals
Ammonium perrhenate	99.0	Sigma-Aldrich
1,8-diazabicyclo [5.4.0] undec-7-ene	98.0	Sigma-Aldrich
Diethyl ether	99.0	Merck-Chemicals
Dichloromethane	99.0	Merck-Chemicals
Dimethyl formamide	99.5	ACE Chemicals
Dimethyl sulfoxide	99.0	Merck-Chemicals
Ethyl acetate	98.8	Sigma-Aldrich
Ethylenediamine	80.0	Sigma-Aldrich
Folic acid	97.0	Sigma-Aldrich
Hexane	97.0	Merck-Chemicals
Hydrochloric acid	32.0	Sigma-Aldrich
Methanol	Analytical grade	Sigma-Aldrich
<i>N</i> -Boc-Ethylene diamine	99.9	Sigma-Aldrich
<i>N</i> -Hydroxysuccinimide	98.0	Sigma-Aldrich
<i>N,N'</i> -Dicyclohexylcarbodiimide	99.0	Fluka
<i>N,N'</i> -Dimethyl formamide	99.9	Sigma-Aldrich
4-Nitrophthalonitrile	99.9	Fluoro-Chem
<i>n</i> -Octanol	99.0	Sigma-Aldrich
Pyridine	90.0	Merck-Chemicals
Pyridine-HCl	98.0	Alfar-Aesar
Triethylamine	99.0	Merck-Chemicals
Trifluoro acetic acid	99.0	Riedel-dehaen
Sodium acetate	99.0	ACE Chemicals
Sodium borohydride	98.0	Sigma-Aldrich
Sodium chloride	99.5	ACE chemicals
Sodium sulphide hydrate	98.0	Sigma-Aldrich
Zinc(III) chloride	98.0	Sigma-Aldrich

Table 2.2: Reagents used for biological studies

Chemical name	% Purity	Supplier
Leibovitz's L15 medium	-	Gibco
Dulbecco modified eagle medium	-	Biowest
Fetal bovine serum	-	Biowest
Trypsin	-	Sigma-Aldrich
Potassium chloride	99.0	Sigma-Aldrich
Disodium phosphate	98.0	Sigma-Aldrich
Monopotassium phosphate	99.5	Sigma-Aldrich
Ethylenediaminetetraacetic	99.9	Sigma-Aldrich
3-(4,5-Dimethylthiazol-2-yl)-2,5-diphenyltetrazolium bromide	-	Sigma-Aldrich
Ham's F12 medium	-	Biowest
Insulin	-	Gibco
Hydrocortisone	-	Sigma-Aldrich

2.2 Instrumentation

2.2.1 Spectroscopic techniques

2.2.1.1 Nuclear magnetic resonance (NMR spectroscopy)

The capping agents and products were determined by using ^1H NMR and ^{13}C NMR spectroscopy on a Bruker AMX 400 MHz spectrometer and reported relative to tetramethylsilane (δ 0.00).

2.2.1.2 Infrared spectroscopy

The infrared spectra were recorded on a Bruker, Tensor 27 platinum ATR-FTIR spectrophotometer in the range 4000–400 cm^{-1} .

2.2.1.3 UV-Vis electronic spectroscopy

The absorption spectra of the phthalocyanine derivatives were recorded on a Thermo Scientific UV-Vis spectrophotometer using a 1 cm quartz cells. The spectra were recorded in the wavelength range between 300–900 nm using DMSO as a solvent. Absorption spectra of

rhenium(III) oxide nanoparticles were also recorded using the same instrument settings but in an aqueous medium.

2.2.1.4 Spectrofluorimetry

The excitation and emission spectra of the nanoparticles were measured with a Perkin Elmer LS45 Fluorescence spectrometer. The nanoparticles were excited at a wavelength of 331 nm.

2.2.1.5 Powerwave spectrophotometer (Biotek)

The Biotek Epoch|2 powerwave microplate reader spectrophotometer is a single channel absorbance microplate reader that has a capability of measuring absorbance after counting the cells on the microscope using a Haemocytometer. This monochromator-based instrument has a wavelength range of 200–999 nm.

2.2.1.6 LC-MS

Conjugating tetraaminophthalocyanine and ethylenediamine with folate was confirmed with the use of Water Synapt G2 liquid chromatography-mass spectroscopy using methanol as a solvent at 15 V.

2.2.2 Transmission electron microscopy (TEM)

TEM images of the rhenium nanoparticles were acquired with a Zeiss Libra 120 transmission electron microscope equipped with an EDAX detector and Gatan Crystorage. To prepare the samples, few drops of the nanoparticle suspension were placed on a 3 mm carbon-coated copper grid and left to dry at room temperature overnight. The images were captured using the embedded self-imaging system using a Mega-view III digital camera.

2.2.3 Zeta potential

Rhenium (III) oxide nanoparticles were confirmed using Zetasizer Nano ZS instrument (Malvern Instruments) that has a Direct Light Scattering (DLS) for measuring the size of the nanoparticles and the surface charge. The nanoparticles were prepared in freshly deionised water.

2.2.4 Other instruments

2.2.4.1 Melting point

The melting points of the compounds were determined with the Stuart Lasec SM|30 Melting point apparatus.

2.2.4.2 Centrifuge

Labofuse 200 Heraeus sepatech centrifuge was extensively used for phthalocyanine purification and for Biochemistry studies, to rapidly sediment cells into a pellet before they were sectioned to be viewed on the TEM for cell uptake.

2.2.4.3 Class 2 Microbiological safety cabinet

Bioflow-II (hood) Labiobic model 650 was used for cell culture studies.

2.2.4.4 Incubator

Thermo Electron Corporation Forma Direct Heat CO₂ Incubator 311 was used to grow and maintain cell cultures. *In vitro* cell cultures should mimic the *in vivo* environment therefore the incubator must maintain an optimal temperature (37°C), carbon dioxide (% CO₂ = 5%), and humidity (95%).

2.2.4.5 Microscope

Regular monitoring of cells is essential as it will provide a lot of information regarding cell growth and general health of culture.

2.3 Methodology

2.3.1 Synthesis *N*-boc-ethylenediamine-folate

According to the literature [114], functionalisation of the diamines at one end is required as biological application require monofunctionalised diamines so that they can hold functional molecules such as targeting biomolecule at one end, while the other end is free to be attached on the solid surface (nanoparticle). Among the various amine protecting groups, *tert*-butyloxycarbonyl (Boc) protecting group is extensively used due to its ability to protect one side with HCl and this protected form is the stable physical state can be used in subsequent reactions. The reaction scheme for preparation of ethylenediamine-folate are presented in **Figure 2.1**.

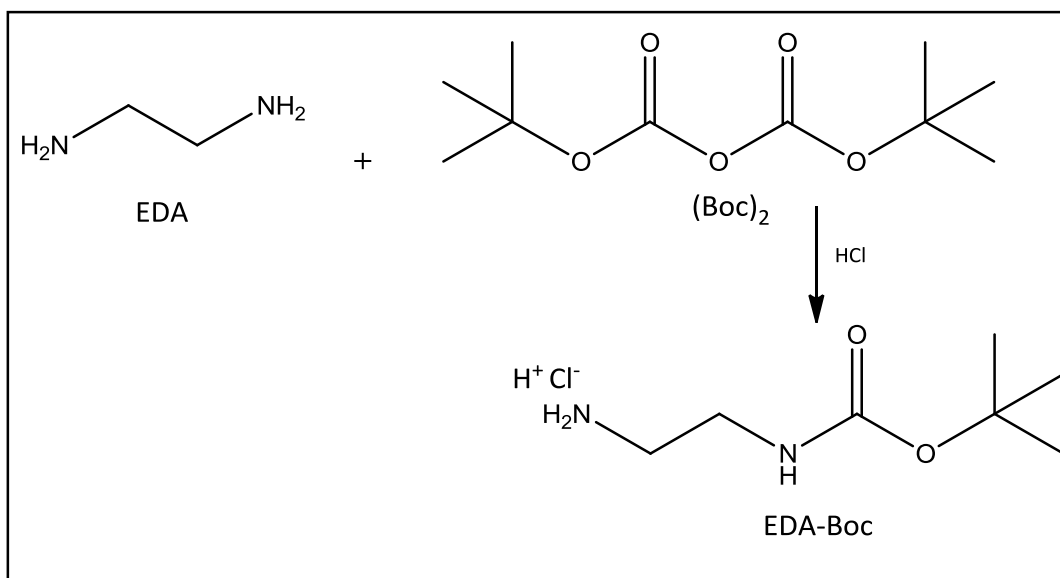


Figure 2.1: Proposed synthetic route of protecting one side of ethylenediamine with *tert*-butyloxycarbonyl protecting group.

2.3.1.1 *N*-Boc-ethylenediamine-folate (*N*-BOC-EDA-FA)

The protocol used for the conjugation of folate and ethylenediamine *via* amide bond formation was modified from Trindade [103] (**Figure 2.2**). Briefly, 640 mg of folic acid (1.34 mmol, 1 eq. dehydrated powder) was dissolved in 25 mL of DMSO for approximately 30 minutes with mild heating. To this 308 mg (2 eq.) of *N*-hydroxysuccinimide and 552 mg of

N,N'-dicyclohexylcarbodiimide were added successively. The reaction mixture was stirred for 16 hours at room temperature. The urea which contained unreacted starting material was filtered off. The solution was then added to 0.376 mL (2 eq.) of triethylamine followed by 429 mg (2 eq) of *N*-*boc*-ethylene diamine dissolved in 5 mL of DMSO. The mixture was left stirring overnight at room temperature. The solution was added to a mixture of 20% acetone in diethyl ether, enough to precipitate the product. The thin yellow precipitate was centrifuged and washed four times with acetone and two times with diethyl ether and dried under vacuum (0.56 g = 65.5% yield). Melting point = 292°C.

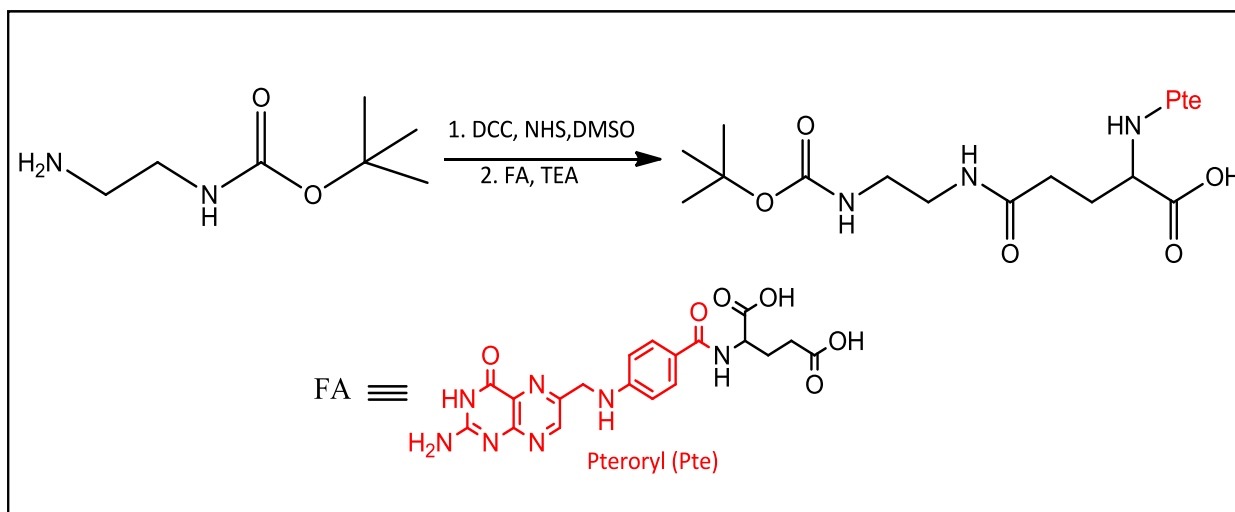


Figure 2.2: Synthetic route of ethylenediamine-folate conjugate

2.3.1.2 Synthesis of ethylenediamine-folate (EDA-FA) (deprotection step)

N-*Boc*-ethylenediamine-folate conjugate (**Figure 2.3**) (205 mg) was dissolved in 2 mL of trifluoroacetic acid (10 mM) and stirred for 2 hours. The solvent was removed under pressure with the aid of dichloromethane, the red residue was dissolved with a minimal amount of dry 5 mL of DMF and then 2 mL of triethylamine was added. The addition of triethylamine resulted in the precipitation of a yellow powder, which was washed and centrifuged four times with acetone and two times with diethyl ether (1.36 g = 80% yield). Melting point = 294.8°C.

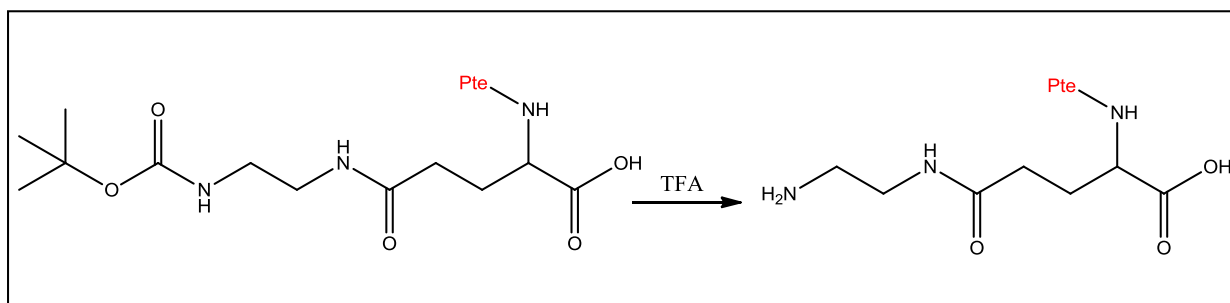


Figure 2.3: Synthetic route of deprotecting the *tert*-butyloxycarbonyl (BOC) protecting group.

2.3.2 Synthesis of Tetraamino-phthalocyanine (TAPc)

Tetraamino phthalocyanine (TAPc) was synthesised according to the method by Ogbodu and co-workers [115] which involves three steps: (i) synthesis of tetranitro-zinc-phthalocyanine (TNZnPc), (ii) reduction of tetranitro-zinc-phthalocyanine to tetraamino-zinc-phthalocyanine (TAZnPc); and (iii) removal of zinc(II) to form tetraamino phthalocyanine.

2.3.2.1 Tetranitro-zinc-phthalocyanine (TNZnPc)

The synthesis of TNZnPc was prepared according to the method by Ogbodu and the co-workers [115]. Zinc chloride (1.23 g, 7.42 mmol) and 4-nitrophthalonitrile (5.14 g, 29.7 mmol) were added to *n*-octanol (8 mL), and catalytic amounts of 1,8-diazabicyclo-[5.4.0]-undec-7-ene (DBU) (0.226 g, 1.485 mmol) was added into the reaction mixture (**Figure 2.4**). The reaction was allowed to proceed at 180°C for 4 hours. Thereafter, the reaction mixture was cooled and diluted with toluene (80 mL), and the precipitate that resulted was collected by centrifugation at 6400 rpm for 30 minutes. The solid was filtered and washed with 10 mL of toluene, water, MeOH/ether (1:9) and then EtOAc/hexane (2:1). The dark green precipitate was dried and weighed (3.85 g = yield of 68%). The melting point was measured with melting point apparatus, and it was observed that the phthalocyanine compounds are thermally very stable up to 500°C.

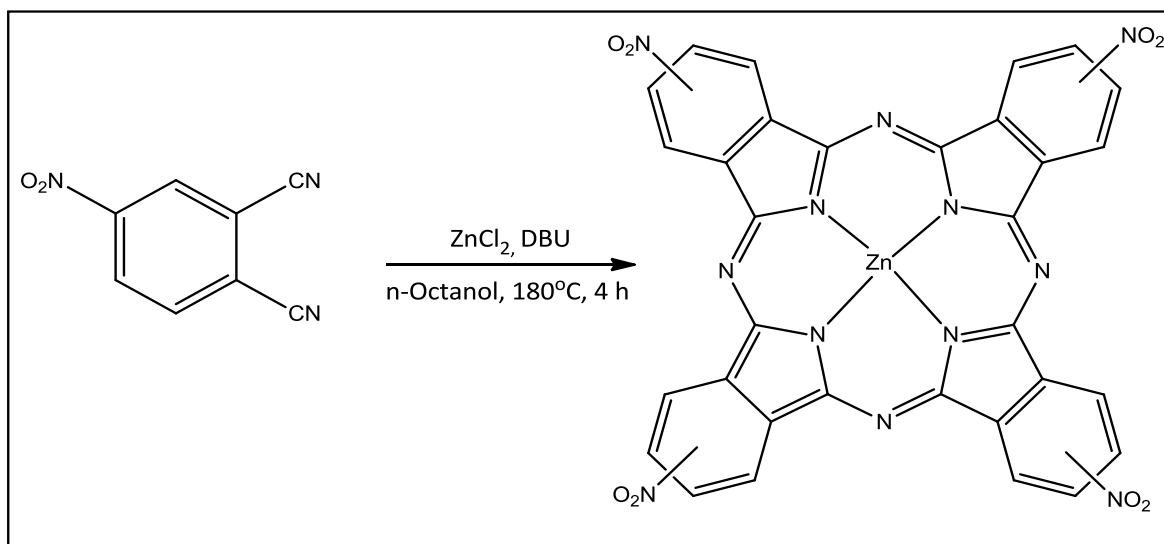


Figure 2.4: The synthesis of tetranitro-zinc-phthalocyanine (TNZnPc) from 4-phthalonitrile.

2.3.2.2 Tetraamino-zinc-phthalocyanine (TAZnPc)

TAZnPc was synthesised under a nitrogen atmosphere at 65°C by dissolving 4.08 g (5.35 mmol) of TNZnPc in 80 mL DMF, followed by addition of 15.88 g (66.1 mmol) of sodium sulfide hydrate. The reaction mixture was allowed to continue heating overnight, and then cooled to room temperature (**Figure 2.5**). Cold water (200 mL) was added and the resulting precipitate was collected by centrifugation at 6400 rpm for 30 minutes. The precipitate was washed three times with MeOH/ether (1:9), EtOAc and dried (1.968 g = 57% yield).

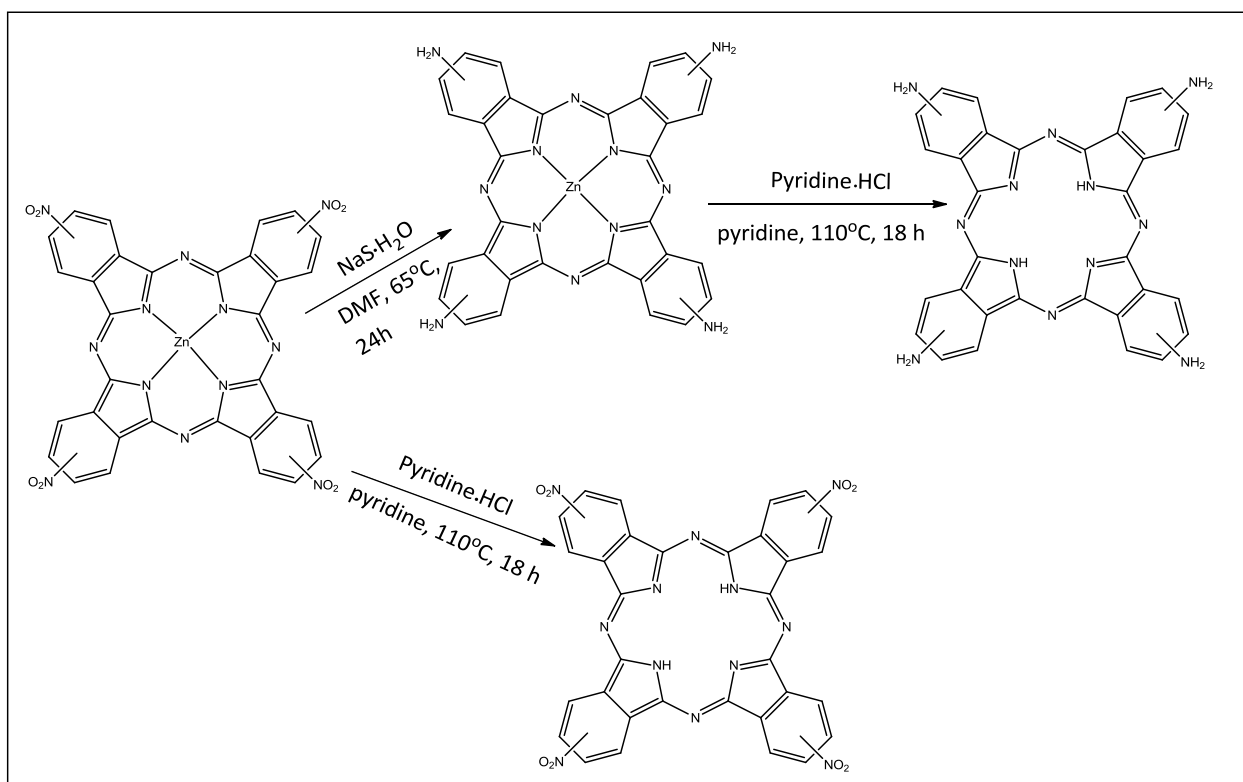


Figure 2.5: The synthesis of tetraaminophthalocyanine (TAPc) and tetranitrophthalocyanine (TNPC).

2.3.2.3 Tetraaminophthalocyanine (TAPc) and tetranitrophthalocyanine (TNPC).

The synthesis of TNPC was achieved by dissolving TNZnPc (0.65 g) in a mixture of pyridine (2 ml) and pyridine·HCl (1 g) while being stirred, under nitrogen, at 110°C for 18 hours. After the reaction run to completion, 10 ml of ice-cold H₂O was poured in the mixture. Centrifugation was used to collect the dark green precipitate at 6400 rpm for 30 minutes, followed by filtration and washing repeatedly with H₂O, MeOH and EtOAc. The tetranitrophthalocyanine was not used to conjugate to folate due to solubility challenges. TAZnPc was demetalated by dissolving 0.75 g in a solution of pyridine (4 mL) and pyridine·HCl (2 g) while being stirred, under nitrogen, at 110°C for 17 hours (**Figure 2.5**). The reaction was stopped, and 20 mL of H₂O was used to cool the mixture. Centrifugation was used to collect the dark green precipitate at 6400 rpm for 30 minutes, followed by filtration and washing three times with 15 mL of each of H₂O, MeOH and EtOAc (0.35 g = 50% yield).

2.3.2.4 Synthesis of TAPc-folate conjugate

The synthesis of folate-conjugated tetraaminophthalocyanine was performed according to a literature method [116], with minor adjustments. Briefly, 100 mg of folic acid (0.23 mmol) was added to 25 mL of H₂O and DMSO (1:9) and was stirred along with 70 mg *N,N'*-dicyclohexylcarbodiimide (DCC) and 39 mg *N*-hydroxysuccinimide (NHS) for 24 hours. A solution of 313 mg of TAPc (0.55 mmol) in DMSO was then added and the solution was stirred at room temperature for 48 hours (**Figure 2.6**). The solid precipitate was acquired through centrifugation at 7000 rpm for 10 minutes, and it was washed four times with 10 mL of acetone and two times with 10 mL of diethyl ether (0.25 g = 59.5% yield). The synthesis of folate-conjugated ethylenediamine was performed according to method.

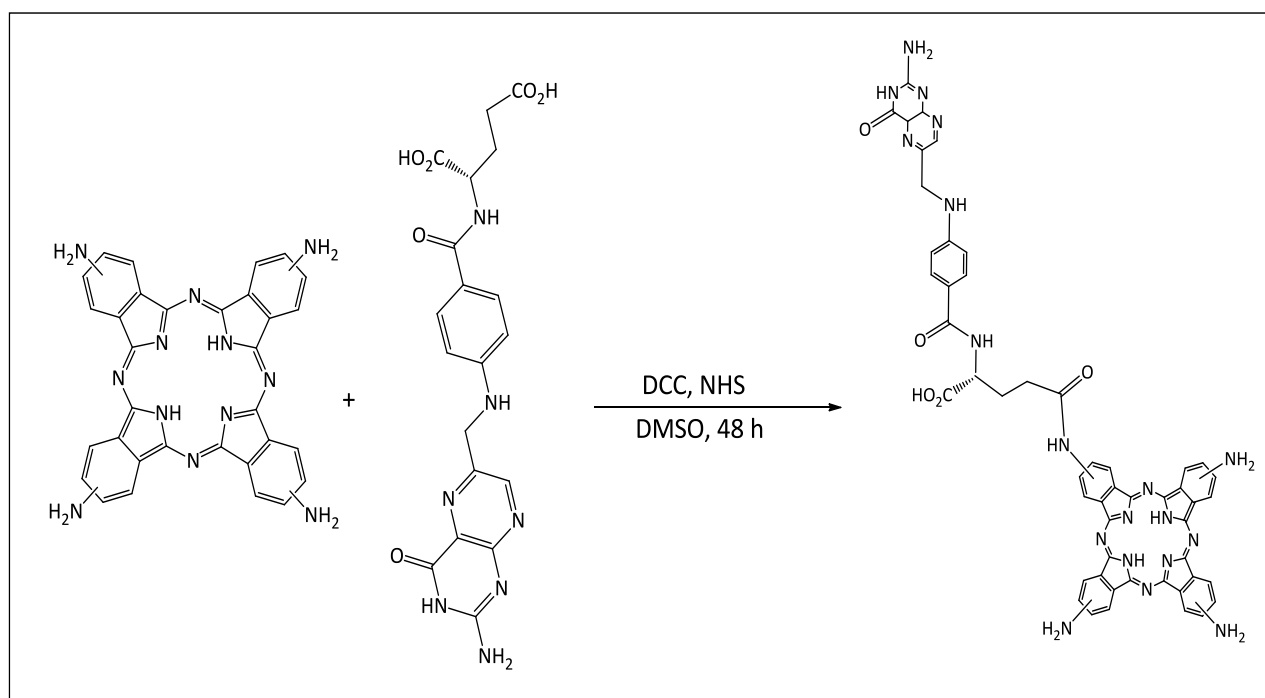


Figure 2.6: Conjugation of tetraaminophthalocyanine (TAPc) to folate, 1:1 ratio.

2.3.3 Synthesis of rhenium(III) oxide nanoparticles

The synthesis of rhenium(III) oxide nanoparticles followed a reported procedure [117] (**Figure 2.7**) with some modifications. In a typical synthesis of rhenium(III) oxide nanoparticles, 80 μ L of ammonium perrhenate (100 mM), 2 mL acetate buffer and 450 μ L deionized water were

mixed and stirred under nitrogen for 30 minutes at room temperature. After 30 minutes, 400 μL of freshly prepared NaBH_4 (100 Mm) was added drop wise to the reaction mixture over a period of a minute. After which, FA-TAPc solution in DMSO (10 mg/mL) was added slowly. The solution was further stirred for another 30 minutes under nitrogen (**Figure 2.8**).

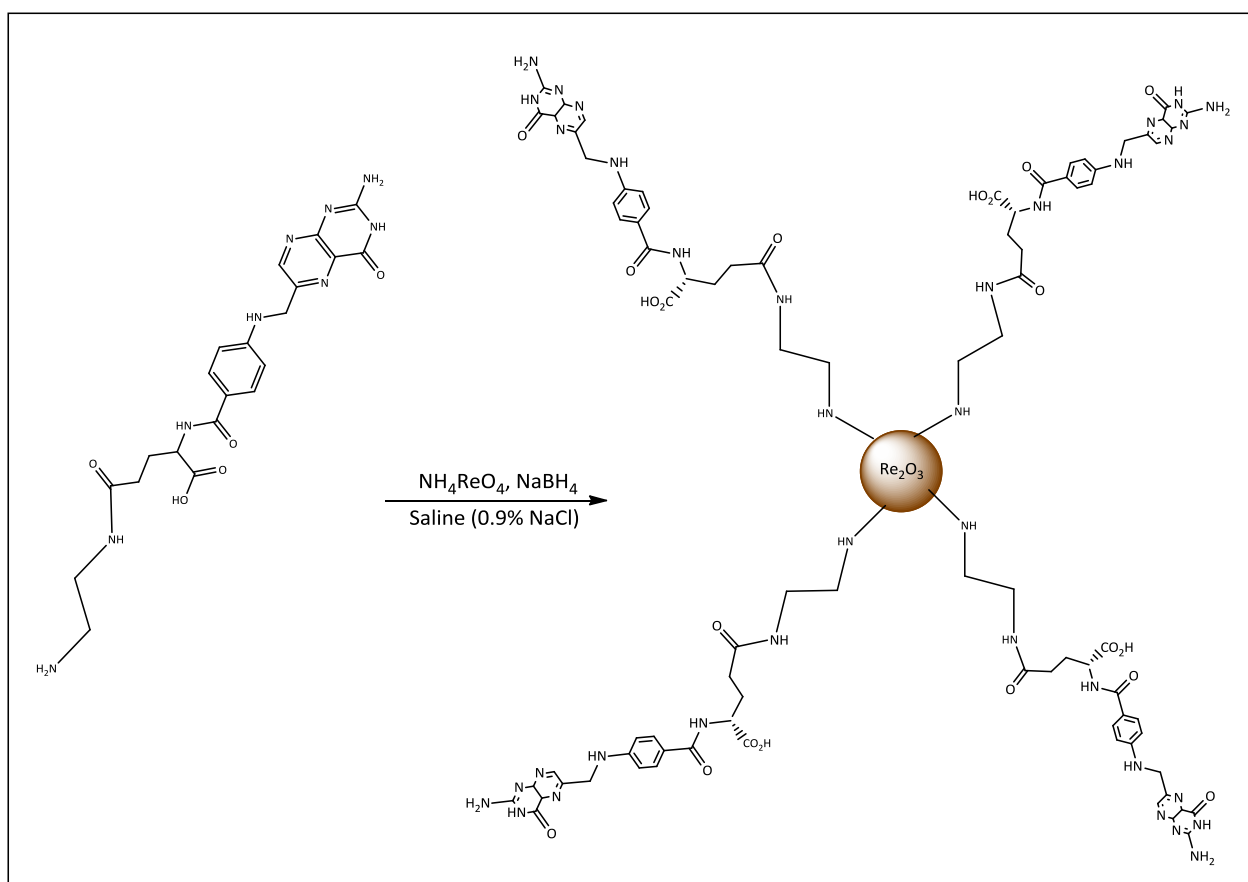


Figure 2.7: Synthetic route of capped rhenium (III) oxide nanoparticles with ethylenediamine-folate. Four capping agents are shown for simplicity.

The solution was then transferred to polyethylene tubes and centrifugated at 3500 rpm. The nanoparticles pellet was washed with deionised water. The NPs were kept in solution and prepared for TEM analysis. The rhenium(III) oxide nanoparticles production was optimised by controlling temperature, amount of capping agent, amount of reducing agent and concentration of rhenium salt. Refer to page 49 for quantification used for Re-EDA NP, Re-EDA-FA NP, Re-TAPc-FA NP, Re-TAPc NP and Re NP.

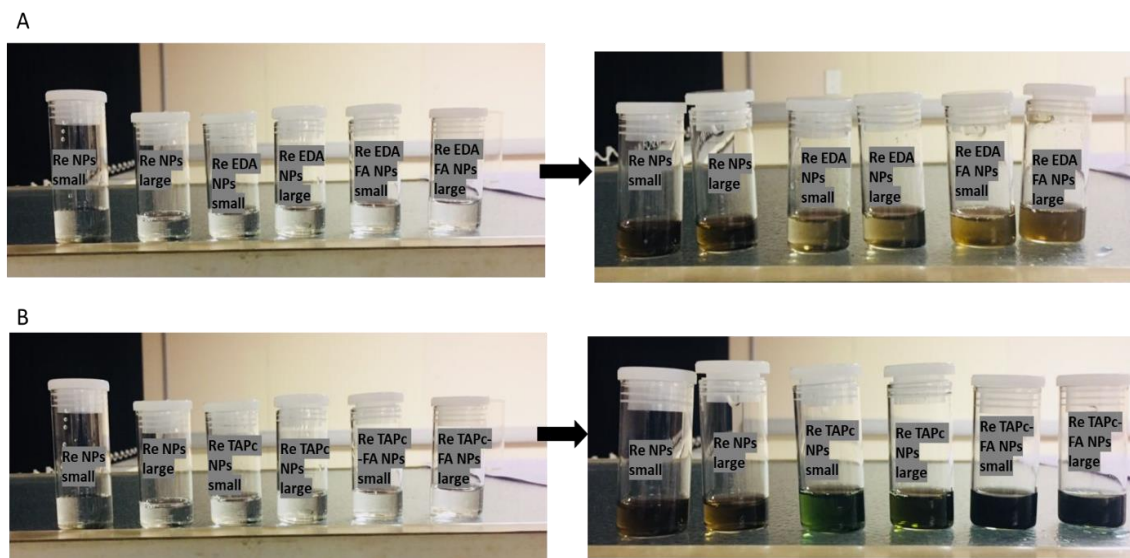


Figure 2.8: Photographs of the sample vials containing ammonium perrhenate in water (100 mM), (A) before and after adding ethylenediamine, ethylenediamine-folate (capping agents) and sodium borohydride (reducing agent), and (B) before and after adding tetraaminophthalocyanine, tetraaminophthalocyanine-folate (capping agents) and sodium borohydride (reducing agent).

2.3.4 Cell culture and maintenance

The cell lines used in this study were MCF-7, MCF-10A (non-tumourigenic), MDA-MB-231, and MDA-MB-468. MCF-7 cell lines were cultured in DMEM media supplemented with 10% (v/v) FBS, while MDA-MB-231 and MDA-MB-468 were cultured in L15 (Leibovitz) media supplemented with 10% (v/v) FBS and Hams F12 media supplemented with 5% v/v Donor horse serum, 20 $\mu\text{g}/\text{mL}$ EGF, 10 $\mu\text{g}/\text{mL}$ Insulin, 0.5 $\mu\text{g}/\text{mL}$ hydrocortisone was used for MCF-10A. The cells were grown in Thermo Electron Corporation Forma Direct Heat CO₂ incubator at 37°C with 5% CO₂. The cell monolayer was washed 2–3 times using PBS (pH 7.4) to remove media, free/unattached nanoparticles and cellular debris. PBS was prepared as follows: 400 mL of distilled water was prepared in a suitable container. A 4 g of NaCl (0.137 M), 100 mg of KCl (0.0027 M), 720 mg of Na₂HPO₄ (0.01 M) and 120 mg of KH₂PO₄ (0.0018 M) were added to the solution. The solution was adjusted to a pH \approx 7.4 using a pH meter. Then the solution was filled with distilled water up to 500 mL.

Table 2.3: Preparation of the media for cell culture:

Media	Reagents
DMEM	10% FBS
L15	10% FBS
F12	5% v/v Donor horse serum, 20 µg/mL EGF, 10 µg/mL Insulin, 0.5 µg/mL hydrocortisone

2.3.5 Cell viability assay

Cell viability assay were completed using the MTT Assay for the various treatments listed below in four different cell lines (MDA-MB-468, MDA-MB-231, MCF-10A, and MCF-7). Cell viability studies of the cells treated with rhenium(III) oxide nanoparticles were evaluated using MTT assay [118]. Firstly, cells were checked if they were contaminated using a microscope. Then the media was removed using vacuum aspirator and the cells were washed with PBSA. The cells were trypsinised with 300 µL of 0.25% (v/v) trypsin solution twice in order to detach cells from the surface of the plate. This was done by incubating the cells at 37°C for minimum time of 5–10 minutes. A media (5 mL) was added to re-suspend the cells, and small aliquot (20 µL) to count the cells using haemocytometer with the aid of trypan blue and were calculated using the following equation (1).

$$\text{Cell Viability (\%)} = \frac{\text{total viable cells (unstained)}}{\text{total cells (stained and unstained)}} \times 100 \quad (1)$$

The cells were seeded at 10,000 cells per well in a 96-well plate and allowed to attach for 24 hours. The cells were treated for 24 hours with different nanoparticle concentrations prepared from transferring 50 µL of 0.6 mM rhenium oxide nanoparticles to 3mL of cell culture media to yield 10 µM solutions. The treatments were varied to maintain the same concentration. Differently capped and sized nanoparticles were used. The controls used were; methotrexate (positive control) and untreated cells (negative control). The effects of simple compounds were investigated. These include folate (FA), tetraaminophthalocyanine (TAPc), and ethylenediamine (EDA). The effects of ethylenediamine-folate (EDA-FA) and tetraaminophthalocyanine-folate (TAPc-FA) conjugates were also investigated. The effects of

nanoparticles capped with sodium borohydride (Re NP), Re-EDA NP, Re-EDA-FA NP, Re-TAPc NP and Re-TAPC-FA NP were also compared. The effects of size were explored using small-sized nanoparticles (1–10 nm) and big-sized nanoparticles (10–100 nm). To determine the effect of all the treatments on cell viability, the standard MTT assay was used. After each screening experiment, the media was removed and 200 μ L of 0.5 mg/mL of MTT was added and cells were incubated for 2 hours. The purple formazan crystals were dissolved in 200 μ L of DMSO and the absorbance was measured at 560 nm using Epoch 2 Powerwave spectrophotometer BioTek Powerwave. The data was normalised using an MTT standard curve for each of the cell lines used.

2.3.6 Statistics

The untreated cells were used as a neutral control, with methotrexate as a positive control. The small-sized nanoparticles were between 1–10 nm and big-sized nanoparticles were between 10–100 nm. Statistical analysis was done using ANOVA, $P^* < 0.05$, with 3 experiments ($N = 3$) for each cell line.

2.3.7 Cell accumulation studies: Transmission electron microscope (TEM)

The preparation of biological samples for electron microscopy requires several stages which included sample washing, fixation, dehydration, embedding, sectioning and analysis. The cell preparations for electron microscopy was performed based on the methodology previously described by Schrand and other co-workers [119, 120] in order to verify the internalisation of the nanoparticles into the cells. The cells were seeded in 10 cm tissue culture treated plates, grown and treated with the following controls (folate, methotrexate, ethylenediamine, tetraaminophthalocyanine, ethylenediamine-folate, tetraaminophthalocyanine-folate) and with rhenium(III) oxide nanoparticles (at 10 μ M). Preparations of the cells for viewing under TEM was done as follows:

Sample washing and harvesting: The cell monolayer was washed 2–3 times using PBS (pH 7.4) to remove media, free/unattached nanoparticles and cellular debris [119, 121].

Primary fixing: After the cells had been washed they were fixed using 2.5 % of phosphate buffered (pH 7.4) glutaraldehyde which was incubated at 4°C for 4 hours. After 4 hours the cells were scrapped and transferred to micro-centrifuge tubes for secondary fixing [122, 123].

Secondary fixing and dehydration: Osmium tetroxide was added to the cells and kept for 90 minutes at room temperature. After 90 minutes, the cells were washed with two times 0.1 M phosphate buffer (pH 7.4) for 10 minutes. Subsequently, the cells were subjected to washing with different solutions [123, 124].

Solvents that were used to wash the cells after fixation:

- 100 mL buffer (phosphate buffer, 7.4 pH)
- 5 mL osmium tetroxide solution (1% in phosphate buffer)
- 50 mL 30% ethanol
- 50 mL 50% ethanol
- 50 mL 70% ethanol
- 50 mL 80% ethanol
- 50 mL 90% ethanol
- 50 mL absolute ethanol

Solvents that were used to wash the cells

- 50 mL propylene oxide
- 20 mL propylene oxide: embedding medium mixture 75:25
- 20 mL propylene oxide: embedding medium mixture 50:50
- 20 mL propylene oxide: embedding medium mixture 25:75
- 20 mL embedding medium

Cell embedment: The cells were suspended in pure resin for 12 hours, pure resin was added again into cells and the cells were placed in an oven at 600°C for 36 hours [125, 126].

Thin cell sectioning: The solidified resin containing the cells were cut into 80 nm sections, at the cutting speed of 0.7 mm/sec, using an ultramicrotome [119]. The cell sections are currently submitted for TEM viewing as part of the broader scope of the study. TEM studies will be carried out on stained and unstained cell sections to establish the presence of rhenium(III) oxide nanoparticles in cells without confusing it with effect of the stains.

Chapter 3 : Synthesis and characterization of capping agents and nanoparticles

3.1 General introduction

Rhenium has isotopes ($^{188}\text{Re}/^{186}\text{Re}$) that have been considered as a prospect for radiotherapy and cancer imaging due to the favourable nuclear properties such as short half-lives (17 hours for ^{188}Re and 3.7 days for ^{186}Re) and beta emission energies (2.11 MeV for ^{188}Re and 1.07 MeV for ^{186}Re) [20, 69, 104]. The key to the development of these radiopharmaceuticals is the selective localisation of the compounds in cancerous sites.

This section focuses on the formation of the rhenium(III) oxide nanoparticles, which were produced *via* the reduction of perrhenate (ReO_4^-). The two amine compounds comprised of ethylenediamine and aminated phthalocyanine were used as capping agents. The diamines were conjugated to folate *via* an amidation reaction on one side of the diamine (unsymmetrical substitution). The rhenium(III) oxide nanoparticles were successfully produced at room temperature by optimising the amount of capping agent, amount of reducing agent and concentration of rhenium salt. The nanoparticles were synthesised using “cold isotopes” of the rhenium metal and synthesised in an aqueous saline medium to imitate the environment in which perrhenate (ReO_4^-) will be produced from the reactor.

Folate is overexpressed in cancer cells and this has provided an avenue for exploiting the internalisation of drugs into cancer cells *via* its folate receptors [127, 128]. The synthetic tools available for conjugation of folic acid has not been extensively studied [129, 130]. Folate (vitamin B9) is structurally constituted of pteric acid covalently bond to a glutamic acid residue. However, only the γ -conjugates have medicinal relevance, since they have a higher affinity toward the receptors compared with α -conjugates (**Figure 1.7**) [131]. Fortunately, the γ -conjugates are intrinsically obtained as the major product from amidation of folate with diamines (from 55–90% selectivity) [132, 133].

3.2 Results and discussion

3.2.1 Ethylenediamine-folate conjugate

The synthesis of the EDA-FA conjugate, which involved the amidation and BOC deprotection step, was confirmed using FT-IR spectroscopy (**Figure 3.1**). The essential peaks (for N-H and C=O stretching vibrations) (**Figure 3.1**) show evidence of structural changes in *N*-BOC-EDA-FA and EDA-FA. The compound is comprised of dissimilar carbonyls, namely an amide stretch was found at 1500 cm^{-1} (C=O (C)), carboxylic acid stretch was found at 1613 cm^{-1} (C=O (B)) and an ester stretch was found at 1710 cm^{-1} (C=O (A)). On the EDA-FA spectrum the peak for C=O (ester) had disappeared due to the deprotection of BOC which confirmed a successful amidation process between folate and monoprotected ethylenediamine due to the disappearance of the ester peak [134]. The peak at 3341 cm^{-1} in the IR spectrum of EDA-FA was due to the N-H stretching vibration and it appeared after the deprotection step, suggesting that the amine is free on one end of ethylenediamine. The peak at 2358 cm^{-1} was due to the stretching vibrations of C-H. It was also observed that after the deprotection of *N*-BOC-EDA-FA, C-H stretch was not prominent, and we concluded that it was due to the removal of *tert*-butyloxycarbonyl (BOC).

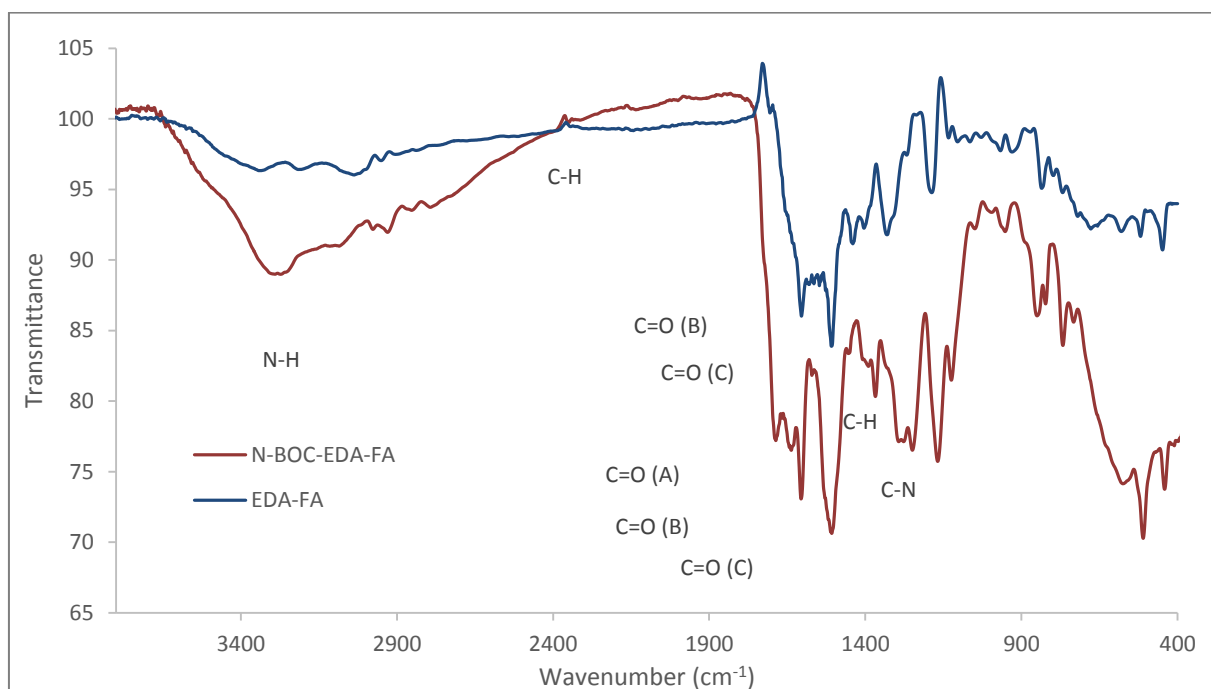


Figure 3.1: FT-IR spectra of *N*-boc-ethylenediamine-folate (*N*-BOC-EDA-FA) and ethylenediamine-folate (EDA-FA).

UV-Vis spectroscopic characterization (**Figure 3.2**) does not prove the deprotection step as the spectra are similar but serves as the characterization of the absorption spectrum for the conjugate with peaks at 280 and 360 nm. The structure was also confirmed using $^1\text{H-NMR}$ (**Figure 3.3**). The $^1\text{H-NMR}$ of *N*-BOC-EDA-FA was observed with the following results: (400 MHz, DMSO) δ 8.64 (s, 1H) and 8.61 (m, 1H), 8.0 (m, 2H), 6.66–7.99 (m, 3H), 6.50–6.60 (m, 2H), 4.25–4.5 (bs, 2H), 2.9–3.3 (m, 1H), 3.45 (water), 1.45 (m, 9H). The deprotection of *N*-BOC-EDA-FA was confirmed by the disappearance of the *tert*-butyloxycarbonyl (BOC) protons at 1.5 ppm (**Figure 3.3** and **3.4**) [114].

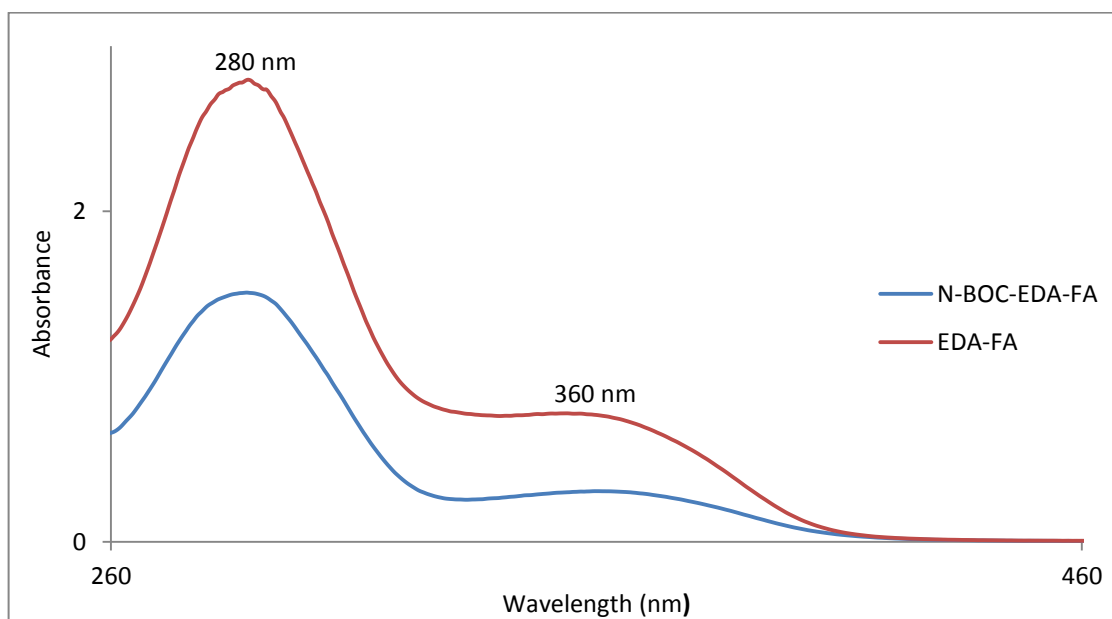


Figure 3.2: UV-Vis spectra of *N*-boc-ethylenediamine-folate (*N*-BOC-EDA-FA) and ethylenediamine-folate (EDA-FA).

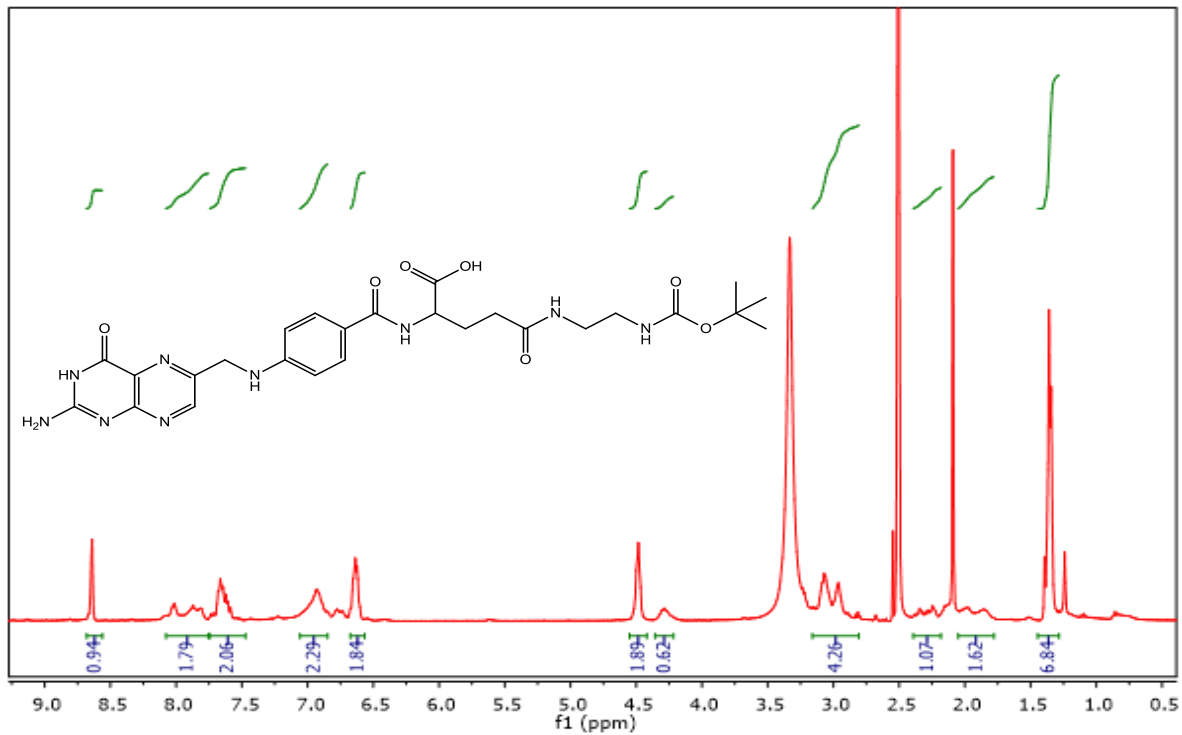


Figure 3.3: ¹H-NMR of Conjugated folate with *N*-boc-ethylenediamine.

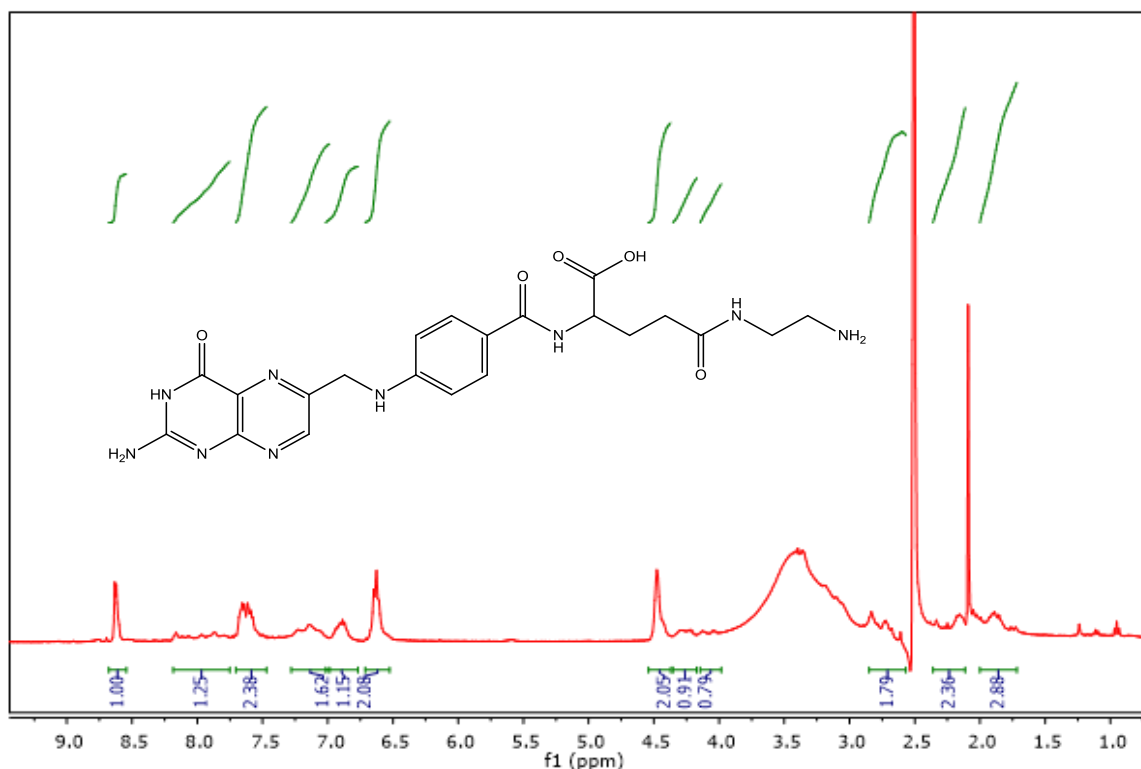


Figure 3.4 : ¹H-NMR ethylenediamine- folate (EDA-FA) after deprotection.

Figure 3.5 shows the LC-MS spectra of EDA-FA, showing some small molecules which confirmed that some of the ethylenediamine molecules were not conjugated to the folate molecules, the spectrum also confirmed some of the ethylenediamine molecules were successfully conjugated to folate molecules with the following molecular ions, 484.2 and 485.0 m/z corresponding to the molecular weight of EDA-FA (483.5 g/mol), one of the molecular ions in the spectrum indicated that EDA: FA ratio was 1:1. During the deprotection of di-*tert*-carbonyl some of the compounds were not completely removed as it showed on some of the molecular ions 531.39, 555.22, 569.57, 570.24 m/z (**Table 3.1**).

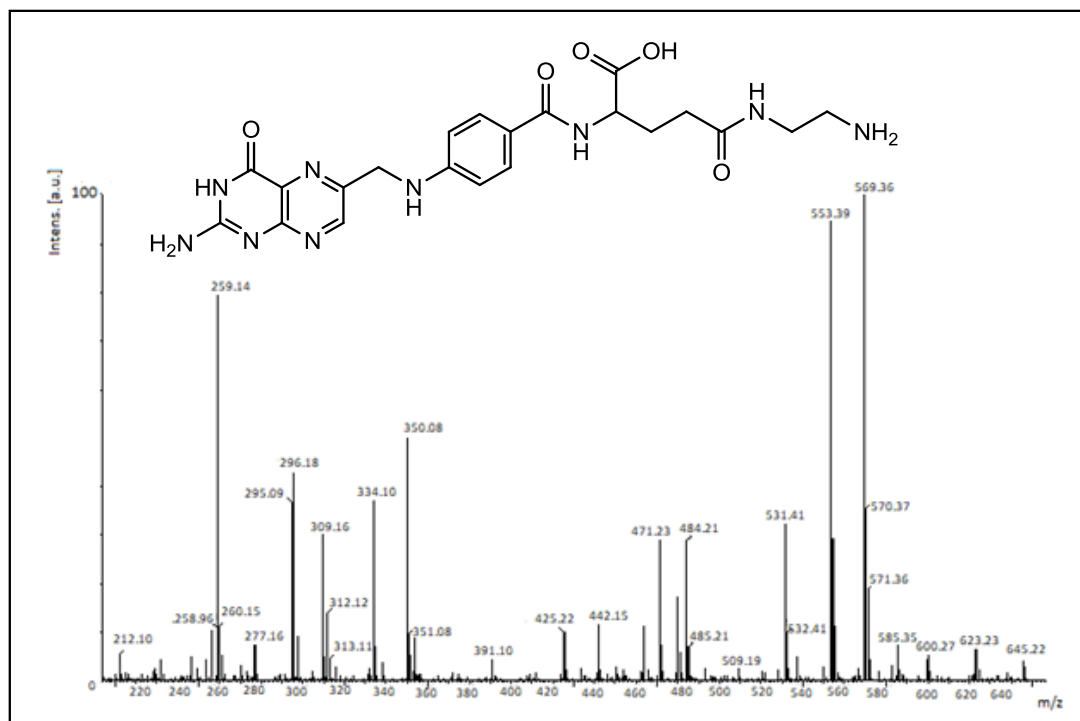


Figure 3.5: Ethylenediamine-folate (EDA-FA) obtained from the Electrospray Ionization (ESI) using LC-MS.

Table 3.1: Chemical structure and molecular ions of ethylenediamine-folate (EDA-FA) obtained from the Electrospray Ionization (ESI) using LC-MS.

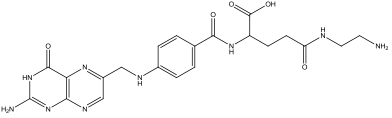
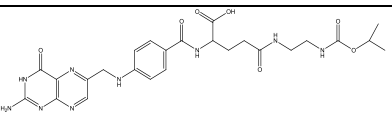
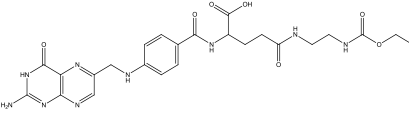
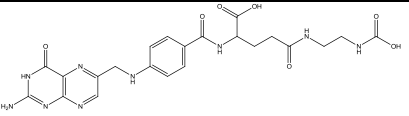
Chemical structure	m/z	Molecular ion
 EDA-FA	484.21	M+H
	485.20	M+2H
 EDA-FA + BOC	569.57	M ⁺
	570.24	M+H

Table 3.1: Continued.

 <p>EDA-FA + BOC</p>	555.22	M ⁺
 <p>EDA-FA + BOC</p>	531.39	M+2H

3.2.2 Tetraaminophthalocyanine-folate (TAPc-FA) conjugate

UV-Vis spectroscopy (**Figure 3.6**) and FT-IR spectroscopy (**Figure 3.7**) were used to confirm the synthesis of TAPc [117]. In comparison to the previous techniques used, UV-Vis provided conclusive evidence for the formation of Pcs and MPs. Phthalocyanine had a very strong absorption in the far-red region of the UV spectrum (approximately 700 nm), known as the Q band, and is usually accompanied by a vibronic shoulder. The peak at 350 nm is a B (soret) band. A metal-free phthalocyanine would have a split band at 700 nm but in this case the metal was not completely removed.

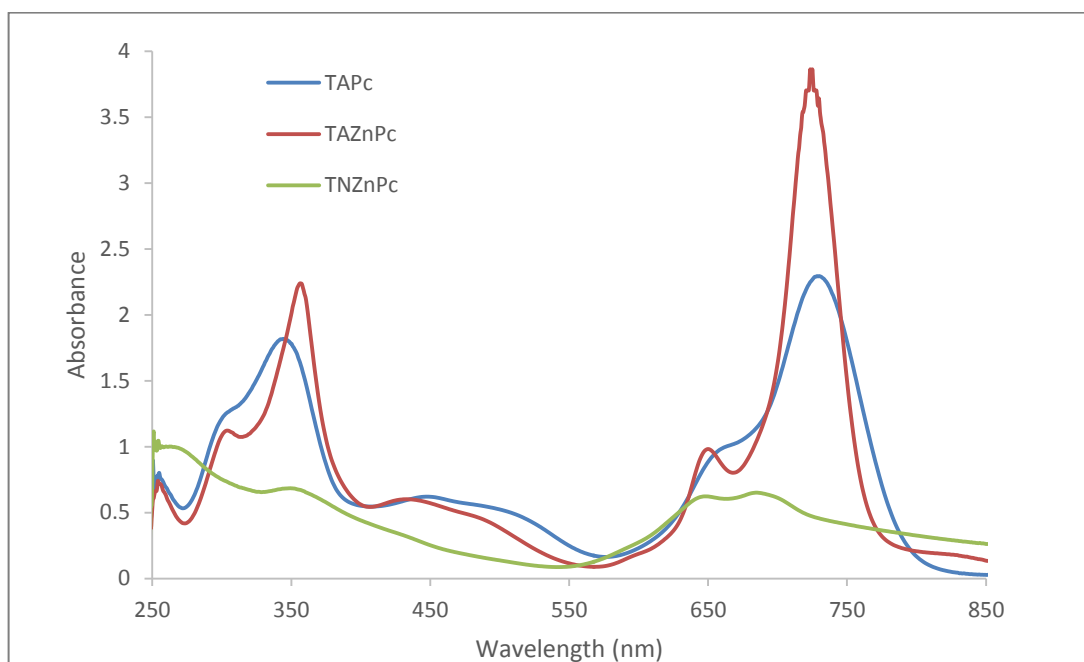


Figure 3.6: UV-Vis spectra of tetranitro-phthalocyanine (TNZnPc), tetraamino-zinc-phthalocyanine (TAZnPc) and tetraaminophthalocyanine (TAPc) dissolved in DMSO.

Figure 3.7 shows FT-IR spectroscopy confirmed the structure of phthalocyanines. The FT-IR spectrum of TAZnPC and TAPc had two peaks at 3310 and 3080 cm^{-1} corresponding to N-H stretches of the amino group that substituted the nitro group (TNZnPC) and at which was accompanied by N-H bending at 1500 cm^{-1} (**Figure 3.7**). The disappearance of the peaks at 1531 and 1333 cm^{-1} (nitro groups) further confirmed the reduction of nitro groups to amino groups.

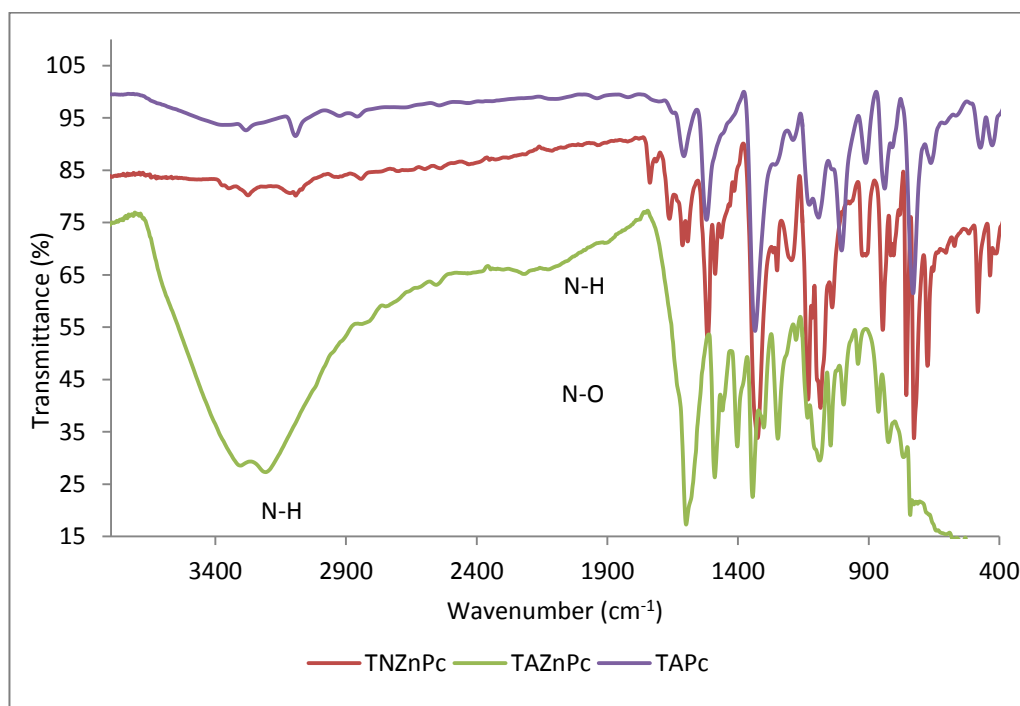


Figure 3.7: FT-IR spectra of tetranitro-zinc-phthalocyanine (TNZnPc), tetraamino-zinc-phthalocyanine (TAZnPc) and tetraaminophthalocyanine (TAPc).

Conjugating the tetraaminophthalocyanine with folate was also confirmed by the LC-MS using Electrospray Ionization (ESI) as a source (**Figure 3.8**). The spectrum confirmed the molecules were conjugated with a 1:1 phthalocyanine: folate ratio with the molecular ions $M^+ = 999.34$ amu.

The large m/z in the LC-MS were further investigated using Chem-draw software, it was analysed as follows: 1061.76 – 1147.36 amu were found to be TAZnPc-FA with some water molecules (this indicate that the product was not fully dry). 1176.04 amu confirmed that although a demetallation of TAZnPc was not fully successful, also when we were activating folate with NHS and DCC, there are some molecules of NHS that are still attached to the folate. Lastly 1177.40 amu and 1211.85 amu showed that that product still has some few molecules of TNZnPc that were conjugated to folate and NHS molecules.

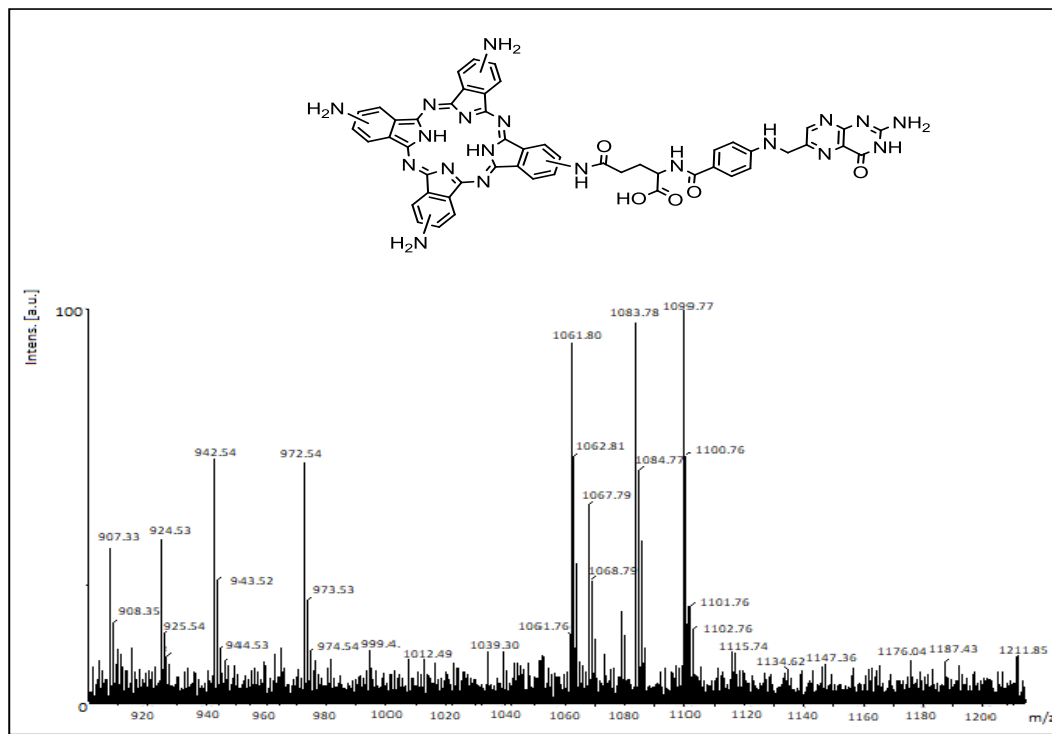


Figure 3.8 : LC-MS of tetraaminophthalocyanine-folate (TAPc-FA) obtained using Electrospray Ionization (ESI) as a source.

Table 3.2: Analysed Chemical structure and molecular ions of tetraaminophthalocyanine-folate (TAPc-FA) obtained from the Electrospray Ionization (ESI) using LC-MS.

Chemical structure	m/z
TAZnPc-FA + water molecules	1061.74- 1147.36
TAZnPc-FA + water molecules + <i>N</i> -Hydroxysuccinimide molecules (NHS)	1176.04
TNZnPc-FA	1177.40
TNZnPc-FA + <i>N</i> -Hydroxysuccinimide molecules (NHS)	1211.85

3.2.3 Rhenium(III) oxide nanoparticles

3.2.3.1 General introduction

Nanoparticles are known to be multipurpose agents with a diversity of biomedical applications [135]. The application of the nanoparticles includes, being used in highly sensitive diagnostic assays, radiotherapy enhancement as well as gene and drug delivery. Metal nanoparticles have been applied as non-toxic carriers for gene and drug use [136]. The key to the successful application of nanoparticles in medicinal use, one needs to take into consideration the size of the nanoparticles. Nanoparticles with sizes more than 100 nm exhibit *in vivo* toxicity in the spleen and liver because of their accumulation. Larger nanoparticle sizes are therefore not suitable for therapeutic use [117].

3.2.3.2 Synthetic aspects

It is quite challenging to control the size of the nanoparticles, regardless of the agglomeration of nanoparticles. The size can be controlled by changing these variables: concentration of the metal, the amount of the capping agent, the amount of the reducing agent and the use of a buffer to control the pH environment (**Table 3.1**). For example, maintaining neutral and slightly basic (7.4 pH) pH resulted in the production of larger nanoparticles, whereas in an acidic environment smaller nanoparticles were obtained. In this study the nanoparticles were synthesised in an aqueous saline solution to mimic the conditions in which rhenium would be obtained.

The nanoparticles were synthesised using a reducing agent (sodium borohydride) under a nitrogen environment. The nanoparticles were found to be stable in a suspension for a period of two weeks. Afterwards, the suspension slowly changed back to a transparent colour. Rhenium oxides may undergo oxidation to ReO_2 in acid or neutral solution and to ReO_4^- in alkaline solutions [117].

Table 3.3: Optimisation synthesis of rhenium(III) oxide nanoparticles capped with different capping agents.

Sample code	Amount of NH_4ReO_4 (100 mM)	Amount of Capping (EDA, EDA-FA, TAPc, TAPc-FA) (10 mg/mL)	Amount of NaBH_4 (100 mM)
Re NP s	60 μL	-	700 μL
Re NP m	80 μL	-	500 μL
Re NP b	100 μL	-	500 μL
Re-EDA NP s	60 μL	800 μL	700 μL
Re-EDA NP m	60 μL	700 μL	500 μL
Re-EDA NP b	80 μL	500 μL	500 μL
Re-EDA-FA NP s	80 μL	700 μL	700 μL
Re-EDA-FA NP m	80 μL	600 μL	700 μL
Re-EDA-FA NP b	80 μL	500 μL	500 μL
Re-TAPc NP s	60 μL	700 μL	700 μL
Re-TAPc NP m	60 μL	600 μL	500 μL
Re-TAPc NP b	80 μL	500 μL	500 μL
Re-TAPc-FA NP s	60 μL	700 μL	700 μL
Re-TAPc-FA NP m	80 μL	600 μL	500 μL
Re-TAPc-FA NP b	80 μL	500 μL	500 μL

s = small (1-10 nm), m = medium (10-50 nm), b = big (50-100 nm)

Reaction conditions were optimised to achieve varied nanoparticle sizes. The use of minimal amounts of capping and reducing agents resulted in larger nanoparticle sizes and increasing the concentration of perrhenate also increased the size of nanoparticles and *vice versa*.

3.2.3.3 Spectroscopic characterization

The spectrum of rhenium(III) oxide nanoparticles capped with ethylenediamine (Re-EDA NP s) (Figure 3.9) showed in a prominent peak at 230 nm after the reducing agent (sodium borohydride) was added this indicated the quantum confinement effect in rhenium(III) oxide nanoparticles.

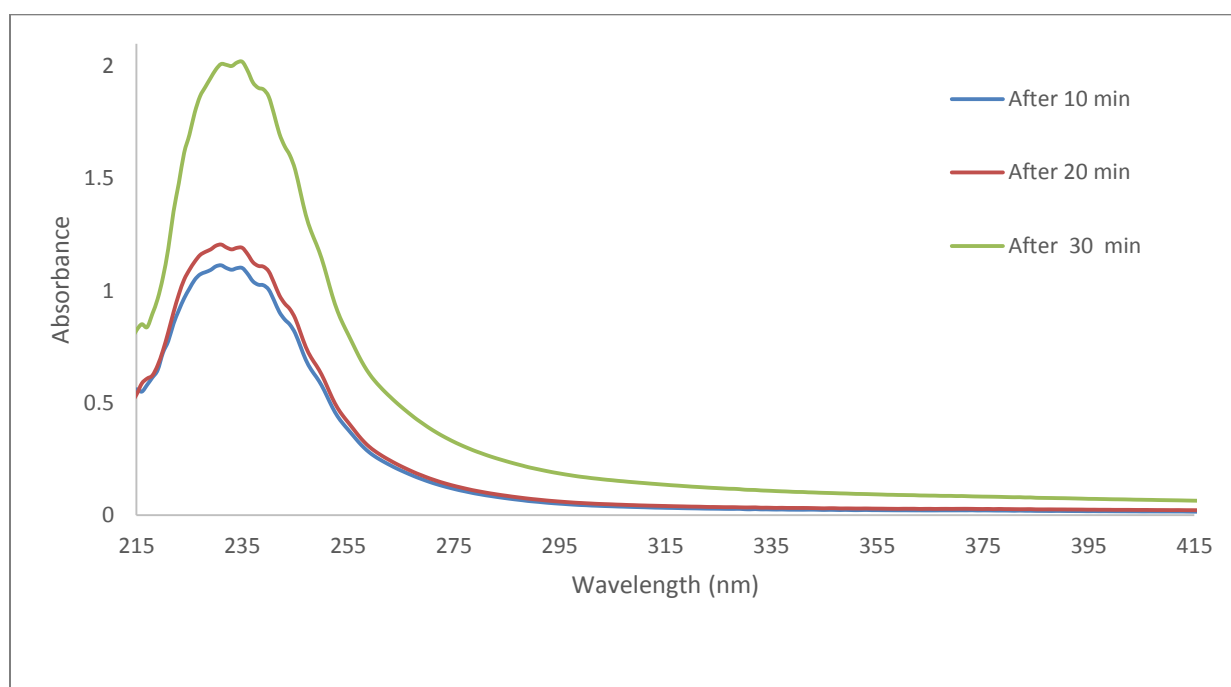


Figure 3.9: Optical spectra of rhenium(III) oxide nanoparticles capped with ethylenediamine (Re-EDA NP s), dissolved in deionised water.

From what had been already been confirmed in **Figure 3.2** for ethylenediamine-folate (EDA-FA) between the two observed peaks at 280 and 360 nm due to the conjugate, an additional peak at 300 nm was observed which could be due to the quantum confinement effect in rhenium(III) oxide nanoparticles (**Figure 3.10**). Various concentrations were used, which then resulted in small-sized nanoparticles (0.1 M), medium-sized nanoparticles (0.125 M) and big-sized nanoparticles (0.15 M).

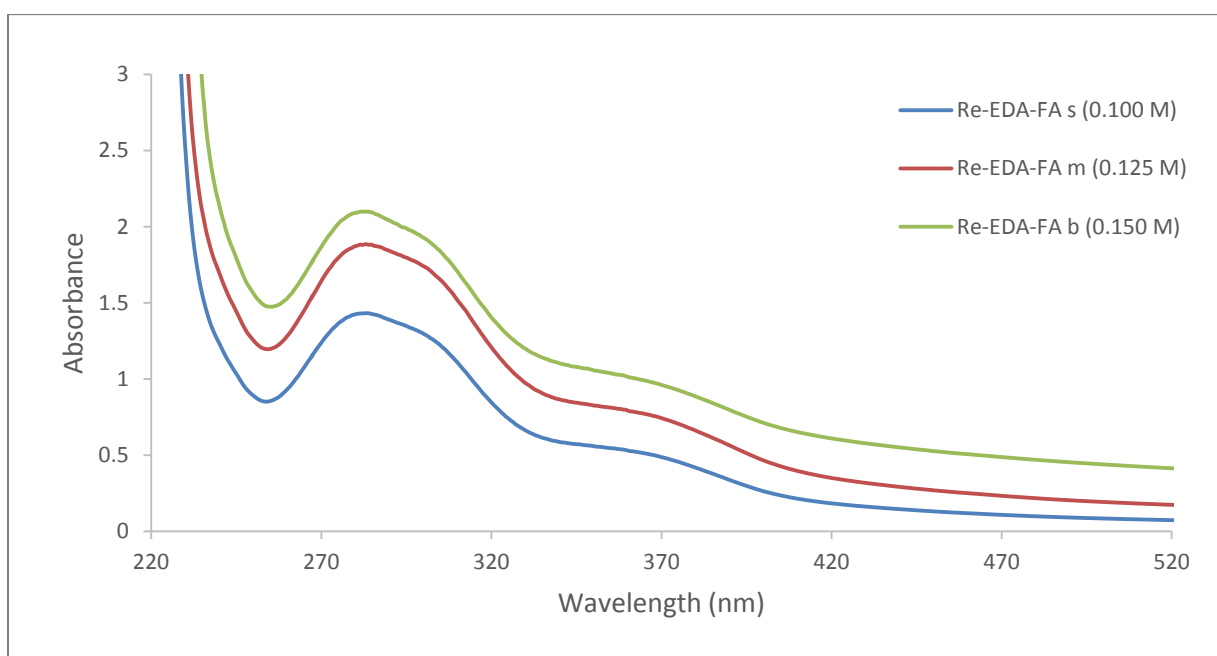


Figure 3.10: Optical spectra of rhenium(III) oxide nanoparticles capped with ethylenediamine-folate (Re-EDA-FA NP) compared with the spectra of rhenium(III) oxide nanoparticles capped with ethylenediamine (Re-EDA NP), dissolved in deionised water.

The absorption spectra of rhenium(III) oxide nanoparticles capped with conjugated tetraaminophthalocyanine-folate (Re-TAPc-FA NP) showed an increase in absorbance and wavelength with an increase in size and concentration (**Figure 3.11**) with peaks at 210 nm for rhenium and at 240 nm indicating the folate conjugated with TAPc. Various concentrations were used, which then resulted in small-sized nanoparticles (0.1 M), medium-sized nanoparticles (0.125 M) and big-sized nanoparticles (0.15 M).

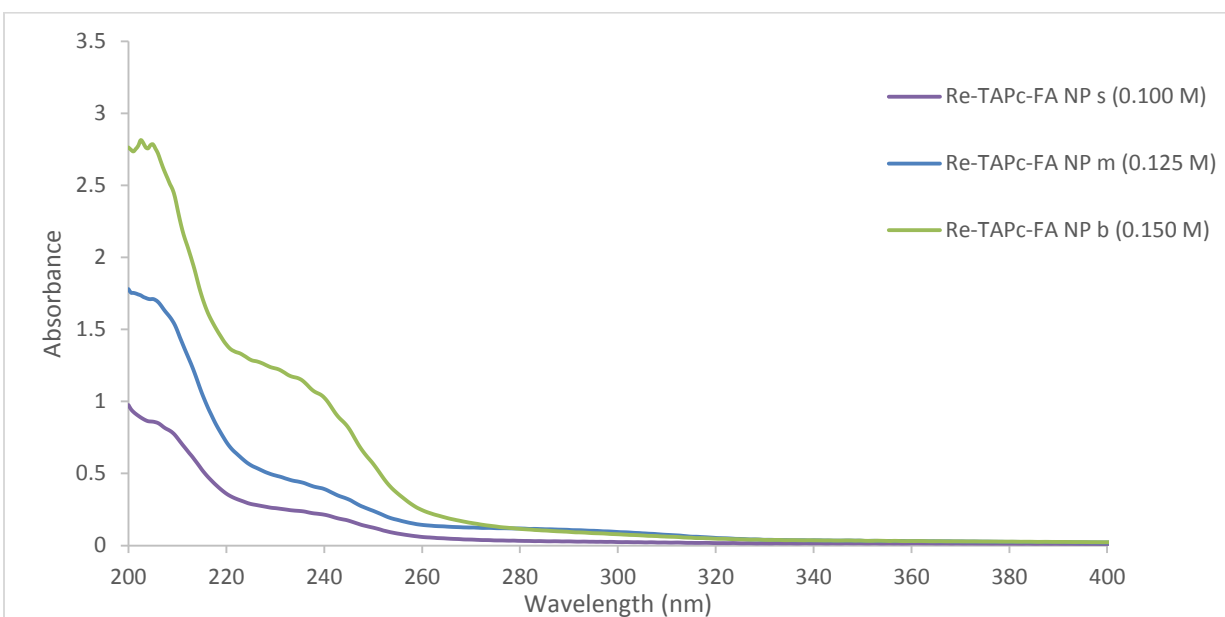


Figure 3.11: Optical spectra of rhenium(III) oxide nanoparticles capped with tetraaminophthalocyanine-folate (Re-TAPc-FA NPs), dissolved in DMSO.

The fluorescence properties of rhenium(III) oxide nanoparticles were studied with a spectrofluorimeter (**Figure 3.12**). It is crucial to examine the fluorescence properties of the material to provide information for possible cell localisation ability on cancer cells using a confocal microscope. Different capping agents were used on the surface of the rhenium nanoparticles; hence it was of interest to investigate the fluorescent properties of these nanoparticles that are capped with different capping agents. The nanoparticles were excited at a wavelength of 331 nm. An emission peak was observed at 475 nm. It was observed that nanoparticles that consisted of capping agents had a higher intensity than the nanoparticles that were not capped as the size also increases. The size of rhenium(III) oxide nanoparticles increased as the concentration increases. Therefore, as the size of the nanoparticles increased the intensity also increases.

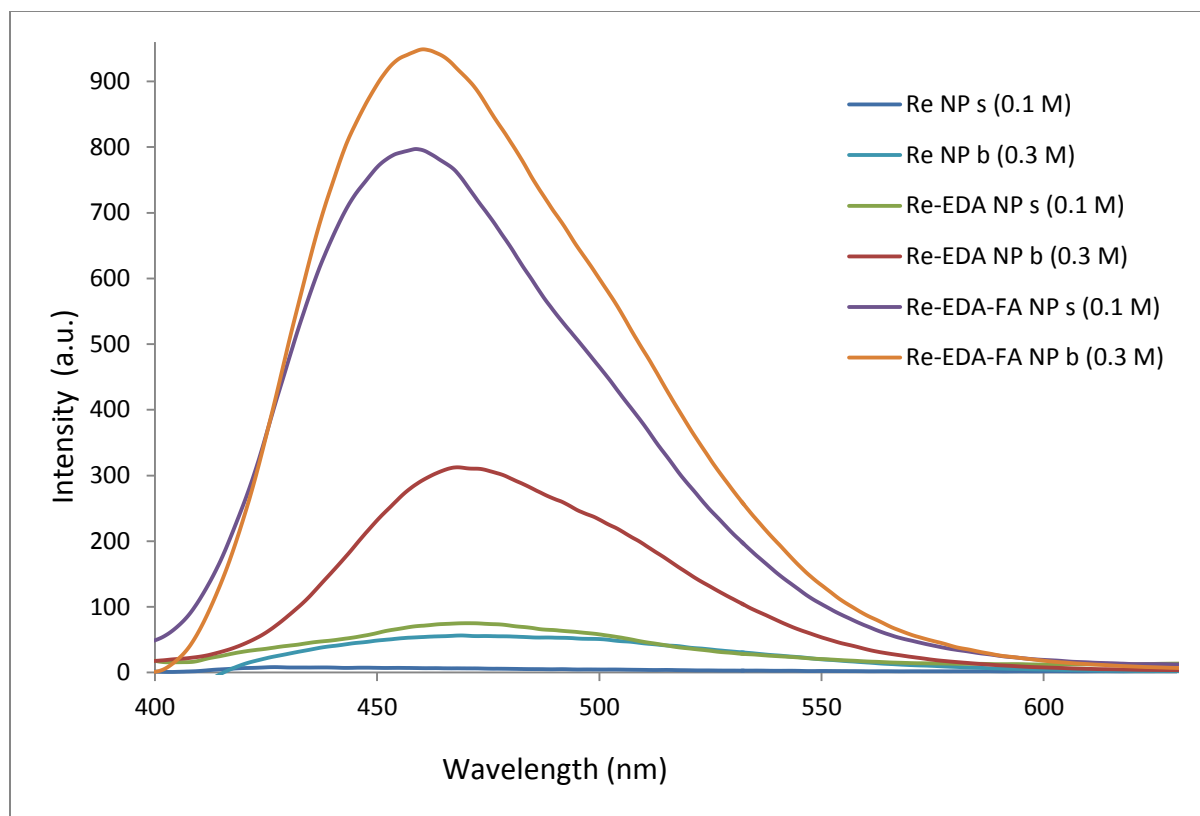


Figure 3.12: Emission spectra of rhenium(III) oxide nanoparticles capped with sodium borohydride and ethylenediamine and ethylenediamine-folate in various concentrations, dissolved in deionised water.

3.2.3.4 TEM characterization

The morphology and size of rhenium(III) oxide nanoparticles was obtained from TEM analysis. The TEM micrographs illustrated in **Figure 3.13**, **3.14** and **3.15** display the varied sizes of nanoparticles that were synthesised with different capping agents. **Figure 3.13** shows TEM micrographs of rhenium(III) oxide nanoparticles capped with ethylenediamine (Re-EDA NP) with their subsequent particle size distributions, and an average particle size was obtained is 2 nm. The actual shape could not be seen under microscope (HR-TEM) due to the incredibly small size of the NPs and the fact that the nanoparticles kept moving, this may be caused by the parameters of the instrument if it was not well set for instance the temperature from which the beam of electrons are produced. However, **Figure 3.13** also showed nanoparticles with a size of 6 nm were obtained when increasing the concentration of perrhenate and with decreasing the amount of the reducing agent. To achieve varied sizes of nanoparticles, one

variable was changed at a time. Small-sized nanoparticles generally showed a spherical shape that is well dispersed, unlike the big-sized nanoparticles.

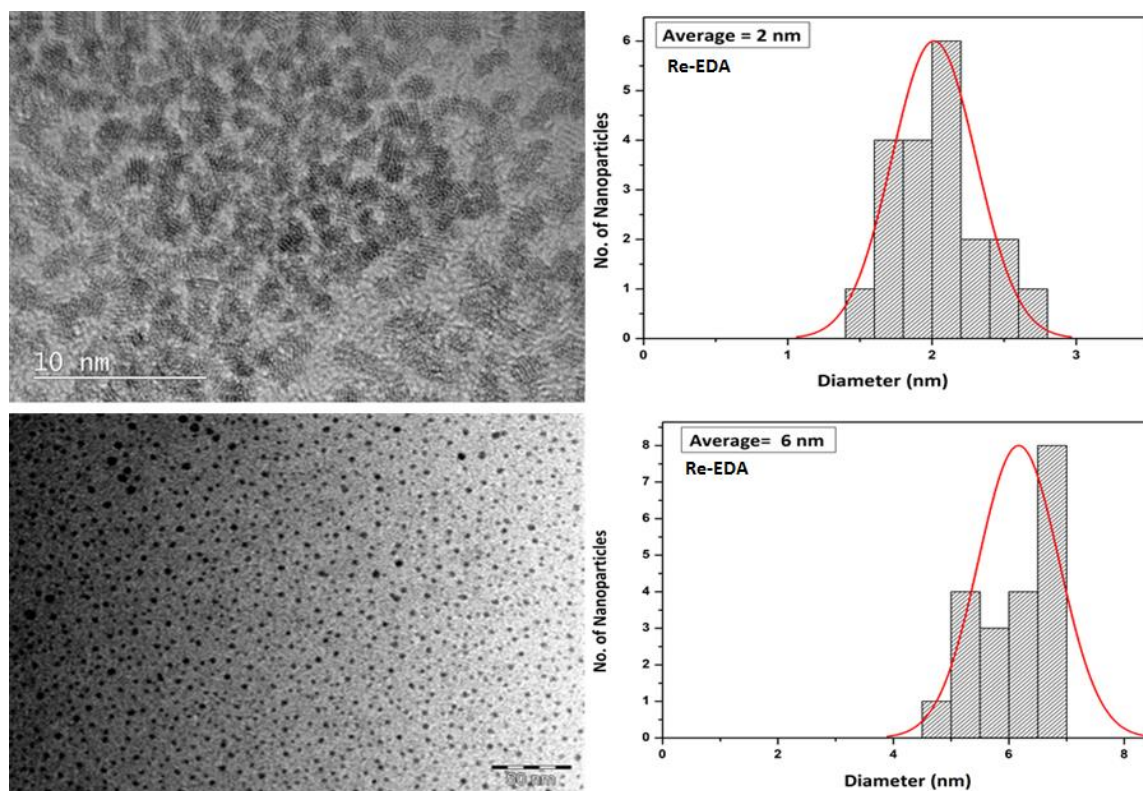


Figure 3.13: TEM micrographs of rhenium(III) oxide- ethylenediamine (Re-EDA NP) and their subsequent particles size distributions approximately 2 and 6 nm. These small size nanoparticles capped with ethylenediamine resulted from the following optimised conditions: 60 μL of ammonium perrhenate (100 mM), 800 μL of freshly prepared NaBH_4 (100 mM) and 800 μL of EDA-FA solution in DMSO (10 mg/mL). However, 6 nm size resulted by an increase in the concentration of perrhenate (80 μL) and with decreasing the amount of the reducing agent (500 μL).

Figure 3.14 shows the TEM micrographs of rhenium(III) oxide capped with conjugated ethylenediamine-folate (Re-EDA-FA NP) with their subsequent particles size distributions. Very small sizes (~ 2 nm) were obtained because of decreasing the concentration of perrhenate. **Figure 3.14** also displayed larger spherical nanoparticles with trace amounts of capping agent surrounding the particle. **Figure 3.15** shows TEM micrographs of rhenium(III) oxide NPs capped with conjugated ethylenediamine-folate (Re-EDA-FA NP) and tetraaminophthalocyanine-folate (Re-TAPc-FA NP). **Figure 3.15** shows the shapeless

rhodium(III) oxide capped with conjugated ethylenediamine-folate with their subsequent particles size distributions, a medium size of 52 nm was obtained, and **Figure 3.15** also shows rhodium(III) oxide capped with TAPc-FA with sizes of 12 and 32 nm.

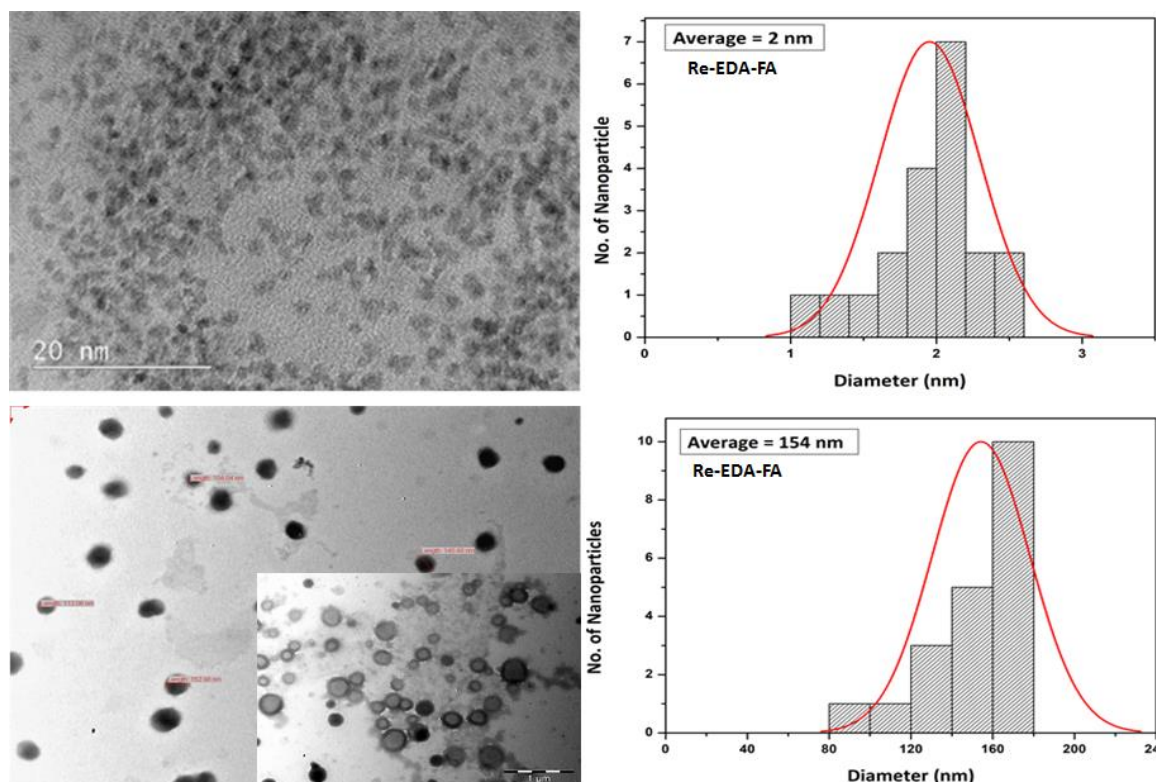


Figure 3.14: TEM micrographs of rhodium(III) oxide-ethylenediamine-folate (Re-EDA-FA) and their subsequent particle size distributions with 2 nm size and 154 nm displayed big spherical nanoparticles with trace amounts of capping agent surrounding the particle. The small size nanoparticles resulted from the following optimised conditions: 60 μL of ammonium perrhenate (100 mM), 700 μL of freshly prepared NaBH_4 (100 Mm) and 700 μL of EDA-FA solution in DMSO (10 mg/mL). However, 154 nm resulted from an increase in the concentration of perrhenate (80 μL) and with decrease of the amount of the reducing agent and capping agent (500 μL).

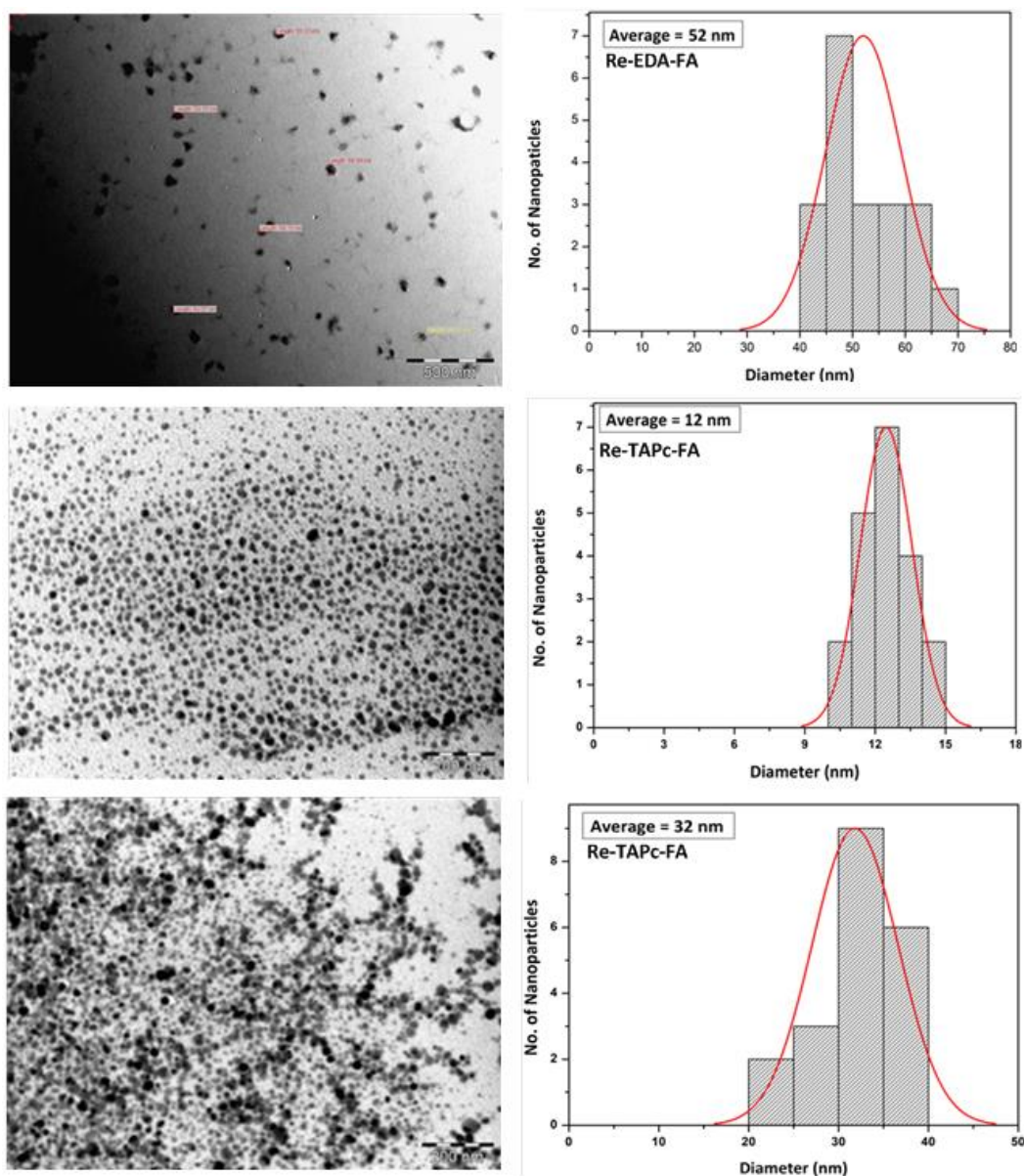


Figure 3.15: TEM micrographs of rhenium(III) oxide nanoparticles capped with ethylenediamine-folate and tetraaminophthalocyanine-folate with their subsequent particle size distributions. The image of rhenium(III) oxide nanoparticles capped with EDA-FA with an average size of 52 nm resulted from the following optimised conditions: 80 μL of ammonium perrhenate (100 mM), 700 μL of NaBH_4 (100 Mm) and 600 μL of EDA-FA solution. However, medium (12 nm) size nanoparticles capped with TAPc-FA resulted from the following optimised conditions: 60 μL of ammonium perrhenate (100 mM), 500 μL of NaBH_4 (100 Mm) and 600 μL of TAPc-FA. An increase in the concentration of perrhenate (80 μL) and 500 μL of NaBH_4 resulted in the medium size (32 nm) nanoparticles capped with TAPc-FA.

3.2.3.5 Zeta potential analysis

The stability and physicochemical behaviour of the nanoparticles require the characterization of the interfacial properties. Such a characterization may be achieved using the Zeta potential, which is related to the surface charge and electric double layer (EDL) of colloidal particles. Furthermore, the Zeta potential is a powerful parameter of the EDL and an appropriate way of predicting the suspension stability [137]. The EDL can be regarded as consisting of two regions or layers. A region closest to the surface that is considered immobile and an outer region allows diffusion of ions to be distributed according to the influence of electrical forces and random thermal motion. The boundary between the edge of this solvated layer and bulk liquid is termed the slipping plane. The potential of the bulk solution is defined as zero, and the electrokinetic potential termed ZP is the potential at the slipping plane [138, 139].

Figures 3.16 and **3.17** shows the Zeta-size of the small-sized rhenium(III) oxide nanoparticles capped with ethylenediamine (Re-EDA NP s) and ethylenediamine-folate (Re-EDA-FA NP s). These nanoparticles formed large sediments under the Zeta-sizer (dynamic light scattering (DLS)) instrument due to the hydrodynamical environment that the nanoparticles are immersed to and this was mostly observed on the small-sized nanoparticles. Whereas **Figures 3.18** and **3.19** shows the Zeta-size of the medium and big-sized rhenium(III) oxide nanoparticles capped with ethylenediamine (Re-EDA NP m) and ethylenediamine-folate (Re-EDA-FA NP b). These nanoparticles they are not easily aggregating and active under the Zeta-sizer instrument.

The Zeta potential values showed both negative and positive charges depending on the surface charge of the particle, but for a particle to be considered as stable, it must be -30 to +30 mV. The Zeta potentials of rhenium(III) oxide nanoparticles (with different capping agents) is summarized in **Table 3.2**. The nanoparticles were found to be negatively charged, and some with a capping agent have some mixed charges which can be concluded that not all the rhenium particles were capped with the capping agent. The nanoparticles were found to be stable although they started to aggregate. The nanoparticles capped with sodium borohydride

were found to be unstable as compared with amine capped nanoparticles. The results can be concluded that the nanoparticles with the capping agent have weak repulsive forces which prevent them from aggregating.

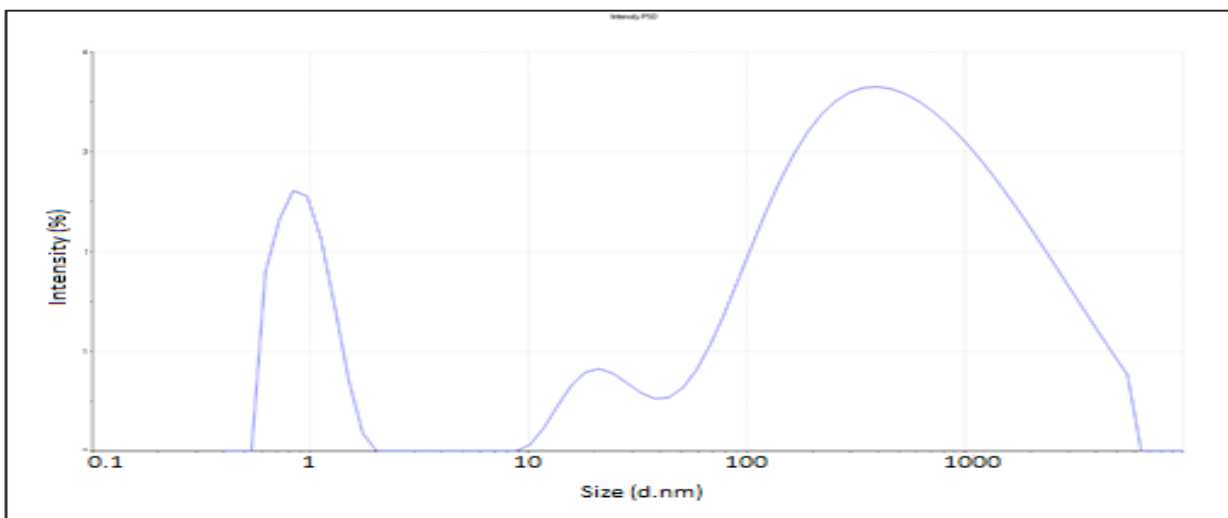


Figure 3.16: Dynamic light scattering (DLS) measurements of rhenium(III) oxide nanoparticles capped with ethylenediamine (Re-EDA NP s) from Zeta-sizer.

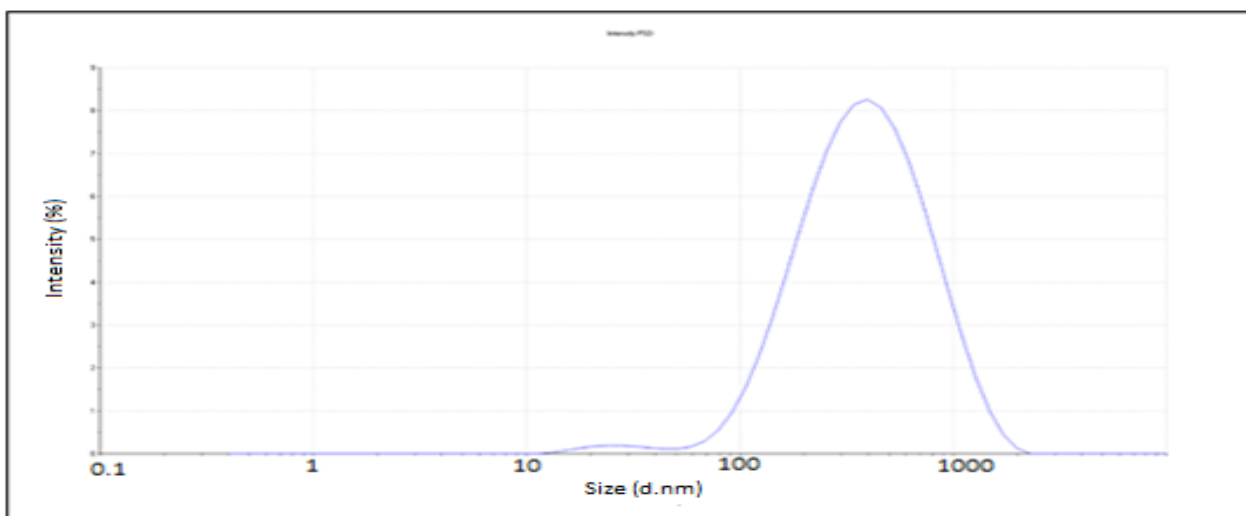


Figure 3.17: Dynamic light scattering (DLS) measurements of rhenium(III) oxide nanoparticles capped with ethylenediamine-folate (Re-EDA-FA NP s) from Zeta-sizer.

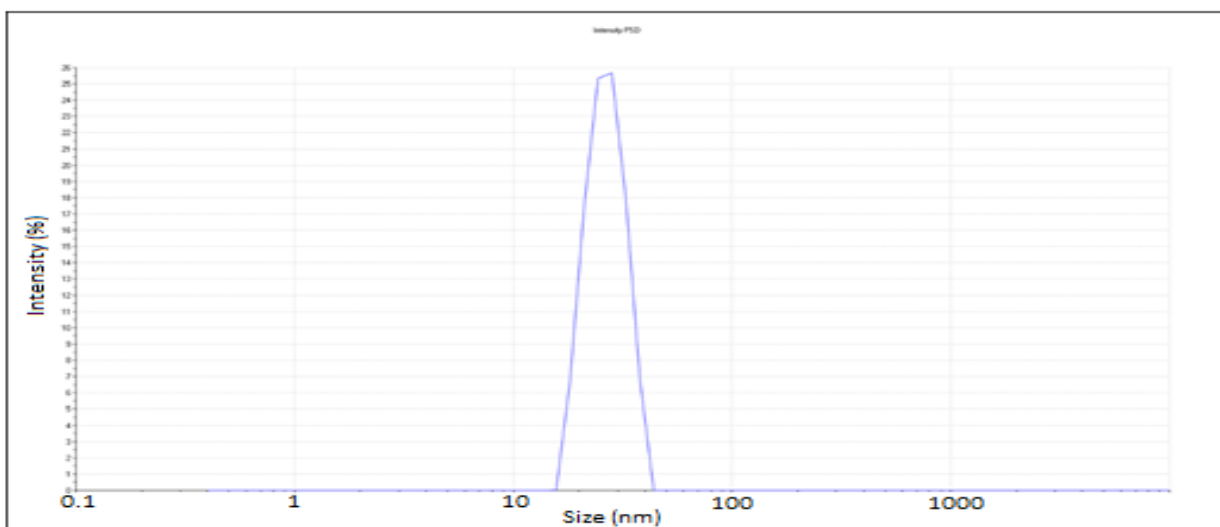


Figure 3.18: Dynamic light scattering (DLS) measurements of rhenium(III) oxide nanoparticles capped with ethylenediamine (Re-EDA NP m) from Zeta-sizer.

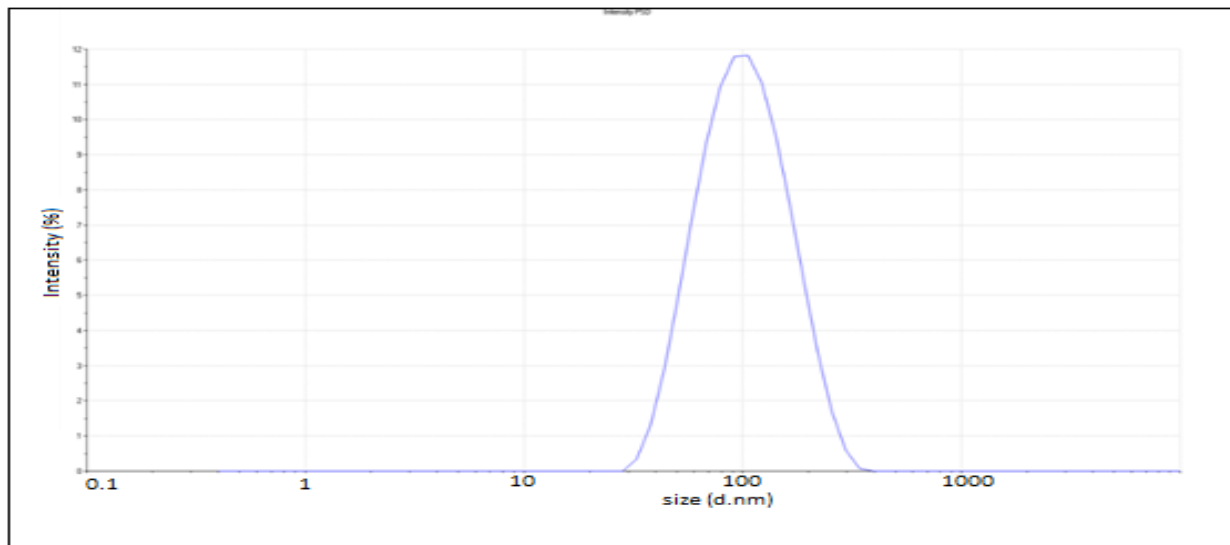


Figure 3.19: Dynamic light scattering (DLS) measurements of rhenium(III) oxide nanoparticles capped with ethylenediamine-folate (Re-EDA-FA NP m) from Zeta-sizer.

The Zeta-size of the rhenium(III) oxide nanoparticles capped with ethylenediamine (Re-EDA NP m) was compared with the TEM size, it was observed that due to the hydrodynamic environment the nanoparticles from dynamic light scattering (DLS) measurements revealed large-sized nanoparticles as compared with the results from TEM. The nanoparticles capped with ethylenediamine-folate (Re-EDA-FA NP b) were also compared with TEM results, it was observed that the big-sized nanoparticles were not easily aggregating and active under the dynamic light scattering (DLS) measurements, hence TEM result gave almost the same uniform sizes. For example, nanoparticle sizes of 35 and 164 nm were observed from dynamic light scattering (DLS) measurements (Figures 3.18 and 3.19) which were confirmed using TEM (Figures 3.13 and 3.14) were found to be 6 and 154 nm.

Table 3.4: Summarised results of rhenium(III) oxide nanoparticles sizes (Zeta-sizer) and charge (Zeta potential). The experiment was carried out at 25°C.

Sample name	Z- Ave (d.nm)	Peak 1 mean (d.nm)	Peak 2 mean (d.nm)	Peak 3 mean (d.nm)	Zeta Potential (mV)
Re NP b	133.8	165.1	4081	0.00	-47.9 (-47.4, -65.4)
Re NP s	81.21	91.69	0.949	23.04	-49.2
Re-EDA NP m	118.4	35.05	0.00	0.00	-18.6 (-18.7, 18.9)
Re-EDA NP s	44.27	0.7334	188.4	1245	-6.13 (-10.3, 10,8)
Re-EDA-FA NP b	121.3	164.8	0.00	0.00	-3.01 (-23.3, 49.6)
Re-EDA-FA NP s	38.8	36.6	2415	0.00	-4.35
Re-TAPc NP b	117.9	144.8	0.00	0.00	-40.4 (-36.3, -49.7)
Re-TAPc NP s	68.11	6.610	289.4	0.00	-36.5
Re-TAPc-FA NP b	97.75	107.0	0.00	0.00	-26.1
Re-TAPc-FA NP s	120.6	162.3	9.315	0.00	-18.1 (-18.9, 11.1)

*d.nm illustrates the diameter of the particle in nanoscale.

3.2.4 General conclusion

The capping agents (tetraaminophthalocyanine, ethylenediamine-folate and tetraaminophthalocyanine-folate) were successfully synthesised and characterised using Ultraviolet-Visible Spectroscopy (UV-Vis), Fourier Transform-Infrared Spectroscopy (FT-IR), Proton Nuclear Magnetic Resonance ($^1\text{H-NMR}$), and Liquid Chromatography-Mass Spectroscopy (LC-MS) to confirm their structure. Rhenium(III) oxide nanoparticles were successfully prepared *via* reducing agent (sodium borohydride) and capping agents. The

nanoparticles were then characterised using UV-Vis, spectrofluorimetry, Transmission Electron Microscopy (TEM), dynamic light scattering (DLS) and Zeta potential. UV-Vis confirmed the presence of rhenium reduced ion and the presence of the capping agent (EDA-FA, TAPc-FA). TEM (**Figures 3.13, 3.14.and 3.15**) confirmed the morphology and the size of the nanoparticles. DLS and Zeta potential confirmed the size and surface charge (negative) of the nanoparticles. Zeta potential and TEM analysis confirmed that the material was classified at nanoscale, however, some of particles resulted in large sediment particles due to the hydrodynamic environment which resulted for the nanoparticles to aggregate. The Zeta potential results confirmed that the use of capping agent increased the nanoparticle stability when comparing the charges of nanoparticles capped with capping agents. The Zeta-size of the rhenium(III) oxide nanoparticles capped with ethylenediamine (Re-EDA NP m) was compared with the TEM size, it was observed that due to the hydrodynamic environment the nanoparticles they turn to give big-sized nanoparticles than the result from TEM. Nanoparticles capped with ethylenediamine-folate (Re-EDA-FA NP b) were also compared with TEM results and it was observed that the big-sized nanoparticles are not easily aggregating and active under the dynamic light scattering (DLS) instrument, hence TEM results gave almost the same uniform sizes.

Chapter 4 : Biochemical studies

4.1 General introduction

Nanotechnology has prompted new and improved materials for biomedical applications with distinct emphasis in therapy and diagnostics. Special interest has been directed at providing enhanced molecular therapeutics for cancer, where conventional approaches do not effectively differentiate between cancerous and normal cells due to a lack of specificity [15]. This normally causes systemic toxicity, severe and adverse side effects with concomitant loss of quality of life. Because of their small size, nanoparticles can readily interact with biomolecules, both at the surface and inside cells yielding better signals and target specificity for diagnostics and therapeutics [136].

Control of the physicochemical properties of nanomaterials, has the potential to significantly improve diagnostic and therapeutic performance. When working with nanomaterials, it is vital to determine the toxicity of the nanoscale materials as compared to their bulk materials [140]. Particle size and surface area are important material characteristics from a toxicological perspective. As the size of a particle decreases, its surface area per volume increases and allows a greater proportion of its atoms to be displayed on the surface rather than the interior of the material. The change in the physicochemical and structural properties of engineered nanomaterial with a decrease in size could be responsible for some physical interactions within cells that could lead to toxicological effects [141].

Biomolecules are captivating macromolecular structures with their unique recognition, transport, and catalytic properties. The conjugation of nanoparticles with biomolecules provides an enhanced targeting ability. Enzymes, antigens and antibodies, and biomolecule receptors have dimensions in the micro and nanoscale, similar to those of nanoparticles. Thus the two classes of materials have potential structural compatibility [142].

Targeted nanoparticles have the potential to deliver a significant amount of drug to cancer cell areas. This targeting requires a ligand on the nanoparticle surface interact with a specific membrane receptor on target cells. However, the contribution of the targeting ligand to nanoparticle delivery is often influenced by non-specific nanoparticle uptake [143]. Nanoparticle-based drug delivery is on the verge of revolutionising cancer therapy, due to superior drug solubility, improved serum stability, longer circulation half-lives, better drug loading and shielding ability, and excellent drug accumulation in the tumour through the enhanced permeability and retention effect and targeting mechanisms [15].

4.1.1 Cell cytotoxicity studies

In this study, the cytotoxic investigation of the rhenium(III) oxide nanoparticles was completed on MDA-MB-468, MDA-MB-231, MCF-10A (non-tumorigenic) and MCF-7 cells lines at 100 and 10 μ M. The main focus was to achieve the concentrations that did not because cell death (i.e. non-cytotoxic concentrations) since the hot isotopes would have an effect on the diagnosis or therapeutic aspect. Nanoparticles can readily interact with biomolecules both at the cell surface and inside cells, allowing for improved signal and the target specificity required for diagnostics and therapeutics. The biological studies were performed to establish if a biological response would be induced by rhenium(III) oxide nanoparticles on different cancer cell lines. These cancer cell lines were chosen based on the presence and/or variation of receptor, with specific focus on folate receptors (**Table 4.1**).

Table 4.1: Different cell lines with the various receptors they express [144–147].

Cell line	Estrogen receptor	Progesterone receptor	HER2 receptor	Endogenous A2B adenosine	Epidermal growth factor receptor	Folate receptor
MCF-7	✓	✓	✗	✗	✗	✓
MCF-10A	✓	✓	✓	✗	✗	✓
MDA-MB-231	✗	✗	✗	✓	✗	✓
MDA-MB-468	✗	✗	✗	✗	✓	✗

*✓ Positive: ✗ negative

The effects of NP-systems were investigated. The preferred results in this study is one that triggers proliferation or has no significant effects, since this is a preliminary study for radiation induced apoptosis (cell death). The initial viability screening was performed at 100 μ M on the different cell lines and the concentration was determined using UV-Vis spectroscopy.

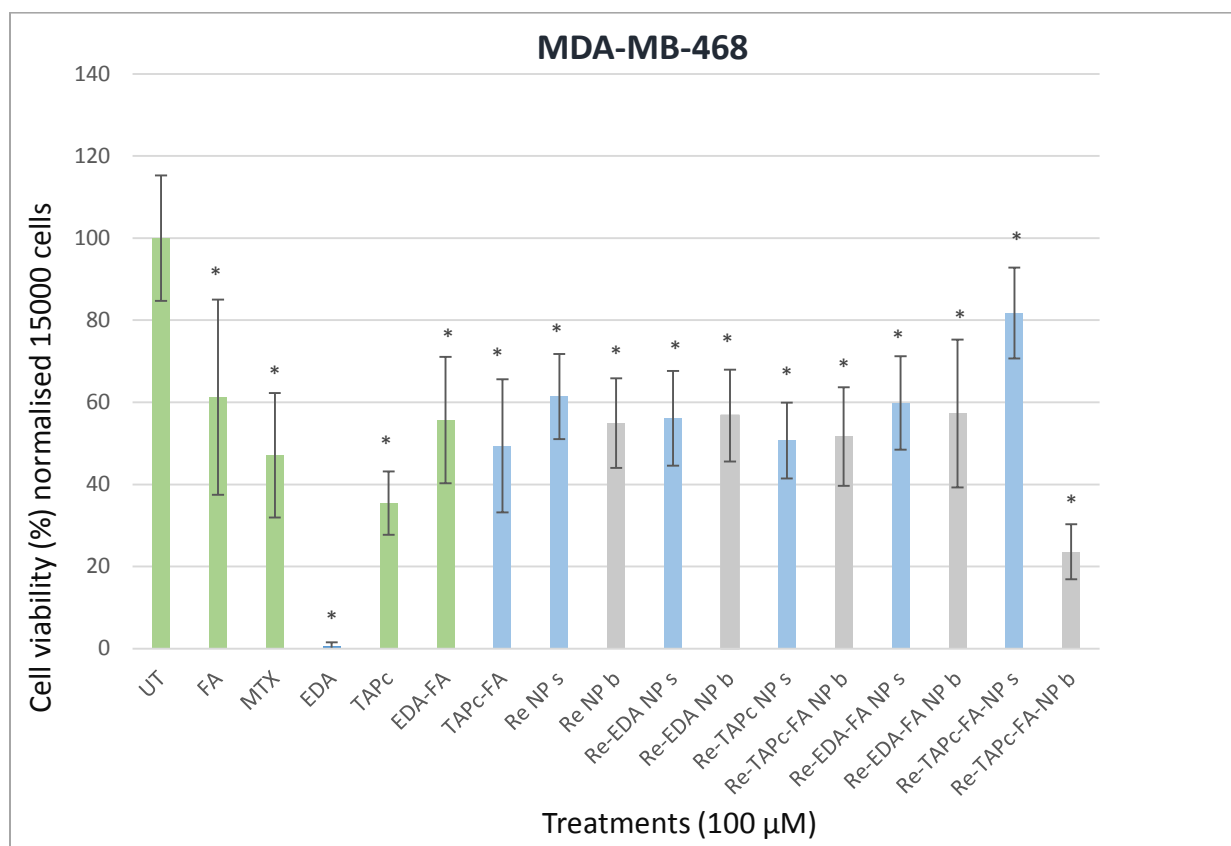


Figure 4.1: The viability profiles of rhenium(III) oxide nanoparticles studied using MDA-MB-468 at 100 µM. Different colors represent the following: controls (green), small-sized nanoparticles (blue) and large (big)- sized nanoparticles (grey). The following compounds were investigated; folate (FA), methotrexate (MTX), ethylenediamine (EDA), tetraaminophthalocyanine (TAPc), ethylenediamine-folate (EDA-FA), tetraaminophthalocyanine-folate (TAPc-FA), small and big-sized sodium borohydride capped nanoparticles (Re NP), small and big-sized ethylenediamine capped nanoparticles (Re-EDA NP), small and big-sized tetraaminophthalocyanine capped nanoparticles (Re-TAPc NP), small and big-sized ethylenediamine-folate capped nanoparticles (Re-EDA-FA NP), and small and big-sized tetraaminophthalocyanine-folate capped nanoparticles (Re-EDA-FA NP). The untreated cells were used as a neutral control, with methotrexate as a positive control. The small-sized nanoparticles are between 1–10 nm and big-sized between 10–100 nm. Statistics analysis was done using ANOVA, $P^* < 0.05$, and 3 experiments were done ($N = 3$) for each cell line.

The first treatment was screened with MDA-MB-468 at 100 μM (**Figure 4.1**) and the cell viability was too low for the study (since the study focuses on the non-cytotoxic concentrations of preferable more than 80% cell viability would be considered as non-toxic) (**Figures 4.2–4.4**) and 10 μM was used in subsequent assays. Thereafter cell viability was determined on the different rhenium(III) oxide nanoparticles obtained at 10 μM concentration showed more than 80% cell viability for MCF-7, MCF-10A and MDA-MB-468 cell lines. For this work, a non-cytotoxic concentration is required and therefore the 10 μM concentration was selected, as this concentration could be used for cell uptake and for *in vivo* studies. A comparison was conducted based on different nanoparticle sizes, bioconjugates and folate receptor that is present on some of the cell lines.

There was a 100% cell viability on the untreated cells for all the cell lines hence they were used as neutral control. MTX (a positive control) as a cancer treatment that is folate analogue showed the expected percentage of cell proliferation (> 80%) for all the cell lines (**Figures 4.2–4.4**). The folate (FA) was used as a control, since this study focuses on the folate conjugate that would introduce the nanoparticles to the folate receptors. Folate on its own did not cause cell death (apoptosis) in all the cell lines. Ethylenediamine-folate (EDA-FA) and tetraaminophthalocyanine-folate conjugate (TAPc-FA) also did not cause cell death which showed that folate favoured all the cell lines even with MDA-MB-468 that did not have folate receptors. A significant effect was observed with EDA, resulted in a low percentage of cell viability. This might be caused by two factors, the cell line does not have folate receptors and it is a triple negative cell line. It does not have estrogen, progesterone, HERS and adenosine receptors as compared with other cell lines, and this may have resulted in it being more reactive with the chelating ethylenediamine.

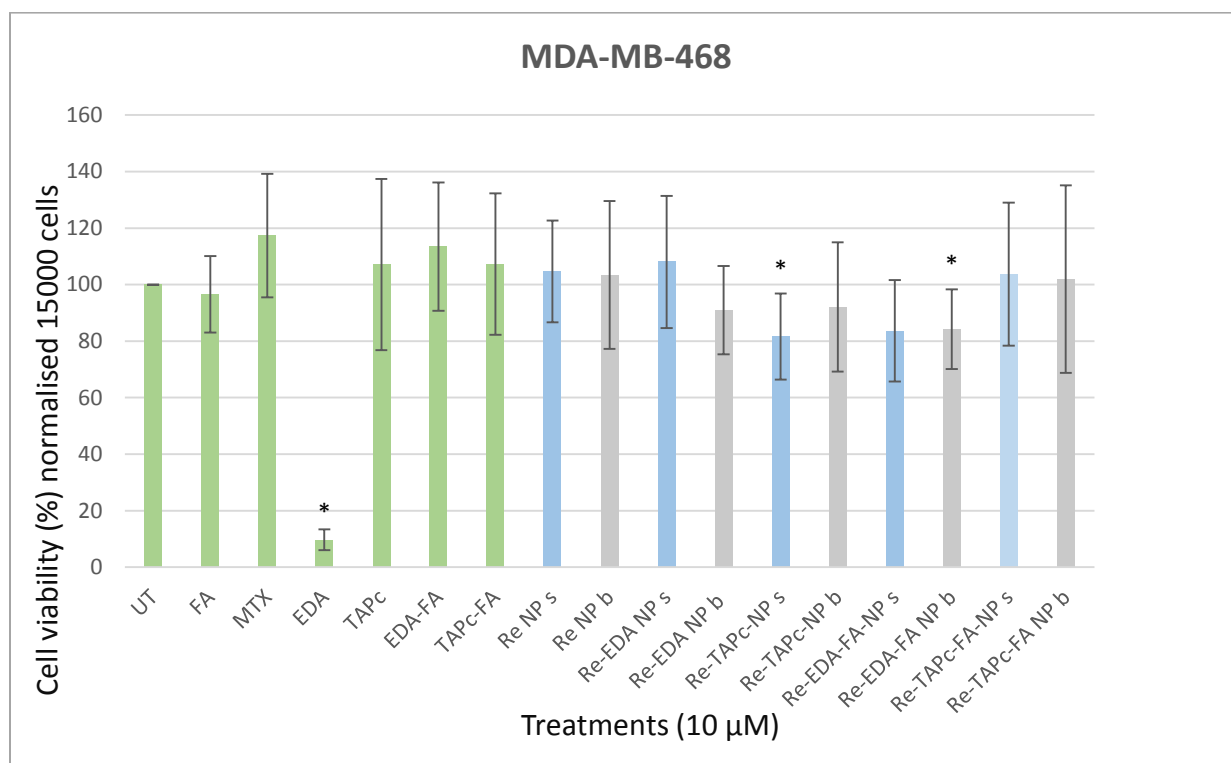


Figure 4.2: The viability profiles of rhenium(III) oxide nanoparticles studied using MDA-MB-468 at 10 μM. Different colors represent the following: controls (green), small-sized nanoparticles (blue) and large (big)- sized nanoparticles (grey). The following compounds were investigated; folate (FA), methotrexate (MTX), ethylenediamine (EDA), tetraaminophthalocyanine (TAPc), ethylenediamine-folate (EDA-FA), tetraaminophthalocyanine-folate (TAPc-FA), small and big-sized sodium borohydride capped nanoparticles (Re NP), small and big-sized ethylenediamine capped nanoparticles (Re-EDA NP), small and big-sized tetraaminophthalocyanine capped nanoparticles (Re-TAPc-NP), small and big-sized ethylenediamine-folate capped nanoparticles (Re-EDA-FA NP), and small and big-sized tetraaminophthalocyanine-folate capped nanoparticles (Re-TAPc-FA NP). The untreated cells were used as a neutral control, with methotrexate as a positive control. The small-sized nanoparticles are between 1–10 nm and big-sized nanoparticles are between 10–100 nm. Statistics analysis was done using ANOVA, $P^* < 0.05$, and 3 experiments were done ($N = 3$) for each cell line.

The MDA-MB-468 cell line (**Figure 4.2**) has no folate receptor. Nanoparticles capped with different capping agents were compared according to their small-sized (1-10 nm) and big-sized nanoparticles (50-100 nm). Nanoparticles capped with sodium borohydride (Re NP s and Re NP b) did not show any toxicity and there was no significant effect on the cell viability of both small and big-sized nanoparticles. The nanoparticles capped with ethylenediamine (Re-EDA NP s and Re-EDA NP b) were compared, these nanoparticles did not cause much of the cell death as the ethylenediamine on its own, although there was a slight difference, a low percentage was observed for the big-sized nanoparticles. It might be possible that large nanoparticles were not washed properly to remove all the free ethylenediamine which were confirmed to be toxic on the MDA-MB-468 cell line. Nanoparticles capped with tetraaminophthalocyanine were compared according to their size (Re-TAPc-NP s and Re-TAPc-NP b), and it was observed that big-sized nanoparticles favour the MDA-MB-468 cell line, since the small-sized nanoparticles had a lower cell viability. Nanoparticles capped with ethylenediamine-folate (Re-EDA-FA NP s and Re-EDA-FA NP b) were compared a significance was observed when comparing them with the untreated cells this might be caused by the toxic free ethylenediamine or ethylenediamine conjugated with folate does not favour this cell line (MDA-MB-468). Nanoparticles capped with tetraaminophthalocyanine-folate (Re-TAPc-FA NP s and Re-TAPc-FA) were compared *via* sizes and there was no significance observed. The effect caused by folate to this non-folate receptor cell line was not significant except that this cell line seems to be aggressive and can react fast with the ethylenediamine.

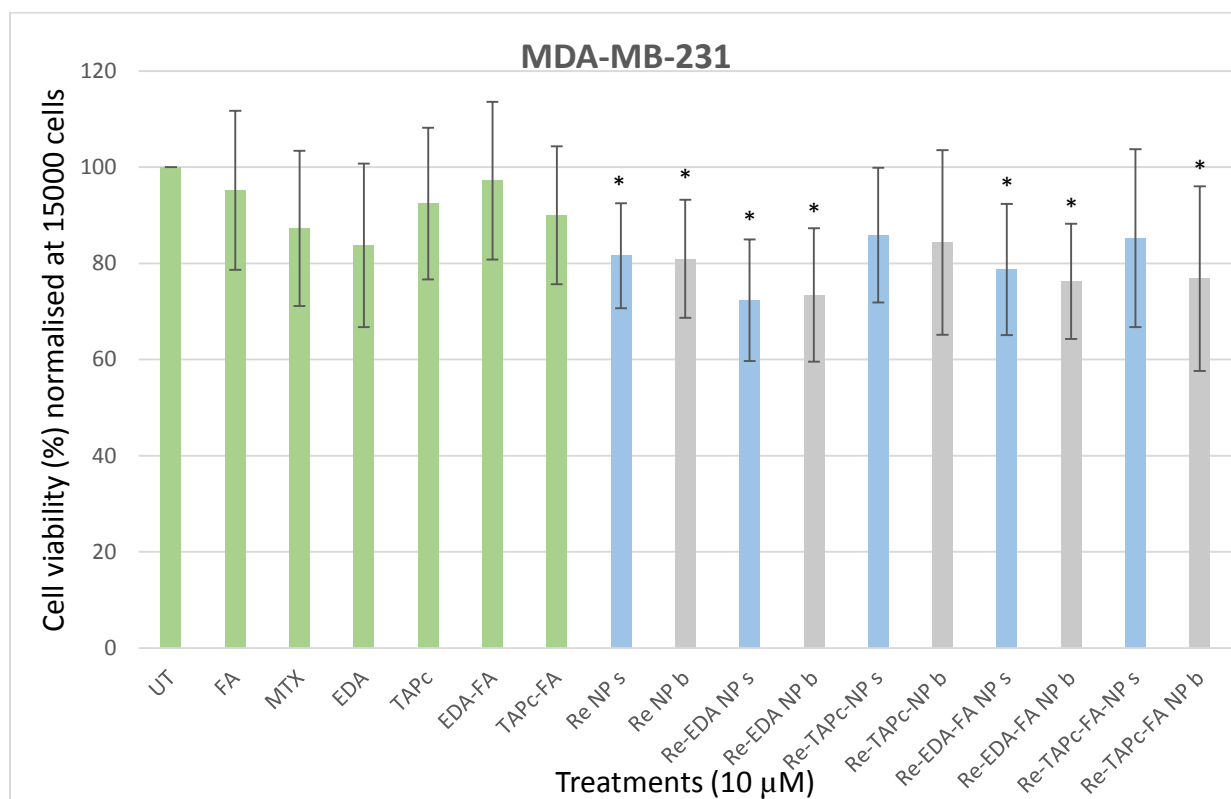


Figure 4.3: The viability profile of rhenium(III) oxide nanoparticles studied using MDA-MB-231 at 10 µM. Different colors represent the following: controls (green), small-sized nanoparticles (blue) and large (big)- sized nanoparticles (grey). The following compounds were investigated; folate (FA), methotrexate (MTX), ethylenediamine (EDA), tetraaminophthalocyanine (TAPc), ethylenediamine-folate (EDA-FA), tetraaminophthalocyanine-folate (TAPc-FA), small and big-sized sodium borohydride capped nanoparticles (Re-NP), small and big-sized ethylenediamine capped nanoparticles (Re-EDA NP), small and big-sized tetraaminophthalocyanine capped nanoparticles (Re-TAPc NP), small and big-sized ethylenediamine-folate capped nanoparticles (Re-EDA-FA NP), and small and big-sized tetraaminophthalocyanine-folate capped nanoparticles (ReTAPc-FA-NP). The untreated cells were used as a neutral control, with methotrexate as a positive control. The small-sized nanoparticles are between 1–10 nm and big-sized between 10–100 nm. Statistics analysis was done using ANOVA, $P^* < 0.05$, and 3 experiments were done ($N = 3$) for each cell line.

MDA-MB-231 (**Figure 4.3**) cell line has folate receptors; and nanoparticles possible entered the cells through a process called receptor-mediated endocytosis. This occurs when the membrane starts wrapping up the nanoparticle slowly until it is fully inside. Nanoparticles capped with sodium borohydride (Re NP s and Re NP b) did not show any toxicity and there was no significance effect on the cell viability of both small and big-sized nanoparticles, although a significant effect was observed when comparing the cell viability to the untreated cells. The nanoparticles capped with ethylenediamine (Re-EDA-NP s and Re-EDA-NP b) were compared, a significant effect was observed when comparing them with untreated cells, a low percentage of cell viability was observed for both sized nanoparticles. It might be possible that both small and big-sized nanoparticles when they are capped with ethylenediamine they turn to decrease the cell viability of the MDA-MB-231 cells, since the MDA-MB-231 (**Figure 4.4**) cell line is considered to be triple-negative breast cancers and it might be that these cells they more sensitive with ethylenediamine. Nanoparticles capped with tetraaminophthalocyanine were investigated according to their size (Re-TAPc-NP s and Re-TAPc-NP b), there was no significant effect observed. Nanoparticles capped with ethylenediamine-folate (Re-EDA-FA NP s and Re-EDA-FA NP b) were compared and a significant effect was observed when comparing them with the untreated cells. Nanoparticles capped with tetraaminophthalocyanine-folate (Re-TAPc-FA NP s and Re-TAPc-FA NP b) were compared, there was no significant effect observed on small-sized nanoparticles, but a significant effect was observed on the big-sized nanoparticles. The effect caused by folate to this folate receptor cell line was significant and this cell line seems to be more sensitive when treated with compounds conjugated with folate.

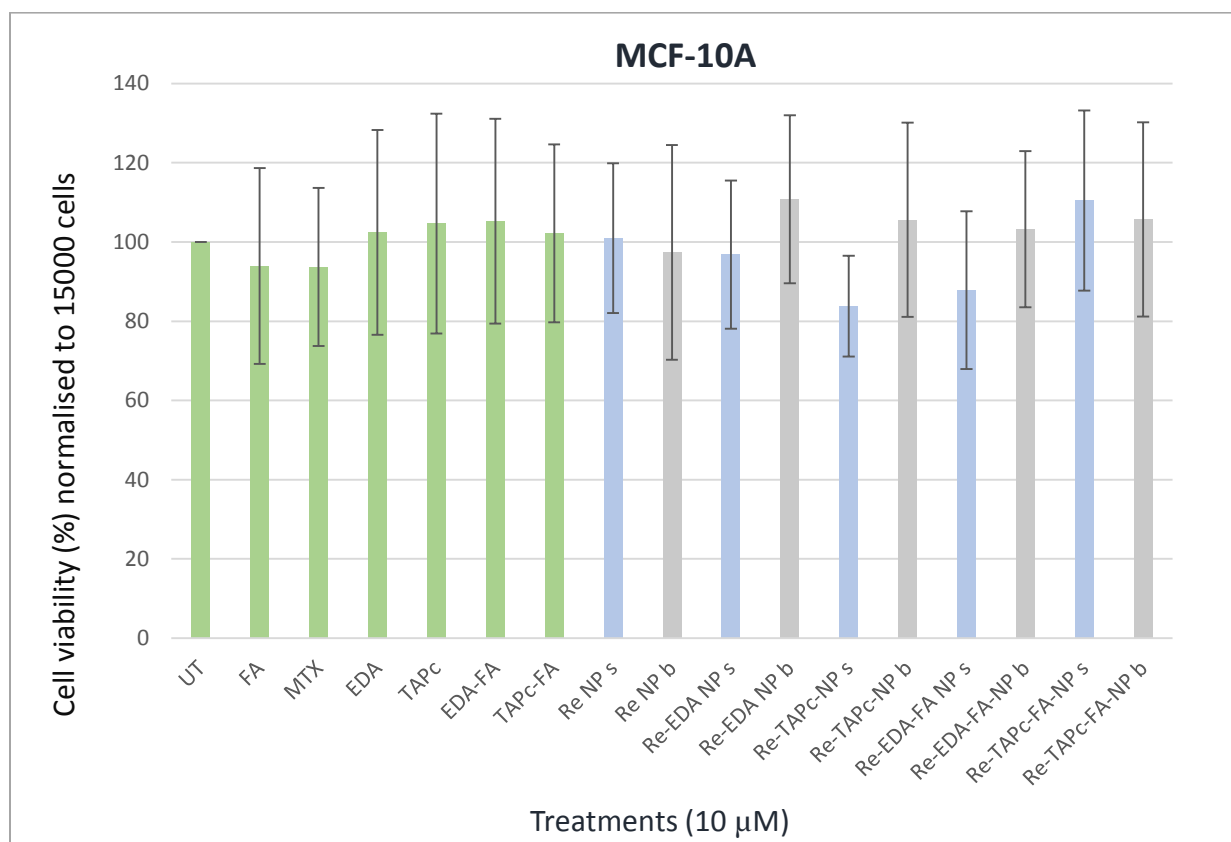


Figure 4.4: The viability profiles of rhenium(III) oxide nanoparticles studied using MCF-10A at 10 µM. Different colors represent the following: controls (green), small-sized nanoparticles (blue) and large (big)- sized nanoparticles (grey). The following compounds were investigated; folate (FA), methotrexate (MTX), ethylenediamine (EDA), tetraaminophthalocyanine (TAPc), ethylenediamine-folate (EDA-FA), tetraaminophthalocyanine-folate (TAPc-FA), small and big-sized sodium borohydride capped nanoparticles (Re NP), small and big-sized ethylenediamine capped nanoparticles (Re-EDA NP), small and big-sized tetraaminophthalocyanine capped nanoparticles (Re-TAPc NP), small and big-sized ethylenediamine-folate capped nanoparticles (Re-EDA-FA NP), and small and big-sized tetraaminophthalocyanine-folate capped nanoparticles (Re-TAPc-FA NP). The untreated cells were used as a neutral control, with methotrexate as a positive control. The small-sized nanoparticles are between 1–10 nm and big-sized nanoparticles are between 10–100 nm. Statistics analysis was done using ANOVA, $P^* < 0.05$, and 3 experiments were done ($N = 3$) for each cell line. All the treatments showed no significant deviation.

MCF-10A cell line (**Figure 4.4**) has folate receptors, and nanoparticles could be considered to be taken up by cells through a process called receptor-mediated endocytosis. Nanoparticles capped with sodium borohydride (Re NP s and Re NP b) did not show any toxicity, and there was no significant difference for the cell viability of both small and big-sized nanoparticles. The nanoparticles capped with ethylenediamine (Re-EDA NP s and Re-EDA NP b) were compared, and a low percentage of cell viability was observed for small-sized nanoparticles as compared to the big-sized nanoparticles. The same sequence was observed for the nanoparticles capped with ethylenediamine-folate (Re-EDA-FA NP s and Re-EDA-FA-NP b) and tetraaminophthalocyanine (Re-TAPc-NP s and Re-TAPc-NP b); ie small-sized nanoparticles seem to have a decreased cell viability than the big-sized nanoparticles in MCF-10A. Nanoparticles capped with tetraaminophthalocyanine-folate (Re-TAPc-FA NP s and Re-TAPc-FA NP b) were compared *via* sizes and there was no significant difference observed. The effect caused by folate to this folate receptor cell line was significant. The nanoparticles were compared according to the ones that are capped with the folate conjugate and the ones that were not conjugated with folate. It was observed that nanoparticles capped with ethylenediamine when they are capped with ethylenediamine-folate, a lower percentage of cells were deemed viable was and *vice-versa* when the nanoparticles were capped with tetraaminophthalocyanine-folate instead of tetraaminophthalocyanine, where more cells survived.

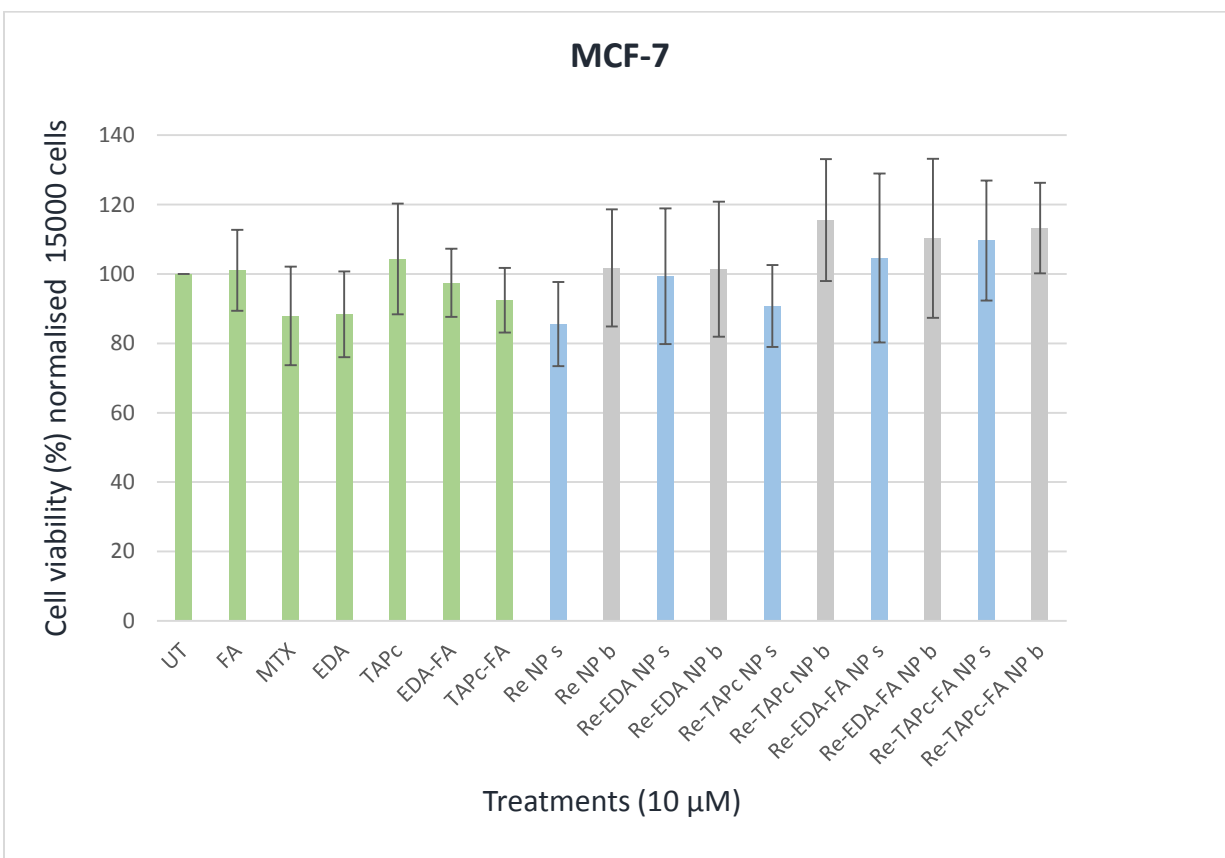


Figure 4.5 The viability profiles of rhenium(III) oxide nanoparticles studied using MCF-7 at 10 µM. Different colors represent the following: controls (green), small-sized nanoparticles (blue) and large (big)- sized nanoparticles (grey). The following compounds were investigated; folate (FA), methotrexate (MTX), ethylenediamine (EDA), tetraaminophthalocyanine (TAPc), ethylenediamine-folate (EDA-FA), tetraaminophthalocyanine-folate (TAPc-FA), small and big-sized sodium borohydride capped nanoparticles (Re NP), small and big-sized ethylenediamine capped nanoparticles (Re-EDA NP), small and big-sized tetraaminophthalocyanine capped nanoparticles (Re-TAPc NP), small and big-sized ethylenediamine-folate capped nanoparticles (Re-EDA-FA NP), and small and big-sized tetraaminophthalocyanine-folate capped nanoparticles (Re-TAPc-FA-NP). The untreated cells were used as a neutral control, with methotrexate as a positive control. The small-sized nanoparticles are between 1–10 nm and big-sized nanoparticles are between 10–100 nm. Statistics analysis was done using ANOVA, $P^* < 0.05$, and 3 experiments were done ($N = 3$) for each cell line. All the treatments for this cell line showed no significant deviation.

MCF-7 cell line (**Figure 4.5**) has folate receptors, and nanoparticles were considered taken by the cells through a process called receptor-mediated endocytosis. Nanoparticles capped with sodium borohydride (Re NP s) did show a decrease in cell viability for small-sized nanoparticles as compared with big-sized nanoparticles (Re NP b). The nanoparticles capped with ethylenediamine (Re-EDA NP s and Re-EDA NP b) were compared, no significant effect was observed. A low percentage of cell viability was observed for small-sized nanoparticles as compared to the large sized nanoparticles for ethylenediamine-folate (Re-EDA-FA NP s and Re-EDA-FA NP b), and the same sequence was observed for the nanoparticles capped with tetraaminophthalocyanine (Re-TAPc NP s and Re-TAPc NP b) and tetraaminophthalocyanine-folate (Re-TAPc-FA NP s and Re-TAPc-FA NP b). Small-sized nanoparticles seem to be toxic than the big-sized nanoparticles in MCF-7. The effect of folate to this folate receptor cell line was significant. The nanoparticles were compared according to ones that are capped with folate conjugate and the ones that are not conjugated with folate, it was observed that when the nanoparticles were capped with ethylenediamine, it resulted into a low cell viability percentage but when the nanoparticles were conjugated with folate, a high percentage of cells were viable and the same sequence was observed when the nanoparticles were capped with tetraaminophthalocyanine-folate instead of tetraaminophthalocyanine.

4.1.2 General conclusion

Table 4.2: Overall comparison on how the different cell lines responded to the control treatments. Results are presented in % viability of cells.

Cell line	FA	MTX	EDA	TAPc	EDA-FA	TAPc-FA
MDA-MB-468	97	117	10	107	113	107
MDA-MB-231	95	87	84	92	97	90
MCF-10A	94	94	102	105	105	102
MCF-7	101	88	88	104	97	92

Table 4.3: Overall comparison on how the different cell lines responded to the nanoparticle's treatments. Results are presented in % viability of cells.

Re NP s	Re NP b	Re-EDA NP s	Re-EDA NP b	Re-TAPc NP s	Re-TAPc NP b	Re-EDA-FA NP s	Re-EDA-FA NP b	Re-TAPc-FA NP s	Re-TAPc-FA NP b
107	103	108	91	82	92	84	84	104	102
82	81	72	73	86	84	79	76	85	77
101	97	97	111	84	106	88	103	110	106
86	102	99	101	91	116	105	110	110	113

*MDA-MB-468 (non-folate receptors), MDA-MB-231 (folate receptor), MCF-10A (folate receptor), MCF-7 (folate receptor), nanoparticles.

In summary all the cell lines were compared, it was observed that MCF-7 (tumorigenic breast cell line) had high percentage of cell viability especially when the cells were treated with folate conjugated nanoparticles. Further investigation was done on the effects of folate conjugate and the effects of size, it was observed that tetraaminophthalocyanine-folate (TAPc-FA) had a high cell viability as compared to the ethylenediamine-folate (EDA-FA) in MCF-7, more especially when treated with large sized nanoparticles.

Due to the nature of the treatise, the investigation of the localisation of nanoparticles on cancer cells by TEM and micro-SPECT kits and model mice (using the "hot" isotopes of rhenium in a radiopharmacy laboratory) is currently being done as part of the bigger scope of the project. This mini thesis has presented only work achieved up to cell viability studies.

Chapter 5 : Conclusion, recommendations, and future work

5.1 Conclusion

Capping agents: Functionalization of the diamines at one end was required to ensure the production of monofunctionalised diamines, to allow the functional molecules (receptors) to bind at one end, so that the other end is free to bind to the solid surface of the nanoparticle. Both tetraaminophthalocyanines and diamines were linked with a biomolecule (folic acid) to enable and enhance the targeting ability of the nanoparticles. The capping agents (tetraaminophthalocyanine, ethylenediamine-folate and tetraaminophthalocyanine-folate) were prepared and characterized by UV-Vis, FT-IR, NMR and LC-MS to confirm their structure. The synthesis of the EDA-FA conjugate, which involved the amidation and BOC deprotection, was confirmed using FT-IR spectroscopy. The essential peaks (for N-H and C=O stretching vibrations), showed evidence of structural changes in *N*-BOC-EDA-FA and EDA-FA. UV-Vis spectroscopic characterization serves as the characterization of the absorption spectrum for the conjugate and it only confirmed the folate that was present in ethylenediamine and *N*-boc-ethylenediamine with similar spectra but did not prove the deprotection step. Thus, the success of the synthesis was also confirmed using $^1\text{H-NMR}$, which also highlighted structural changes, and LC-MS confirmed the molecular ions of the compounds. The synthesis of the TAPc-FA was also confirmed by UV-Vis and LC-MS.

Rhenium(III) oxide nanoparticles: The size of nanoparticle governs its interactions with biological systems, including absorption, distribution, cellular internalization, metabolism, and excretion [15]. Nanoparticles with a diameter of 50 nm are more efficiently internalized by cells than smaller (about 15–30 nm) or larger (about 70–240 nm) particles. Nanoparticles with a diameter of 30–50 nm efficiently recruit and interact with membrane receptors and are subsequently taken up by receptor-mediated endocytosis [141]. Therefore, to be an effective drug carrier, the nanoparticle should have a diameter of 10–150 nm. This size range will ensure longer circulation time and increased accumulation in the interstitial cell tumour [142].

The synthesis of rhenium(III) oxide nanoparticles was achieved by employing sodium borohydride as a two-electron reducing agent, capped with the phthalocyanines and ethylenediamine conjugated to folate. The nanoparticles were characterized with UV-Vis and, spectrofluorimetry, TEM and Zeta potential. Nanoparticles between 10 and 100 nm were envisaged as suitable for applications in biological systems. For particles to be considered stable and suitable for the cells, the Zeta potential must be between -30 and +30 Mv. Re_2O_3 NPs capped with sodium borohydride were found to be unstable with Zeta potential of -49 mV in comparison to the NPs capped with ethylenediamine (-18.6 mV).

Biological studies: Nanoparticles can readily interact with biomolecules both at surface and inside cells, yielding better signals and target specificity for diagnostics and therapeutics. The biological studies were performed to establish if the biological responses would be induced by rhenium(III) oxide nanoparticles on several cancer cell lines, that are distinguished by variation in the receptor, with specific focus on the folate receptor. Cytotoxicity investigation of the rhenium(III) oxide nanoparticles was done on MDA-MB-468, MDA-MB-231, MCF-10A (non-tumourigenic) and MCF-7 cells lines. The cell viability on the different rhenium(III) oxide nanoparticles obtained at 10 μM concentration showed more than 80% cell viability for MCF-7, MCF-10A and MDA-MB-468 cell lines, since the study focuses on the non-cytotoxicity concentrations of preferable more than 80% cell viability. A comparison was conducted based on different nanoparticle sizes, capping agents especially bioconjugates across the four cell lines and the folate receptor in some of the cell lines. All the cell lines were compared, it was observed that MCF-7 (tumorigenic breast cell line) had a high percentage of cells viable when the cells were treated with folate conjugated nanoparticles. Further investigation was done on the effects of folate conjugate and the effects of size, it was observed that tetraaminophthalocyanine-folate favoured the MCF-7, more especially when treated with large sized nanoparticles. The promising results of MCF-7 treated with nanoparticles capped with tetraaminophthalocyanine-folate (Re-TAPc-FA NP s and Re-TAPc-FA NP b) require additional experiment to be completed. In future studies the uptake of the nanoparticles into

the cells using TEM and ICP and micro-SPECT kits and model mice (using the “hot” isotopes of rhenium in a radiopharmacy laboratory) will be completed.

5.2 Recommendations and future work

Recommendations:

- Using ligands that can cause significant change in the fluorescent properties so that it can increase chances of the nanoparticles being used for imaging and therapy.
- Some successes were observed in this study, the synthesis of rhenium(III) oxide nanoparticles capped with conjugated folate phthalocyanine and ethylenediamine, tested on four different breast cancer cell lines (MCF-7, MCF-10A, MDA-MB-231 and MDA-MB-468). However, a few alterations maybe required to increase the efficacy of the NPs, this may include changing the capping agents or changing the stabilizers for instance the use of different diamine linker molecules such as polymers can be explored. Polymers would provide better capping compared to the smaller diamines. They also pose reduced purification challenges and few unexpected side products during bioconjugation.
- The rhenium(III) oxide nanoparticles: were found to be stable for approximately three weeks, thus, for these nanoparticles to be used as a potential therapeutic agent, it would be recommended that using stabilizing agents for their stability for the use in a biological study.

Future work:

- The use of XPS technique to characterize further the rhenium(III) oxide nanoparticles in order to confirm the oxidation state of rhenium.
- The investigation of tumour internalization ability of the rhenium(III) oxide nanoparticles capped with ethylenediamine-folate and tetraaminophthalocyanine-folate using TEM and ICP studies.
- The tumour and organ biodistribution studies of the nanoparticles would be completed using micro-SPECT kits and model mice (using the “hot” isotopes of rhenium in a radiopharmacy laboratory).

REFERENCES

- [1] F. R. Schram and P. K. L. Ng, "What is Cancer?," *J. Crustac. Biol.*, vol. 32, no. 4, pp. 665–672, 2012.
- [2] A Sudhakar, "History of Cancer, Ancient and Modern Treatment Methods Akulapalli," *J Cancer Sci Ther.*, vol. 1, no. 2, pp. 1–4, 2010.
- [3] A. Caraceni and S. M. Weinstein, "Classification of cancer pain syndromes.," *Oncology (Williston Park)*. vol. 15, no. 12, pp. 1642–3, 2001.
- [4] P. Barros-Núñez, M. A. Rosales-Reynoso, and C. I. Juárez-Vázquez, *The classification, mechanisms of activation and roles in cancer development of oncogenes*. pp. 1–2, 2013.
- [5] V. Thomas, B. Mathew, D. R. Dean, and E. Nyairo, *Biodegradable polymeric nano-biomaterials for cancer therapeutic applications*. pp. 445–474, 2012.
- [6] K. Schneider, "Cell Biology and Cancer," *Couns. about cancer Strateg. Genet. Couns.*, pp. 1–17, 2001.
- [7] R. L. Siegel, K. D. Miller, and A. Jemal, "Cancer statistics, 2018," *CA. Cancer J. Clin.*, vol. 68, no. 1, pp. 7–30, 2018.
- [8] A. Wicki, D. Witzigmann, V. Balasubramanian, and J. Huwyler, "Nanomedicine in cancer therapy: Challenges, opportunities, and clinical applications," *J. Control. Release*, vol. 200, pp. 138–157, 2015.
- [9] D. A. Vorobiof, F. Sitas, and G. Vorobiof, "Breast cancer incidence in South Africa.," *J. Clin. Oncol.*, 2001.
- [10] H. Van Oers and L. Schlebusch, "Anxiety and the patient with breast cancer: a review of current research and practice," *South African Fam. Pract.*, 2013.
- [11] R. L. Siegel, K. D. Miller, and A. Jemal, "Cancer statistics," *CA Cancer J Clin*, vol. 66, no. 1, pp. 7–30, 2016.
- [12] B. N. Ames and L. S. Gold, "The causes and prevention of cancer: the role of environment," *Biotherapy*, vol. 11, no. 2–3, pp. 205–220, 1998.
- [13] E. J. BENZ, "The Jeremiah Metzger Lecture Cancer in the Twenty-First Century: An Inside View from an Outsider.," *Trans. Am. Clin. Climatol. Assoc.*, vol. 128, no. 2, pp. 275–297,

- 2017.
- [14] E. G. Jones, "Eli G. Jones Cancer - Its Causes, Symptoms and Treatment." pp. 302, 2014.
- [15] I. Brigger, C. Dubernet, and P. Couvreur, "Nanoparticles in cancer therapy and diagnosis," *Advanced Drug Delivery Reviews*, vol. 54, no. 5. pp. 631–651, 2002.
- [16] K. Hayashi, M. Zhao, K. Yamauchi, N. Yamamoto, H. Tsuchiya, K. Tomita and R. Hoffman "Cancer metastasis directly eradicated by targeted therapy with a modified Salmonella typhimurium," *J. Cell. Biochem.*, vol. 106, no. 6, pp. 992–998, 2009.
- [17] J. B. Engel, A. V. Schally, G. Halmos, B. Baker, A. Nagy, and G. Keller, "Targeted therapy with a cytotoxic somatostatin analog, AN-238, inhibits growth of human experimental endometrial carcinomas expressing multidrug resistance protein MDR-1," *Cancer*, vol. 104, no. 6, pp. 1312–1321, 2005.
- [18] M. Partridge, E. Phillips, R. Francis, and S. R. Li, "Immunomagnetic separation for enrichment and sensitive detection of disseminated tumour cells in patients with head and neck SCC.," *J. Pathol.*, vol. 189, no. 3, pp. 368–77, 1999.
- [19] F. Vlems, J. Diepstra, C. Punt, M. Ligtenberg, I. Cornelissen, J. van Krieken, T. Wobbles, G. van Muijen and T. Ruers, "Detection of disseminated tumour cells in blood and bone marrow samples of patients undergoing hepatic resection for metastasis of colorectal cancer.," *Br. J. Surg.*, vol. 90, no. 8, pp. 989–995, 2003.
- [20] B. Azadbakht, H. Afarideh, M. Ghannadi-maragheh, A. Bahrami-samani, and M. Asgari, "PT," *Nucl. Med. Biol.*, vol. 48, pp 26–30, 2016.
- [21] S. J. P. Jonathan R. Dilworth, "The biomedical chemistry of technetium and rhenium," *Chem. Soc. Rev.*, vol. 27, pp. 43–55, 1998.
- [22] E. Deutsch, K. Libson, J. L. Vanderheyden, A. R. Ketrings, and H. R. Maxon, "The chemistry of rhenium and technetium as related to the use of isotopes of these elements in therapeutic and diagnostic nuclear medicine," *Int. J. Radiat. Appl. Instrumentation.*, vol. 13, no. 4, pp. 465–477, 1986.
- [23] M. Assadi, K. Afrasiabi, I. Nabipour, and M. Seyedabadi, "Nanotechnology and nuclear medicine; research and preclinical applications," *Hell. J. Nucl. Med.*, vol. 14, no. 2, pp. 149–198, 2011.

- [24] F. Alexis, E. Pridgen, L. K. Molnar, and O. C. Farokhzad, "Factors affecting the clearance and biodistribution of polymeric nanoparticles," *Mol. Pharmaceutics*, vol. 5, no. 4, pp 505–515, 2008.
- [25] W. T. Tysoe and N. D. Spencer, "Novel nano-carbons," *Tribol. Lubr. Technol.*, vol. 64, no. 10, pp. 72, 2008.
- [26] R. W. Siegel, "Nanomaterials: synthesis, properties and applications," *Nanomater. Synth. Prop. Appl.*, vol. 32, no. 2, pp 201–218, 1996.
- [27] V. V. Narayanan and G. R. Newkome, "Supramolecular chemistry within dendritic structures," *Dendrimers*, vol. 197 pp. 19–77, 1998.
- [28] A. Gentile, F. Ruffino, and M. Grimaldi, "Complex-Morphology Metal-Based Nanostructures: Fabrication, Characterization, and Applications," *Nanomaterials*, vol. 6, no. 6, p. 110, 2016.
- [29] F. X. Gu, R. Karnik, A. Wang, F. Alexis, E. Levy-Nissenbaum, S. Hong, R. Langer and O. Farokhzad, "Targeted nanoparticles for cancer therapy," vol. 2, no. 3 pp. 14–21, 2007.
- [30] G. L. Zwicke, G. Ali Mansoori, and C. J. Jeffery, "Utilizing the folate receptor for active targeting of cancer nanotherapeutics," *Nano Rev.*, vol. 3, no 1, p. 18496, 2012.
- [31] S. Rajesh, W. James, J. R. Lillard, "Nanoparticle-based targeted drug delivery," *Exp. Mol. Pathol.*, vol. 86, no. 3, pp. 215–223, 2009.
- [32] P. Tiwari, K. Vig, V. Dennis, and S. Singh, "Functionalized Gold Nanoparticles and Their Biomedical Applications," *Nanomaterials*, vol. 1, no. 1, pp. 31–63, 2011.
- [33] F. Wypych, N. Seefeld, and I. Denicolo, "Preparation of nanocomposites based on the encapsulation of conducting polymers into 2H-MoS₂ and 1T-TiS₂," *Quim. Nova*, vol. 20, no. 4, pp. 356–360, 1997.
- [34] I. Freestone, N. Meeks, M. Sax, and C. Higgitt, "The Lycurgus Cup — A Roman nanotechnology," *Gold Bull.*, vol. 40, no. 4, pp. 270–277, 2007.
- [35] J. K. Patra and K. H. Baek, "Green Nanobiotechnology: Factors Affecting Synthesis and Characterization Techniques," *J. Nanomater.*, vol. 2014, no. 12, pp. 1–12, 2014.
- [36] C. Underwood, A. Eps, J. Dearling, A. Packard, C. Burke, J. Soo, A. Kim, Y. Hsiang, A. Klibanov, J. Hanes, R. Price, K. Strebhardt, A. Ullrich, K. Whitehead, R. Langer, D.

- Anderson, N. Idris, M. Gnanasammandhan, J. Zhang, P. Ho, R. Mahendran, B. Haley, E. Frenkel, J. Jiang, G. Oberdörster, A. Elder, R. Gelein, P. Mercer, P. Biswas, S. Horikoshi and N. Serpone, "Introduction to Nanoparticles," *Nanotoxicology*, vol. 26, no. 1, pp. 57–64, 2008.
- [37] D. Schaming and H. Remita, "Nanotechnology: from the ancient time to nowadays," *Found. Chem.*, vol. 17, no. 3, pp. 187–205, 2015.
- [38] P. Balaya, "Size effects and nanostructured materials for energy applications," *Energy Environ. Sci.*, vol. 1, no. 6, p. 645, 2008.
- [39] P. H. Cury Camargo, K. G. Satyanarayana, and F. Wypych, "Nanocomposites: Synthesis, Structure, Properties and New Application Opportunities," *Mater. Res. J. Mater.*, vol. 12, no. 1 pp. 1-39, 2009.
- [40] Z. Husain and M. Husain, "Carbon nanotube and its possible applications," *Indian J. Eng. Mater. Sci.*, vol. 12, no. 12, pp. 529–551, 2005.
- [41] T. Panigrahi, "Synthesis and characterization of silver nanoparticles using leaf extract of *Azadirachta indica*," *Dep. Life Sci. Natl. Inst. Technol. Rourkela-769008, Orissa, India*, 2013.
- [42] R. Nagarajan and T. A. Hatton, *Nanoparticles: Synthesis, Stabilization, Passivation, and Functionalization*. vol. 996, pp. 451, 2008.
- [43] H. R. Abid, G. H. Pham, H.-M. Ang, M. O. Tade, and S. Wang, "Journal of Colloid and Interface Science," *J. Colloid Interface Sci.*, vol. 366, no. 1, pp. 621–630, 2012.
- [44] J. B. Castor, S.B., Hendrick, "Rare Earth Elements," *Ind. Miner. Rocks Commod. Mark. Uses*, pp. 769–792, 2006.
- [45] R. Nagarajan, "Nanoparticles: Building blocks for nanotechnology," in *ACS Symposium Series*, vol. 996, pp. 2–14, 2008.
- [46] I. Brigger, C. Dubernet, and P. Couvreur, "Nanoparticles in cancer therapy and diagnosis," *Adv. Drug Deliv. Rev.*, vol. 54, no.5, pp. 631–651, 2002.
- [47] J. Jiang, G. Oberdörster, and P. Biswas, "Characterization of size, surface charge, and agglomeration state of nanoparticle dispersions for toxicological studies," *J. Nanoparticle Res.*, vol. 11, no. 1, pp. 77–89, 2009.

- [48] S. Zhang *et al.*, "Size Dependent Endocytosis of Nanoparticles," *Adv. Mater.*, vol. 21, no. 4, pp. 419–424, 2009.
- [49] H. Kettiger, A. Schipanski, P. Wick, and J. Huwyler, "Engineered nanomaterial uptake and tissue distribution: From cell to organism," *Int. J. Nanomedicine*, vol. 8, pp. 3255–3269, 2013.
- [50] B. Haley and E. Frenkel, "Nanoparticles for drug delivery in cancer treatment," *Urol. Oncol. Semin. Orig. Investig.*, vol. 26, no. 1, pp. 57–64, 2008.
- [51] C. Link, F. Alexis, E. Pridgen, and L. K. Molnar, "reviews Factors Affecting the Clearance and Biodistribution of," *Mol. Pharm.*, vol. 5, no. 4, pp. 505–515, 2008.
- [52] S. D. Steichen, M. Caldorera-Moore, and N. A. Peppas, "A review of current nanoparticle and targeting moieties for the delivery of cancer therapeutics," *Eur. J. Pharm. Sci.*, vol. 48, no. 3, pp. 416–427, 2013.
- [53] N. Bertrand and J. Leroux, "The journey of a drug-carrier in the body : An anatomophysiological perspective" *J. Control. Release*, vol. 161, no. 2, pp. 152–163, 2012.
- [54] J. Wu, X. Xu, N. Kamaly, and C. Link, "Cancer nanotechnology : The impact of passive and active targeting in the era of modern cancer biology" *Adv. Drug Deliv. Rev.* vol. 66, pp. 2–25, 2014.
- [55] K. Strebhardt and A. Ullrich, "Paul Ehrlich's magic bullet concept: 100 years of progress," vol. 8, no.6, pp. 473–480, 2008.
- [56] M. E. Davis, J. Zuckerman, C. Choi, D. Seligson, A. Tolcher, C. Alabi, Y. Yen, J. Heidel, and A. Ribas, "Evidence of RNA in humans from systemically administered siRNA *via* targeted nanoparticles," *Nature*, vol. 464, no. 7291, pp. 1067–1070, 2010.
- [57] J. E. Kipp, "The role of solid nanoparticle technology in the parenteral delivery of poorly water-soluble drugs," vol. 284, pp. 109–122, 2004.
- [58] K. A. Whitehead, R. Langer, and D. G. Anderson, "Knocking down barriers: advances in siRNA delivery," vol. 8, no. 2, pp. 129–138, 2009.
- [59] A. Babu, A. K. Templeton, A. Munshi, and R. Ramesh, "Nanodrug Delivery Systems: A Promising Technology for Detection, Diagnosis, and Treatment of Cancer," *AAPS PharmSciTech*, vol. 15, no. 3, pp. 709–721, 2014.

- [60] L. D. Leserman, J. N. Weinstein, R. Blumenthal, and W. D. Terry, "Receptor-mediated endocytosis of antibody-opsionized liposomes by tumour cells," vol. 77, no. 7, pp. 4089–4093, 2014.
- [61] J. L. Steegmann-Olmedillas, "The role of iron in tumour cell proliferation," *Clin Transl Oncol*, vol. 13, no. 2, pp. 71–76 2011.
- [62] G. J. Weiss, J. Chao, J. D. Neidhart, R. K. Ramanathan, D. Bassett, J. A. Neidhart, C. J. Choi, W. Chow, V. Chung, S. J. Forman, E. Garmey, J. Hwang, D. L. Kalinoski, M. Koczywas, J. Longmate, R. J. Melton, R. Morgan, J. Oliver, J. J. Peterkin, J. L. Ryan, T. Schlupe, T. W. Synold, P. Twardowski, M. E. Davis, and Y. Yen, "First-in-human phase 1/2a trial of CRLX101, a cyclodextrin-containing polymer-camptothecin nanopharmaceutical in patients with advanced solid tumour malignancies," *Invest. New Drugs*, vol. 31, no. 4, pp. 986–1000, 2013.
- [63] R. Wang, P. S. Billone, and W. M. Mullett, "An overview of the marine natural products in clinical trials and on the market," *J. Coast. Life Med.*, vol. 3, no. 6pp. 471–477, 2015.
- [64] K. D. Steffensen, M. Waldstrøm, N. Pallisgård, B. Lund, K. Bergfeldt, J. Wihl, N. Keldsen, C. Marth, I. Vergote and A. Jakobsen, "Panitumumab and pegylated liposomal doxorubicin in platinum-resistant epithelial ovarian cancer with KRA wild-type," *PaLiDo Study, a Phase II Nonrandomized Multicent. Study*, vol. 23, no. 1, pp. 73–80, 2013.
- [65] W. J. Gradishar, S. Tjulandin, N. Davidson, H. Shaw, N. Desai, P. Bhar, M. Hawkins and J. O'Shaughnessy, "Phase III trial of nanoparticle albumin-bound paclitaxel compared with polyethylated castor oil-based paclitaxel in women with breast cancer," *J. Clin. Oncol.*, vol. 23, no. 31, pp. 7794–7803 2005.
- [66] R. L. Coleman, W. Brady, D. McMeekin, P. Rose, J. Soper, S. Lentz, J. Hoffman and M. Shahin, "A phase II evaluation of nanoparticle, albumin-bound (nab) paclitaxel in the treatment of recurrent or persistent platinum-resistant ovarian, fallopian tube, or primary peritoneal cancer: A Gynecologic Oncology Group Study," *Gynecol. Oncol.*, vol. 122, no. 1, pp. 111–115, 2011.
- [67] P. J. Hosein, G. de Lima Lopes, V. Pastorini, C. Gomez, J. Macintyre, G. Zayas, I. Reis, A. Montero A, J. Merchan, C. Rocha Lima, G. De, L. Lopes and C. Lima, "A Phase II Trial of

- nab-Paclitaxel as Second-line Therapy in Patients With Advanced Pancreatic Cancer,” *Am. J. Clin. Oncol.*, vol. 36, no. 2, pp. 1, 2012.
- [68] M. A. Socinski, I. Bondarenko, N. Karaseva, A. Makhson, I. Vynnychenko, I. Okamoto, J. Hon, V. Hirsh, P. Bhar, H. Zhang, J. Iglesias and M. Renschler, “Weekly nab-paclitaxel in combination with carboplatin versus solvent-based paclitaxel plus carboplatin as first-line therapy in patients with advanced non-small-cell lung cancer: final results of a phase III trial.,” *J. Clin. Oncol.*, vol. 30, no. 17, pp. 2055–2062, 2012.
- [69] D. S. Alberts, J. Blessing, L. Landrum, D. Warshal, L. Martin, S. Rose, A. Bonebrake, and L. Ramondetta, “Phase II trial of nab-paclitaxel in the treatment of recurrent or persistent advanced cervix cancer: A gynecologic oncology group study,” *Gynecol Oncol*, vol. 127, no. 3, pp. 451–455, 2012.
- [70] N. M. Idris, M. K. Gnanasammandhan, J. Zhang, P. C. Ho, and R. Mahendran, “Technical Reports In vivo photodynamic therapy using upconversion nanoparticles as remote-controlled nanotransducers,” *Nat. Med.*, vol. 18, no. 10, pp. 1580–1585, 2012.
- [71] H. Huang, S. Delikanli, H. Zeng, D. M. Ferkey, and A. Pralle, “Remote control of ion channels and neurons through magnetic-field heating of nanoparticles,” vol. 5, no. 6, pp. 602–606, 2010.
- [72] C. W. Burke, J. Suk, A. Kim, Y. Hsiang, A. Klibanov, J. Hanes and R. Price, “Markedly enhanced skeletal muscle transfection achieved by the ultrasound-targeted delivery of non-viral gene nanocarriers with microbubbles,” *J. Control. Release*, vol. 162, no. 2, pp. 414–421, 2012.
- [73] L. Zhang, H. Chen, L. Wang, T. Liu, J. Yeh, G. Lu, L. Yang and H. Mao, “Delivery of therapeutic radioisotopes using nanoparticle platforms: Potential benefit in systemic radiation therapy,” *Nanotechnol. Sci. Appl.*, vol. 3, no. 1, pp. 159–170, 2010.
- [74] D. Trau, W. Yang, M. Seydack, F. Caruso, N. T. Yu, and R. Renneberg, “Nanoencapsulated microcrystalline particles for superamplified biochemical assays,” *Anal. Chem.*, vol. 74, no. 21, pp. 5480–5486, 2002.
- [75] G. Ting, C. H. Chang, and H. E. Wang, “Cancer nanotargeted radiopharmaceuticals for tumour imaging and therapy,” *Anticancer Research*, vol. 29, no. 10. pp. 4107–4118,

- 2009.
- [76] H. Hong, Y. Zhang, J. Sun, and W. Cai, "Molecular imaging and therapy of cancer with radiolabeled nanoparticles," *Nano Today*, vol. 4, no. 5, pp. 399–413, 2009.
- [77] T. F. Massoud and S. S. Gambhir, "Molecular imaging in living subjects: seeing fundamental biological processes in a new light.," *Genes Dev.*, vol. 17, no. 5, pp. 545–580 2003.
- [78] V. G. Kessler and G. a. Seisenbaeva, "Rhenium Nanochemistry for Catalyst Preparation," *Minerals*, vol. 2, no. 4, pp. 244–257 2012.
- [79] A. R. Margarita and M. M. Khabib, "Catalytic Properties of Rhenium and Its Compounds," *Russ. Chem. Rev.*, vol. 38, no. 11, pp. 944, 1969.
- [80] H. S. Broadbent and W. J. Bartley, "Rhenium Catalysts. VII. Rhenium(VI) Oxide," *J. Org. Chem.*, vol. 28, no. 9, pp. 2345–2347, 1963.
- [81] M. Grzelczak, J. Pérez-Juste, P. Mulvaney, and L. M. Liz-Marzán, "Shape Control in Gold Nanoparticle Synthesis," *Chem. Soc. Rev.*, vol. 37, no. 9, pp. 1783–1791, 2008.
- [82] S. C. Kim, W. G. Shim, M. S. Lee, S. C. Jung, and Y.-K. Park, "Preparation of platinum nanoparticle and its catalytic activity for toluene oxidation.," *J. Nanosci. Nanotechnol.*, vol. 11, no. 8, pp. 7347–7352, 2011.
- [83] C.-C. Wang, D.-H. Chen, and T.-C. Huang, "Synthesis of palladium nanoparticles in water-in-oil microemulsions," *Colloids Surfaces A Physicochem. Eng. Asp.*, vol. 189, no. 1-3, pp. 145–154, 2001.
- [84] J. Cookson, "The preparation of palladium nanoparticles," *Platinum Metals Review*, vol. 56, no. 2, pp. 83–98, 2012.
- [85] J. V. Rojas and C. H. Castano, "Production of palladium nanoparticles supported on multiwalled carbon nanotubes by gamma irradiation," *Radiat. Phys. Chem.*, vol. 81, no. 1, pp. 16–21, 2012.
- [86] Y. Sun, "Controlled synthesis of colloidal silver nanoparticles in organic solutions: empirical rules for nucleation engineering.," *Chem. Soc. Rev.*, vol. 42, no. 7 pp. 2497–2511, 2012.
- [87] B. Azadbakht, H. Afarideh, M. Ghannadi-Maragheh, M. Asgari, and A. Bahrami-Samani,

- “Development of an electrochemical $^{188}\text{W}/^{188}\text{Re}$ generator as a technique for separation and purification of ^{188}Re in radiopharmaceutical applications,” *Appl. Radiat. Isot.*, vol. 118, no 12, pp. 331–337, 2016.
- [88] B. Azadbakht, H. Afarideh, M. Ghannadi-Maragheh, A. Bahrami-Samani, and M. Asgari, “Preparation and evaluation of APTES-PEG coated iron oxide nanoparticles conjugated to rhenium-188 labeled rituximab,” *Nucl. Med. Biol.*, vol. 48, no. 5, pp. 26–30, 2017.
- [89] S. Anantharaj, K. Sakthikumar, A. Elangovan, G. Ravi, T. Karthik, and S. Kundu, “Ultra-small rhenium nanoparticles immobilized on DNA scaffolds: An excellent material for surface enhanced Raman scattering and catalysis studies,” *J. Colloid Interface Sci.*, vol. 483, no. 12, pp. 360–373, 2016.
- [90] J. V. Rojas and C. H. Castano, “Synthesis of rhenium oxide nanoparticles (RexOy) by gamma irradiation,” *Radiat. Phys. Chem.*, vol. 99, no. 6, pp. 1–5, 2014.
- [91] Ü. Demirbaş, R. Z. U. Kobak, B. Barut, R. Bayrak, A. Koca, and H. Kantekin, “Synthesis and electrochemical characterization of tetra-(5-chloro-2-(2,4-dichlorophenoxy)phenol) substituted Ni(II), Fe(II) and Cu(II) metallophthalocyanines,” *Synth. Met.*, vol. 215, no. 5, pp 7–13, 2016.
- [92] O. Bekaroglu, “Synthesis of phthalocyanines and related compounds,” *J. Porphyr. Phthalocyanines*, vol. 4, no. 5, pp. 465–473, 2000.
- [93] N. B. McKeown, *Phthalocyanine materials: synthesis, structure, and function*. pp. 193, 1998.
- [94] D. K. P. Ng, “Dendritic phthalocyanines: Synthesis, photophysical properties, and aggregation behavior,” *Comptes Rendus Chim.*, vol. 6, no. 8–10, pp. 903–910, 2003.
- [95] S. Gundy, W. Van der Putten, A. Shearer, D. Buckton, A. G. Ryder, and M. Ball, “The use of chloroaluminium phthalocyanine tetrasulfonate (AIPcTS) for time-delayed fluorescence imaging,” *Phys. Med. Biol.*, vol. 49, no. 3, pp. 359–369, 2004.
- [96] B. G. Ongarora, K. R. Fontenot, X. Hu, I. Sehgal, S. D. Satyanarayana-Jois, and M. G. H. Vicente, “Phthalocyanine-peptide conjugates for epidermal growth factor receptor targeting.” *J. Med. Chem.*, vol. 55, no. 8, pp. 3725–3738, 2012.
- [97] Z. Biyiklioğlu, “Water-soluble axially disubstituted non-aggregated silicon

- phthalocyanines and their electrochemical properties," *Dye. Pigment.*, vol. 99, no. 1, pp. 59–66, 2013.
- [98] Z. Biyiklioğlu, V. Çakir, D. Çakir, and H. Kantekin, "Crown ether-substituted water soluble phthalocyanines and their aggregation, electrochemical studies," *J. Organomet. Chem.*, vol. 749, pp. 18–25, no. 1, 2014.
- [99] Z. Biyiklioğlu, "Non-aggregated and water soluble amphiphilic silicon phthalocyanines with two axial substituents and their electrochemical properties," *Polyhedron*, vol. 63, no 10, pp. 1–8, 2013.
- [100] K. Eller, E. Henkes, R. Rossbacher, and H. Höke, "Amines, Aliphatic," *Ullmann's Encycl. Ind. Chem.*, pp. 647–698, 2012.
- [101] R. P. Tripathi, V. Tiwari, N. Tewari, D. Katiyar, N. Saxena, S. Sinha, A. Gaikwad, A. Srivastava, V. Chaturvedi, Y. Manju, R. Srivastava, and B. Srivastava, "Synthesis and antitubercular activities of bis-glycosylated diamino alcohols," *Bioorganic Med. Chem.*, vol. 13, no 19, pp. 5668–5679, 2005.
- [102] M. Köhn, R. Wacker, C. Peters, H. Schröder, L. Soulère, R. Breinbauer, C. Niemeyer and H. Waldmann, "Staudinger Ligation: A New Immobilization Strategy for the Preparation of Small-Molecule Arrays," *Angew. Chemie - Int. Ed.*, vol. 42, no 47, pp. 5830–5834, 2003.
- [103] A. S. Nagle, R. Salvatore, R. Cross, E. Kapxhiu, S. Sahab, C. Yoon, K. Jung, "Selective mono protection of diols, diamines, and amino alcohols using cesium bases," *Tetrahedron Lett.*, vol. 44, no. 30, pp. 5695–5698, 2003.
- [104] D. W. Lee, H. Ha, and W. K. Lee, "Selective Mono-BOC Protection of Diamines," *Synth. Commun.*, vol. 37, no. 5, pp. 737–742, 2007.
- [105] A. Goossens, I. Baret, and A. Swevers, "Allergic contact dermatitis caused by tetrahydroxypropyl ethylenediamine in cosmetic products," *Contact Dermatitis*, vol. 64, no 3, pp. 161–164, 2011.
- [106] P. Roose, K. Eller, E. Henkes, R. Rossbacher, and H. Höke, "Amines, Aliphatic," in *Ullmann's Encyclopedia of Industrial Chemistry*, pp. 1–55, 2015.
- [107] A. R. Vortherms, R. P. Doyle, D. Gao, and P. J. Sinko, "Nucleosides , Nucleotides and

- Nucleic Acids Synthesis , Characterization , and In Vitro Assay of Folic Acid Conjugates Toward Targeted AZT Based Anticancer Therapeutics,” vol. 27, no. 4, pp. 37–41, 2008.
- [108] A. R. Vortherms, R. P. Doyle, D. Gao, O. Debrah, and P. J. Sink, “Synthesis, characterization and in vitro assay of folic acid conjugates of 3'-azido-3'deoxythymidine (AZXT): toward targeted AZT based anticancer therapeutics,” *Nucleosides Nucleotides Nucleic Acids*, vol. 27, no. 2, pp. 173–185, 2009.
- [109] C. Chen, “Acid by folate receptors,” vol. 5, no. 3, pp. 1–5, 2013.
- [110] A. Hashemian, G. Mansoori “Cancer Nanodiagnosics and Nanotherapeutics through the Folate- Conjugated Nanoparticles,” vol. 5, no. 3, pp. 61–64, 2015.
- [111] A. S. Wibowo, M. Singh, K. Reeder, J. Carter, A. Kovach, W. Meng, M. Ratnam, F. Zhang and C. Dann, “Structures of human folate receptors reveal biological trafficking states and diversity in folate and antifolate recognition.,” *Proc. Natl. Acad. Sci. U. S. A.*, vol. 110, no. 38, pp. 15180–8, 2013.
- [112] A. S. G. Ali, M. a Reza, H. Eshghi, A. Sazgarnia, and R. Montazerabadi, “Cancerous Cells Targeting and Destruction Using Folate Conjugated Gold Nanoparticles,” *Dyn. Biochem. Process Biotechnol. Mol. Biol.*, vol. 4, no. 1, pp. 6–12 2010.
- [113] L. Teng, J. Xie, L. Teng, and R. J. Lee, “Clinical translation of folate receptor-targeted therapeutics,” *Expert Opin. Drug Deliv.*, vol. 9, no. 8, pp. 901–908, 2012.
- [114] A. F. Trindade, R. Frade, E. Maçôas, C. Graça, C. Rodrigues, J. Martinho and C. Afonso, “‘Click and go’: simple and fast folic acid conjugation_Supplement,” *Org. Biomol. Chem.*, vol. 12, no. 20, pp. 1–3, 2014.
- [115] Z. O. Repository, “University of Zurich An efficient two-step synthesis of metal-free phthalocyanines using a Zn(II) template An efficient two-step synthesis of metal-free phthalocyanines using a Zn(II) template,” no. 15, pp. 197, 2009.
- [116] R. O. Ogbodu, E. Antunes, and T. Nyokong, “Physicochemical properties of zinc monoamino phthalocyanine conjugated to folic acid and single walled carbon nanotubes,” *Polyhedron*, vol. 60, no. 9, pp. 59–67, 2013.
- [117] S. Ntsimango, “The development of rhenium nanoradiopharmaceuticals,” MSc. Dissertation, NMU, no.1, 2016.

- [118] T. Mosmann, "Rapid colorimetric assay for cellular growth and survival: Application to proliferation and cytotoxicity assays," *J. Immunol. Methods*, vol. 65, no. 1–2, pp. 55–63, 1983.
- [119] A. M. Schrand, J. J. Schlager, L. Dai, and S. M. Hussain, "Preparation of cells for assessing ultrastructural localization of nanoparticles with transmission electron microscopy," *Nat. Protoc.*, vol. 5, no. 4, pp. 744–757, 2010.
- [120] L. C. Cairncross, "An investigation into the localization of peptide-gold nanoparticles in an in vitro and in vivo colorectal cancer model," no. 2, 2015.
- [121] C. Ng, J. Li, and R. Perumalsamy, "Localizing cellular uptake of nanomaterials in vitro by transmission electron microscopy," *Microsc. Sci. Technol.*, no. 1640, pp. 316–320, 2010.
- [122] G. R. Newman, B. Jasani, and E. D. Williams, "The preservation of ultrastructure and antigenicity," *J. Microsc.*, vol. 127, no. 3, pp. 5–6, 1982.
- [123] G. R. Newman, B. Jasani, and E. D. Williams, "A simple post-embedding system for the rapid demonstration of tissue antigens under the electron microscope," *Histochem. J.*, vol. 15, no. 6, pp. 543–555, 1983.
- [124] G. R. Newman and J. A. Hobot, "Resins for combined light and electron microscopy: A half century of development," *Histochem. J.*, vol. 31, no. 8, pp. 495–505, 1999.
- [125] J. F. Hillyer and R. M. Albrecht, "Gastrointestinal persorption and tissue distribution of differently sized colloidal gold nanoparticles," *J. Pharm. Sci.*, vol. 90, no. 12, pp. 1927–1936, 2001.
- [126] W. H. De Jong, M. C. Burger, M. A. Verheijen, and R. E. Geertsma, "Detection of the presence of gold nanoparticles in organs by transmission electron microscopy," *Materials (Basel)*, vol. 3, no. 9, pp. 4681–4694, 2010.
- [127] J. V. Rojas and C. H. Castano, "Synthesis of rhenium oxide nanoparticles (RexOy) by gamma irradiation," *Radiat. Phys. Chem.*, vol. 99, no. 6, pp. 1–5, 2014.
- [128] C. Wittekind, "Pathology," *Color. Cancer*, vol. 23, no. 2, pp. 103–114, 2006.
- [129] A. Gabizon, A. T. Horowitz, D. Goren, D. Tzemach, F. Mandelbaum-Shavit, M. M. Qazen, and S. Zalipsky, "Targeting folate receptor with folate linked to extremities of poly(ethylene glycol)-grafted liposomes: In vitro studies," *Bioconjug. Chem.*, vol. 10, no.

- 2, pp. 289–298, 1999.
- [130] S. Wang, J. Luo, D. Lantrip, D. Waters, C. Mathias, M. Green, P. Fuchs and P. Low, “Design and synthesis of [111In]DTPA-folate for use as a tumour-targeted radiopharmaceutical,” *Bioconjug. Chem.*, vol. 8, no. 5, pp. 673–679, 1997.
- [131] S. Wang, R. J. Lee, C. J. Mathias, M. a Green, and P. S. Low, “Synthesis, purification, and tumour cell uptake of ⁶⁷Ga-deferoxamine-folate, a potential radiopharmaceutical for tumour imaging,” *Bioconjug. Chem.*, vol. 7, no. 1, pp. 56–62, 1996.
- [132] N. Viola-Villegas, A. E. Rabideau, J. Cesnavicious, J. Zubieta, and R. P. Doyle, “Targeting the folate receptor (FR): Imaging and cytotoxicity of Re I conjugates in FR-overexpressing cancer cells,” *ChemMedChem*, vol. 3, no. 9, pp. 1387–1394, 2008.
- [133] O. Aronov, A. T. Horowitz, A. Gabizon, and D. Gibson, “Folate-targeted PEG as a potential carrier for carboplatin analogs. Synthesis and in vitro studies,” *Bioconjug. Chem.*, vol. 14, no. 3, pp. 563–574, 2003.
- [134] S. Singh, H. Singh, T. Karthick, P. Tandon, and V. Prasad, “Phase transition analysis of V-shaped liquid crystal: Combined temperature-dependent FTIR and density functional theory approach,” *Spectrochim. Acta - Part A Mol. Biomol. Spectrosc.*, vol. 188, pp. 561–570, 2018.
- [135] L. Lu, K. Ai, and Y. Ozaki, “Environmentally friendly synthesis of highly monodisperse biocompatible gold nanoparticles with urchin-like shape,” *Langmuir*, vol. 24, no. 3, pp. 1058–1063, Feb. 2008.
- [136] J. Conde, G. Doria, and P. Baptista, “Noble Metal Nanoparticles Applications in Cancer,” *J. Drug Deliv.*, vol. 2012, pp. 1–12, 2012.
- [137] R. R. Retamal Marín, F. Babick, and L. Hillemann, “Zeta potential measurements for non-spherical colloidal particles – Practical issues of characterisation of interfacial properties of nanoparticles,” *Colloids Surfaces A Physicochem. Eng. Asp.*, vol. 532, no. 4, pp. 516–521, 2017.
- [138] G. Perera, M. Zipser, S. Bonengel, W. Salvenmoser, and A. Bernkop-Schnürch, “Development of phosphorylated nanoparticles as zeta potential inverting systems,” *Eur. J. Pharm. Biopharm.*, vol. 97, pp. 250–256, 2015.

- [139] P. Leroy, N. Devau, A. Revil, and M. Bizi, "Influence of surface conductivity on the apparent zeta potential of amorphous silica nanoparticles," *J. Colloid Interface Sci.*, vol. 410, pp. 81–93, 2013.
- [140] A. Elder, H. Yang, R. Gwiazda, X. Teng, S. Thurston, H. He and G. Oberdörster, "Testing nanomaterials of unknown toxicity: An example based on platinum nanoparticles of different shapes," *Adv. Mater.*, vol. 19, no. 20, pp. 3124–3129, 2007.
- [141] A. Nel, "Toxic Potential of Materials," *Science (80-.)*, vol. 311, no. 5726, pp. 622–627, 2007.
- [142] E. Katz and I. Willner, "Integrated nanoparticle-biomolecule hybrid systems: Synthesis, properties, and applications," *Angew. Chemie - Int. Ed.*, vol. 43, no. 45, pp. 6042–6108, 2004.
- [143] H. Jin, J. Lovell, J. Chen, K. Ng, W. Cao, L. Ding, Z. Zhang and G. Zheng, "Investigating the specific uptake of EGF-conjugated nanoparticles in lung cancer cells using fluorescence imaging," *Cancer Nanotechnol.*, vol. 1, no. 1–6, pp. 71–78, 2010.
- [144] R. Yusuf and K. Frenkel, "Morphologic transformation of human breast epithelial cells MCF-10A: dependence on an oxidative microenvironment and estrogen/epidermal growth factor receptors," *Cancer Cell Int.*, vol. 10, pp. 15–20, 2010.
- [145] M. Panjehpour, M. Castro, and K. N. Klotz, "Human breast cancer cell line MDA-MB-231 expresses endogenous A₂B adenosine receptors mediating a Ca²⁺ signal," *Br. J. Pharmacol.*, vol. 145, no. 2, pp. 211–218, 2005.
- [146] N. M. Jackson, "The regulation and mechanisms of EGFR-mediated apoptosis in MDA-MB-468 cells," 2015.
- [147] H. J. Hathaway, K. Butler, N. Adolphi, D. Lovato, R. Belfon, D. Fegan, T. Monson, J. Trujillo, T. Tessier, H. Bryant, D. Huber, R. Larson and E. Flynn, "Detection of breast cancer cells using targeted magnetic nanoparticles and ultra-sensitive magnetic field sensors," *Breast Cancer Res.*, vol. 13, no. 5, pp. 108–108, 2011.